Wayne State University Dissertations

1-1-2015

Photodynamic Therapy As An Effective Therapeutic Approach In Mame Models Of Triple Negative And Inflammatory Breast Cancers

Neha Aggarwal
Wayne State University,

Follow this and additional works at: http://digitalcommons.wayne.edu/oa_dissertations

Part of the Molecular Biology Commons, Oncology Commons, and the Pharmacology Commons

Recommended Citation

PHOTODYNAMIC THERAPY AS AN EFFECTIVE THERAPEUTIC APPROACH IN MAME MODELS OF TRIPLE NEGATIVE AND INFLAMMATORY BREAST CANCERS

by

NEHA AGGARWAL

DISSERTATION

Submitted to the Graduate School

of Wayne State University,

Detroit, Michigan

in partial fulfillment of the requirements

for the degree of

DOCTOR OF PHILOSPHY

2015

MAJOR: PHYSIOLOGY

Approved by

_____

Advisor   Date

_____

_____

_____

_____

_____

DEDICATION

I dedicate this dissertation to my entire family. To my parents, Mrs. Rama and Sudhir Aggarwal: you show unconditional love, support and encouragement always. I would not have been where I am without your support. You are the best parents.

I also dedicate this work to my husband, Lalit for his constant support through the years we have been together. I must recognize the support and love of my sister, Namisha and my brother, Gaurav. I also extend thanks to my in-laws for their support.

ACKNOWLEDGEMENTS

TABLE OF CONTENTS

LIST OF TABLES

LIST OF FIGURES

LIST OF ABBREVIATIONS

2D	two-dimensional
3D	three-dimensional
BPD	benzoporphyrin derivative
CA074	methyl (2S)-1-[(2S)-3-methyl-2-[[(2S,3S)-3-(propylcarbamoyl)oxirane-2-carbonyl]amino]pentanoyl]pyrrolidine-2-carboxylate
CG	calcein AM
DIC	differential interference contrast
EB	ethidium homodimer-1
ECM	extracellular matrix
EGF	epidermal growth factor
EGFR	epidermal growth factor receptor
ER	estrogen receptor
HER2	herceptin receptor 2
IBC	inflammatory breast cancer
IHC	immunohistochemistry
MAME	mammary architecture and microenvironment engineering
MEGM	mammary epithelial cell growth medium
NPe6	N-aspartyl chlorin6
PBS	phosphate buffered saline
PDT	photodynamic therapy
PR	progesterone receptor
rBM	reconstituted basement membrane
RFP	red fluorescence protein

T4MPyP meso-tetrakis (4-N-methylpyridyl) porphine

TNBC triple-negative breast cancer

ZnPc zinc(II) phthalocyanine

CHAPTER 1

INTRODUCTION AND SPECIFIC AIMS OF DISSERTATION

Breast cancer is the most commonly diagnosed cancer and is the second leading cause of cancer-related deaths in females in the United States. Two subtypes for which there are at present no effective targeted therapies are triple negative breast cancer (TNBC) and inflammatory breast cancer (IBC). Conventional therapies (surgery, radiation, chemotherapy) alone or in combination are not effective against TNBC or IBC.

PDT is a treatment that requires administration of a light activable photosensitizer that localizes to specific sub-cellular organelles. Once the photosensitizer is excited by light at an appropriate wavelength, reactive oxygen species are formed that cause cell death. Recent literature has shown that treating with two PSs (i.e., combination PDT) significantly increases apoptotic cell death. Photodynamic therapy (PDT) is an FDA approved therapy and is currently in clinical use for treatment of endobronchial, esophageal and bladder cancers. An essential component for successful PDT is accessibility of the tumors to the light needed for PS excitation. PDT is not in clinical use for treatment of breast cancers. We propose that PDT may have the potential to eradicate chest wall metastases of TNBCs and dermal metastases of IBC, i.e., sites that would be accessible to this therapy.

Pre-clinical PDT studies have mainly used cell lines cultured in monolayers growing on plastic. Cells cultured in monolayers do not recapitulate the *in vivo* architecture that is critical for accurately modeling tumor growth and treatment. In contrast, cells grown in 3D *in vitro* models do recapitulate *in vivo* cell-cell and cell-matrix interactions. Moreover, 3D models are predictive of resistance to chemo- and radiation therapies unlike monolayer cultures. We propose, through the following two Specific Aims, to use 3D models of TNBC and IBC to determine the efficacy of PDT including combination PDT in photokilling.

Specific Aim 1: Determine if PDT is more effective in the photokilling of MAME structures of TNBC and IBC when lysosomes and mitochondria are sequentially targeted as compared to targeting only mitochondria.

Hypothesis: Combination PDT will be more efficacious in photokilling as two critical organelles, lysosomes and mitochondria, will be damaged.

Specific Aim 2: Identify mechanism(s) involved in photokilling by sequential targeting of lysosomes and mitochondria.

Hypothesis: Sequential targeting of lysosomes and mitochondria causes cell death via apoptosis.

In this dissertation research, we used 3D Mammary Architecture and Microenvironment Engineering (MAME) models of TNBC and IBC to determine the efficacy of PDT. In Chapter 3, we describe studies to determine the efficacy of PDT that targets mitochondria (using BPD as photosensitizer) in the photokilling MAME structures of TNBC and IBC cells. We further demonstrate that combination PDT targeting both mitochondria and lysosomes is more efficacious in photokilling MAME structures of IBC cells. In Chapter 4 we describe studies demonstrating that apoptosis is the mechanism of cell death induced by combination PDT in which lysosomal photodamage (using NPe6 as photosensitizer) was followed by mitochondrial photodamage (using BPD). This dissertation research provide evidence that PDT, in particular combination PDT, is an efficacious therapeutic modality against two lethal subtypes of breast cancer (TNBC and IBC) as assessed in cell lines grown in 3D MAME cultures.

CHAPTER 2

BACKGROUND FOR DISSERTATION

2.1 Breast Cancer

The mammary gland is composed of a highly branched ductal network. The ductal network is composed of two cell types: a monolayer of myoepithelial cells underneath the ductal epithelial cells (Lakhani and O'Hare 2001, Adriance, Inman et al. 2005). The myoepithelial cells provide the contractile forces during lactation and also induce ductal cell polarity during development (Gudjonsson, Ronnov-Jessen et al. 2002). The breast stroma makes up about 80% of the mammary gland (Drife 1986) and is comprised of cells like adipocytes, fibroblasts, smooth muscle, macrophages and endothelial cells (Weigelt and Bissell 2008) and non-cellular matrix components. The breast epithelial cells and stromal components are interdependent in terms of normal regulation of signaling.

Signaling occurs through receptors such as integrins that bind cells to the extracellular matrix (ECM) (Hynes 1992, Lochter and Bissell 1995). ECM is secreted from stromal and epithelial cells and plays an important role in cell adhesion, signaling, and survival (Ghajar and Bissell 2008). The ECM is continuously remodeled during physiological processes such as development (Badylak 2005), morphogenesis (Ghajar and Bissell 2008), angiogenesis (Cheresh and Stupack 2008), cell migration, and wound healing (Schultz and Wysocki 2009). Basement membrane (BM) is a specialized form of ECM and is composed of laminin and type IV collagen (Kalluri 2003). BM is present as a continuous layer at the epithelial stromal interface (Kalluri 2003, Weigelt and Bissell 2008). The BM functions as a mechanical barrier that anchors and maintains the organization of an acinus.

Breast cancer is the most commonly diagnosed cancer and is the second leading cause of cancer-related deaths in females in the United States (American Cancer Society). During

malignant progression changes occur both in the breast epithelium and its microenvironment. The transformed epithelial cells proliferate and begin to fill the hollow lumen (Ronnov-Jessen, Petersen et al. 1996, Sternlicht, Kedeshian et al. 1997, Debnath and Brugge 2005). As cancer progresses the epithelial cells breach the basement membrane leading to invasion and metastasis. Malignant progression from benign hyperplasia to very aggressive lethal tumors takes a long time leaving a large window of opportunity to offer therapeutic interventions if detected early in time (American Cancer Society). Breast cancer is not a single disease but has many subtypes based on expression of estrogen receptor (ER), progesterone receptor (PR) and human epidermal growth factor receptor 2 (HER2) receptors in primary tumors. These subtypes are referred to as luminal A (when ER and/or PR is present but HER2 is not amplified), luminal B (when ER and/or PR is present along with HER2 amplification), HER2-like (when ER and PR are absent but HER2 is amplified) and basal-like or triple negative (when all three receptors are absent) (American Cancer Society).

2.1.1 Inflammatory breast cancer (IBC)

IBC is a rare and very aggressive type of locally advanced breast cancer. Based on expression of ER, PR and HER2, IBC tumors are also classified as luminal A, luminal B, HER2-like and basal-like or triple negative. IBC is characterized by erythema, edema and/or *peau d'orange* with or without a palpable mass in the breast causing inflammation of the breast, hence the name inflammatory breast cancer (Figure 2.1). The cancer cells do not generally form a lump, but instead form emboli that metastasize to the dermal lymphatic vasculature. Due to the absence of a palpable mass, diagnosis of this subtype of breast cancer is difficult and it is not generally detected by mammography. Additionally, due to the presence of edema and erythema, IBC is often confused with an inflammatory condition like mastitis. IBC is characterized by rapid proliferation of cancer cells, chemo-resistance and poor prognosis. By the time a correct

diagnosis is made, IBC has advanced to stages III or IV (Wingo, Jamison et al. 2004). To date,

no targeted therapy has been approved for IBC; a combination of conventional chemotherapy

and radiation remain the standard therapies.

Figure 2.1: Clinical characteristics of IBC and variations in symptoms. IBC patient with redness in both breasts (bilateral erythema) with minimal breast inflammation (edema) (A) in contrast to another IBC patient with increased breast size due to edema and peau d'orange (appearance of skin like peel of an orange) with minimal erythema (B) (Robertson, Bondy et al. 2010).

IBC is the most lethal type of breast cancer with a three-year survival rate of 42% as

compared to 85% for non-IBC (Chang, Parker et al. 1998). In the same study, the authors

observed that after 10 years of follow-up, most of the IBC patients had died, whereas more than half of the patients with other types of breast carcinoma were still alive. In another study, a comparison among IBC patients of stages IIIB, IIIC and IV revealed that the two-year survival among these women was 81%, 67% and 42%, respectively (Dawood, Ueno et al. 2012).

The incidence of IBC is relatively low but varies depending on geographic region. For example, IBC accounts for approximately 2.5% of all breast cancer cases in the USA (Hance, Anderson et al. 2005), whereas in parts of northern Africa (Egypt, Morocco and Tunisia) rates may be as high as 6-10% (Soliman, Kleer et al. 2011). The clinical characteristics of patients are also variable by geographic location. A study on patients from Egypt, Tunisia and Morocco showed that Egyptian IBC patients had the highest combined erythema, edema, *peau d'orange*, and metastasis among the 3 IBC groups (Soliman, Kleer et al. 2011). This study also showed that Egyptian IBC tumors had the highest RhoC expression among the three populations under study and might be a potential therapeutic target. In another study by the same group, a comparison between Egyptian and US IBC patient population was made showing that erythema, edema, and peau d'orange were found in 77% of the Egyptian patients as compared with 29% of the U.S. patients and that the expression of RhoC was significantly higher in Egyptian patient tumors (Lo, Kleer et al. 2008). In the U.S. IBC incidence rates are significantly higher in African-American women than in Caucasian women (Chang, Parker et al. 1998, Hance, Anderson et al. 2005). Thus IBC appears to result from interplay of epidemiologic, genetic and environmental factors, which lead to distinct clinical and molecular characteristics among different populations.

Molecular markers besides RhoC GTPase have also been studied in patient populations. IBC tumors have a higher occurrence of *p53* gene mutations as compared to non-IBC tumors (Riou, Le et al. 1993, Gonzalez-Angulo, Sneige et al. 2004) and increased expression of

angiogenic and lymphangiogenic factors including IL-6, IL-8, VEGF, and VEGF receptor 3 (Van der Auwera, Van Laere et al. 2004). Previous studies from our lab have shown that the cysteine protease cathepsin B, the serine protease urokinase-type plasminogen activator (uPA) and the urokinase-type plasminogen activator receptor (uPAR) are associated with caveolar fractions (caveolae are lipid-rich invaginations of the plasma membrane and are involved in important cellular processes such as endocytosis, cholesterol transport and cell signaling events) in IBC cells (Victor and Sloane 2007, Victor, Anbalagan et al. 2011). These reports also showed that caveolin-1 and cathepsin B are co-expressed in IBC patient samples and this co-expression contributes to the aggressive behavior of IBC. Additional studies have shown that high levels of cathepsin B correlate with an increase in numbers of metastatic lymph nodes in IBC patients (Nouh, Mohamed et al. 2011).

2.1.2 Triple Negative Breast Cancer (TNBC)

At the molecular level, breast cancer is characterized based on expression of hormone receptors. The most lethal breast cancers are those that are characterized by the absence of estrogen receptor (ER) and progesterone receptor (PR) and the amplification of human epidermal growth factor receptor type 2 (HER2) and are referred to as triple negative breast cancer (TNBC) (Bosch, Eroles et al. 2010, de Ruijter, Veeck et al. 2011, Lehmann, Bauer et al. 2011, Chiorean, Braicu et al. 2013). Of all breast cancers, TNBCs account for about 10-20% cases (Morris, Naidu et al. 2007, Bosch, Eroles et al. 2010, Lehmann, Bauer et al. 2011, Dreyer, Vandorpe et al. 2013). TNBC (like IBC) is more likely to affect younger women and occurs before ages of 40 or 50 whereas age of onset for other breast cancers is 60 or older (Dent, Trudeau et al. 2007, Bowen, Duffy et al. 2008, Lund, Trivers et al. 2009). TNBC is more common in African-American women and women of Hispanic origin than in Asian and non-Hispanic women (Stead, Lash et al. 2009, Lara-Medina, Perez-Sanchez et al. 2011). The rate of recurrence for TNBCs is

~7% -11% that is higher compared to other breast cancer subtypes (2%-6%) (Steward, Conant et al. 2014). TNBCs also have shorter times to recur that range from 19 to 40 months compared to 35 to 67 months for non-TNBCs (Steward, Conant et al. 2014). In addition, about 20-40% of IBC cases are also triple negative; in contrast to 15-20% of non-IBC cases being triple negative (Lehmann, Bauer et al. 2011, Dawood, Ueno et al. 2012). Common treatments such as endocrine therapy and targeting of HER-2 receptor become ineffective for TNBC (both IBC and non-IBC) patients. Due to lack of targeted therapy, the prognosis for triple negative IBC is worse than IBCs that express ER, PR, and/or HER2 (Zell, Tsang et al. 2009, Dawood, Ueno et al. 2011, Li, Gonzalez-Angulo et al. 2011, Masuda, Baggerly et al. 2013).

Due to the absence of receptors, TNBC is non-responsive to the therapies available for breast cancer treatment including hormonal therapy such as tamoxifen and aromatase inhibitors) or therapies that target HER2 receptors such as Herceptin (or trastuzumab) (Bosch, Eroles et al. 2010). According to recent literature, correlation between TNBC and several genetic abnormalities have been seen such as mutation of p53, BRCA1, epidermal growth factor receptor (EGFR) expression, and androgen receptor expression (Zhang, Fang et al. 2015). These genetic aberrations have generated an interest for developing targeted therapies for treatment of TNBC. For example, chemotherapy with EGFR antagonists has shown an enhanced tumor response compared to traditional chemotherapy (Corkery, Crown et al. 2009, Nogi, Kobayashi et al. 2009). TNBCs with BRCA1 mutations showed good response to poly-adenosine diphosphate ribose polymerase (PARP) inhibitors in a Phase II clinical trial (Tutt, Robson et al. 2010) and PARP III inhibitors are now in a Phase III trial (NCT02032277). In another clinical trial using Bevacizumab, a monoclonal antibody directed against vascular endothelial growth factor A (VEGF A) (intratumoral expression of VEGF is higher in TNBCs as compared to non-TNBCs), an overall improvement in survival of TNBC patients was not seen (Linderholm, Hellborg et al.

2009). A major reason for failure of these recent therapies is that TNBCs are heterogeneous. Currently, there are no effective targeted therapies for TNBC and there is an unmet need for one (de Ruijter, Veeck et al. 2011, Chiorean, Braicu et al. 2013).

2.2 Photodynamic Therapy (PDT)

Photodynamic Therapy (PDT) is a process that can eradicate malignant cells and their vasculature. PDT is a treatment that has three components: 1) a photosensitizer that localizes primarily in sub-cellular organelles of neoplastic cells, 2) dissolved oxygen in cells and tissues, and 3) light to activate the photosensitizer (Figure 2.2). The resulting photochemistry leads to formation of reactive oxygen species that are cytotoxic and can evoke cellular death pathways (Celli, Spring et al. 2010, Kessel and Oleinick 2010). An essential component to successful PDT is accessibility of the tumors to the light needed for photosensitizer excitation. PDT has been shown to be effective in treating cancers that can be easily accessed by light, including head and neck, esophageal, oral, laryngeal, lung and breast cancer chest wall metastases (Allison, Mang et al. 2001, Biel 2007, Morrison, Hill et al. 2014).

Figure 2.2: Mechanism of Photodynamic Therapy. Photosensitizer (ground state) (PS) is administered to the cells and then activated (to excited state) with light of a particular wavelength. As PS returns to its ground state, energy is transferred to tissue oxygen forming ROS and/or singlet oxygen that cause cell death (Dolmans, Fukumura et al. 2003).
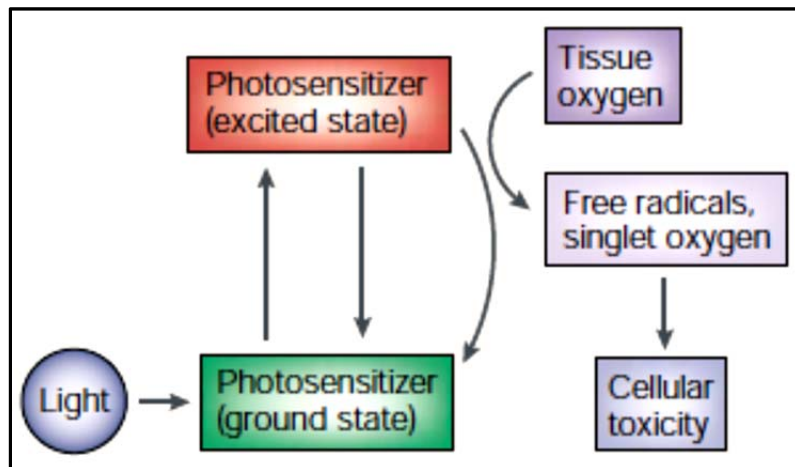
2.2.1 Brief history of PDT

PDT has been known for centuries (Figure 2.3). Exposure to sunlight (phototherapy) to

treat skin diseases and rickets has been used in Egyptian and Indian civilizations since ancient times; however, it was not extensively used in medicine until the 18th century (Epstein 1990, Epstein 1990, Dolmans, Fukumura et al. 2003, Agostinis, Berg et al. 2011). In 1904, Raab discovered the phenomenon of PDT while studying the effect of light and dyes on paramecia (Raab 1904). Later, von Tappeiner and Jodlbauer (von Tappeiner and Jodlbauer 1904, von Tappeiner and Jodlbauer 1907) showed the necessity of oxygen in the process and coined the term "photodynamic therapy"

In the early 20th century the use of PDT was largely confined to treating skin problems such as psoriasis. For treatment of cancer, chemotherapy and ionizing radiotherapy were being used clinically; PDT was not used as a treatment modality. The first pioneering study was by Diamond et al. in 1972 showing regression of glioma in rats when treated with PDT using hematoporphyrin as photosensitizer and white light as activator (Diamond, Granelli et al. 1972). Later, Dougherty and colleagues (Dougherty, Kaufman et al. 1978, Dougherty, Lawrence et al. 1979, Dougherty, Gomer et al. 1998) initiated a clinical trial of PDT in patients with malignant lesions, using hematoporphyrin derivative as photosensitizer that was activated by red light at a wavelength of 630 nm, and proved the effectiveness of this therapy. In 2003, the FDA and other health agencies worldwide approved PDT using Photofrin, a photosensitizer made of a mixture of oligomers of porphyrin, for treatment of esophageal cancer and lung cancer. During use of PDT clinically, surgeons noticed that PDT not only eradicated tumors by direct cell killing but also by shutdown of tumor vasculature. This finding that PDT leads to vasculature shutdown led to one of the major successes in the field, in which a photosensitizer was used for treatment of macular degeneration (Brown and Mellish 2001, Yang 2004). This is a common ailment especially in the older population, leading to impaired vision due to proliferation of blood vessels in the eye. Vascular damage after PDT might also contribute to the success of PDT as a

therapeutic treatment as the tumor cells no longer have access to nutrients and oxygen from the blood stream. The resulting hypoxia/anoxia post-PDT is thought to abrogate tumor growth and progression.
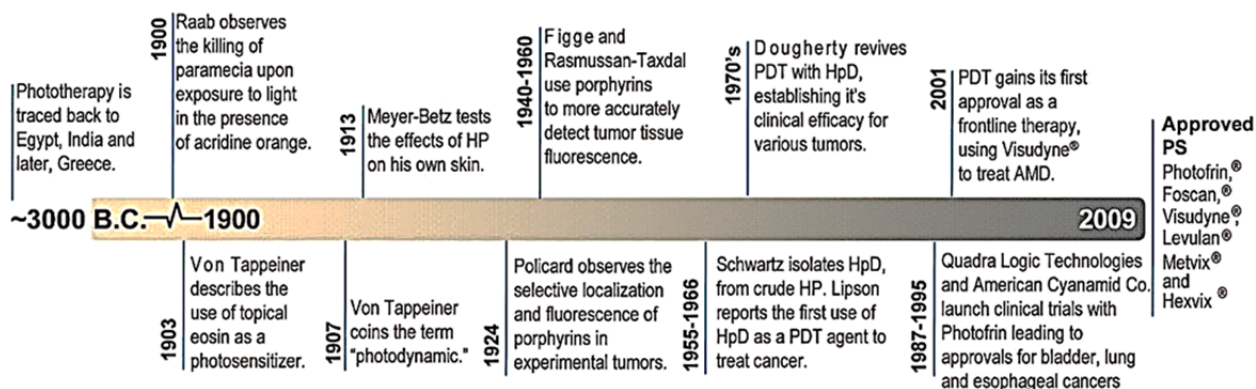
Figure 2.3: History of Photodynamic Therapy. Timeline showing some key discoveries in the field of PDT (Celli, Spring et al. 2010).

2.2.2 Photosensitizers

There are a number of photosensitizers currently known and some of these are registered in at least one country for use in clinical practice (Table 2.1). The second-generation photosensitizers are pure compounds, not mixtures like the photofrin and hematoporphyrin derivative (HPD) and have been shown to localize to sub-cellular organelles such as mitochondria, lysosomes, plasma membrane, endoplasmic reticulum, etc. For instance, the benzoporphyrin derivative monoacid A (BPD, Verteporphin[TM]) and phthalocyanine (Pc4) localize mainly to mitochondria and the mono-L-aspartyl chlorin e6 (NPe6) and meso-tetrakis (4-N-methylpyridyl) porphine (T4MPyP) to lysosomes. Other photosensitizers such as zinc(II) phthalocyanine (ZnPc) localize to the Golgi apparatus and m-tetrahydroxyphenylchlorin (mTHPC) to both endoplasmic reticulum and mitochondria.

Table 2.1. List of Photosensitizers

PHOTOSENSITIZER	STRUCTURE	WAVELENGTH, nm	APPROVED	TRIALS	CANCER TYPES
Porfimer sodium (Photofrin) (HPD)	Porphyrin	630	Worldwide		Lung, esophagus, bile duct, bladder, brain, ovarian
ALA	Porphyrin precursor	635	Worldwide		Skin, bladder, brain, esophagus
ALA esters	Porphyrin precursor	635	Europe		Skin, bladder
Temoporfin (Foscan) (mTHPC)	Chlorine	652	Europe	United States	Head and neck, lung, brain, skin, bile duct
Verteporfin	Chlorine	690	Worldwide (AMD)	United Kingdom	Ophthalmic, pancreatic, skin
HPPH	Chlorin	665		United States	Head and neck, esophagus, lung
SnEt2 (Purlytin)	Chlorin	660		United States	Skin, breast
Talaporfin (LS11, MACE, NPe6)	Chlorin	660		United States	Liver, colon, brain
Ce6-PVP (Fotolon), Ce6 derivatives (Radachlorin, Photodithazine)	Chlorin	660		Belarus, Russia	Nasopharyngeal, sarcoma, brain
Silicon phthalocyanine (Pc4)	Phthalocyanine	675		United States	Cutaneous T-cell lymphoma
Padoporfin (TOOKAD)	Bacteriochlorin	762		United States	Prostate
Motexafin lutetium (Lutex)	Texaphyrin	732		United States	Breast

Abbreviations: ALA, 5-aminolevulinic acid; AMD, age-related macular degeneration; Ce6-PVP, chlorin e6-polyvinylpyrrolidone; HPD, hematoporphyrin derivative; HPPH, 2- (1-hexyloxyethyl)-2-devinyl pyropheophorbide-a; MACE, mono-(L)-aspartylchlorin-e6; mTHPC, m-tetrahydroxyphenylchlorin; nm indicates nanometers; SnEt2, tin ethyl etiopurpurin.

The table shows photosensitizers in use or undergoing clinical trials against cancer types (Agostinis, Berg et al. 2011).

Based on the subcellular localization of photosensitizers, different pathways are activated that lead to cell death. Photosensitizers that target mitochondria and lysosomes generally tend to induce apoptosis whereas the photosensitizers that localize in the plasma membrane are more likely to lead to necrosis (Moan, Pettersen et al. 1979, Schroder, Chen et al. 1988, Agarwal, Clay et al. 1991, Webber, Luo et al. 1996, Kessel and Luo 1998, Kessel, Luo et al. 2000, Kessel and Poretz 2000, Kessel and Oleinick 2010). In addition to sub-cellular localization, concentration of photosensitizer and dose of light are also determining factors in regard to cell death mechanisms (Fingar, Potter et al. 1987, Wyld, Reed et al. 2001). Two photosensitizers that were used in our study are discussed next.

Benzoporphyrin Derivative Monoacid A (BPD)

The trade names of the photosensitizer benzoporphyrin derivative monoacid A are Verteporfin and Visudyne™. BPD is a second-generation photosensitizer (Richter, Waterfield et al. 1990, Richter, Waterfield et al. 1991, Aveline, Hasan et al. 1994). The chemical structure of

BPD resembles that of porphyrins (Figure 2.4). BPD is not soluble in water but is soluble in organic solvents and serum (Allison, Pritchard et al. 1990) and is available as a liposomal formulation for clinical use. Photodynamic therapy using BPD is the only treatment available for wet age-related macular degeneration (Brown and Mellish 2001, Keam, Scott et al. 2003). BPD is not toxic to cells in the absence of light (low cytotoxicity). Once BPD is activated by light of 690 nm wavelength, highly reactive, short-lived singlet oxygen and reactive oxygen radicals are generated resulting in severe damage to cells and eventually cell death (Keam, Scott et al. 2003). BPD localizes to the mitochondria and photodamage upon activation of BPD leads to loss of protection by anti-apoptotic protein BCl2 (Kessel and Luo 1998, Kessel and Luo 1999, Kessel 2006, Osaki, Takagi et al. 2006, Kessel and Oleinick 2010). This results in an increase in mitochondrial membrane permeability and in release of cytochrome c from mitochondria (Granville, Carthy et al. 1998, Kessel and Luo 1999, Kessel 2006, Kessel and Arroyo 2007, Kessel and Oleinick 2010). The release of cytochrome c results in the activation of caspase cascade leading to cell death via apoptosis (Granville, Carthy et al. 1998, Kessel and Luo 1999, Kessel 2006, Osaki, Takagi et al. 2006, Kessel and Oleinick 2010).

Figure 2.4: Chemical structure of Benzoporphyrin Derivative Monoacid A (BPD).
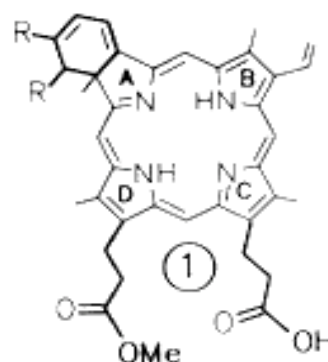
Mono-L-aspartyl chlorin e6 (NPe6)

Mono-L-aspartyl chlorin e6 (NPe6) is also known as also known as talaporfin sodium, MACE, laserphyrin, and LS11 and is trademarked as Aptocine by Light Sciences Oncology.

Chemically, NPe6 is a chlorin-based, second-generation photosensitizer (Figure 2.5) (Usuda, Kato et al. 2006). Upon activation by light of 660 nm wavelength, reactive oxygen species in the form of singlet oxygen are primarily detected (Spikes and Bommer 1993). *In vivo* imaging of NPe6 in an EMT6 mouse tumor model has shown that the photosensitizer undergoes redistribution from vessels into the interstitial space ~3 hours administration (Mitra and Foster 2008). NPe6 primarily localizes to lysosomes (Wan, Liu et al. 2008). Upon photodamage to lysosomes by activating NPe6 with light at 660 nm wavelength, lysosomal proteases including cathepsin B are released into the cytoplasm (Kessel, Luo et al. 2000, Reiners, Caruso et al. 2002, Caruso, Mathieu et al. 2004). Activated cathepsin B (and other lysosomal proteases) cleaves cytoplasmic Bid to its truncated form (t-Bid) that is known to interact with the mitochondrial membrane, leading to release of cytochrome c (Kessel, Luo et al. 2000, Reiners, Caruso et al. 2002, Cirman, Oresic et al. 2004). Once cytochrome c is released, caspase cascade is activated resulting in apoptosis and cell death (Figure 2.6) (Kessel, Luo et al. 2000, Reiners, Caruso et al. 2002, Caruso, Mathieu et al. 2004).

Figure 2.5: Chemical structure of Mono-L-aspartyl chlorin e6 (NPe6).
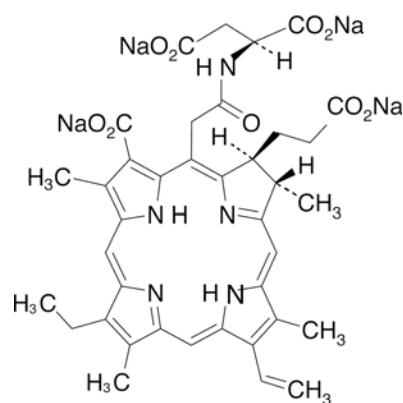
2.2.3 Selectivity of PDT

Multiple factors provide and account for the selectivity of PDT. First, photosensitizing agents show affinity for tumors and their vasculature for reasons not yet completely understood. It is believed that photosensitizers are taken up by LDL receptors that are known to be upregulated in tumor cells (Maziere, Santus et al. 1990, Kessel 1992, Trauner, Gandour-Edwards

et al. 1998). After administration (generally intravenous) of the photosensitizer, there is a non-specific distribution throughout the body but over the next 24-48 hours, the agent localizes to the tumor site (Figure 2.7). Second, photosensitizers are inactive and relatively non-toxic to cells when administered and until irradiated for activation. Light delivery using lasers to tumor site provides another level of selectivity (Figure 2.7). Furthermore, the reactive oxygen species formed upon PDT have a very short half-life of <0.04 microsecond and can affect <20 nm area from the site of formation, thereby limiting the extent of photodamage (Moan and Berg 1991).
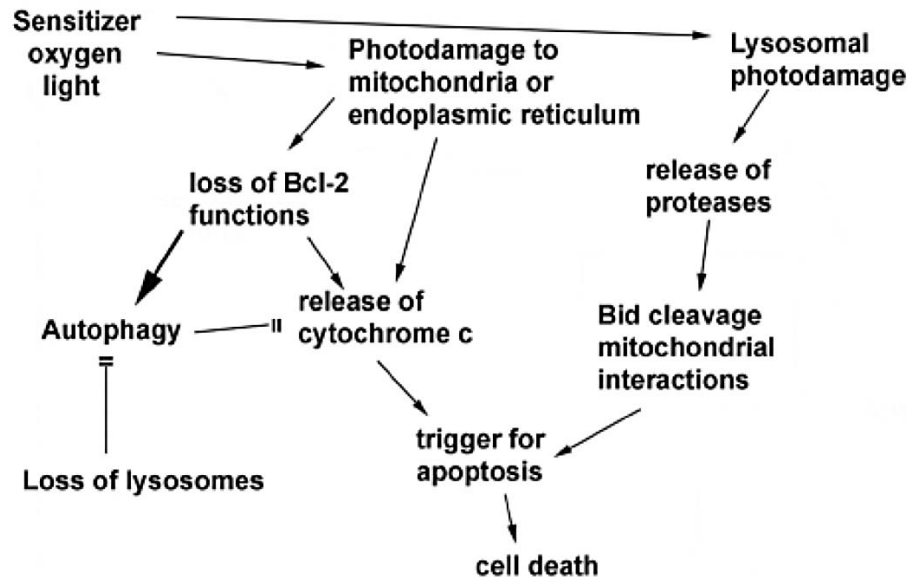
Figure 2.6: Pathways showing photodamage to mitochondria, lysosomes or ER resulting in cell death via apoptosis (Kessel 2015).

2.2.4 PDT and breast cancer

PDT is one of the alternative methods for treatment cancers. Use of PDT to treat recurrent breast carcinoma and chest wall metastasis of breast cancer has been studied, but is considered an underutilized modality (Dougherty, Lawrence et al. 1979, Mang, Allison et al. 1998, Allison, Mang et al. 2001, Dimofte, Zhu et al. 2002). In a study, fourteen patients with more than 500 metastatic lesions of breast cancer were treated with PDT. Patients were administered photosensitizer photofrin (0.8 mg/kg) intravenously and light treatment at 630 nm

from a diode laser at a total light dose of 150 to 200 J/cm2 after 48 hours. All patients showed

tumor necrosis and 9 patients showed complete response (Cuenca, Allison et al. 2004). In

another phase I study, 15 patients were treated with ultra low irradiance (starting at 100 J/cm^2)

continuously over 24 hours but later the light dose was reduced to 50 J/cm^2 (Rogers 2012). Two

patients had complete tumor response and 9 patients showed a partial response to treatment.

Moreover no adverse reaction at the control site and ulceration of the normal skin was seen at 24

hours after treatment. Breast cancer is known to metastasize to bones and PDT on preclinical

murine model of breast cancer metastasis to vertebrae showed that response to PDT was

dependent on both drug dose and light dose (Burch, Bisland et al. 2005, Akens, Yee et al. 2007,

Akens, Hardisty et al. 2010). Recent studies from Hu's group have shown that factor VII-

targeted PDT is an effective treatment for chemoresistant breast cancer (Hu, Rao et al. 2010,

Duanmu, Cheng et al. 2011, Hu, Rao et al. 2011). They have also shown that factor VII-targeted

PDT can selectively kill angiogenic vascular endothelial cells and breast cancer cells *in vitro* and

inhibit tumor growth in mice models (Hu, Rao et al. 2010, Hu, Rao et al. 2011).

2.2.5 Combination PDT

The first study in which two photosensitizers were combined (combination PDT) was

done in 1996 and evaluated the efficacy of BPD and the photosensitizer EtNBS in a mouse

sarcoma model (Cincotta, Szeto et al. 1996). This study showed that combination of these

photosensitizers led to an enhanced synergistic effect when lysosomes were targeted before

mitochondria. Histology of tumor mass 24 hours post-PDT showed almost complete destruction

of tumor without extravasation of red blood cells and damage to normal skin. More recent

literature has shown that treating with two photosensitizers significantly increases cell death

(Villanueva, Stockert et al. 2010, Acedo, Stockert et al. 2014, Kessel and Reiners 2014). A

combination of photosensitizers: zinc (II)-phthalocyanine (ZnPc) and TMPyP on 2D models of

Hela, HaCaT and MCF-7 cell lines, showed that these cells died by apoptosis at dose of 2.4 J/cm^2 and by necrosis at dose of 3.6 J/cm^2 suggesting that mechanism of cell death is dependent on PDT dose (Acedo, Stockert et al. 2014). Additionally, a significant dose-dependent reduction of tumor volume was observed in subcutaneously transplanted amelanotic melanomas in mice after combination PDT treatment (Acedo, Stockert et al. 2014). In another study from the Kessel laboratory the combination of BPD and NPe6 promoted cell death via apoptosis in monolayer cultures of 1c1c7 murine hepatoma cells (Kessel and Reiners 2014). This study also showed that a synergistic response was seen when lysosomes were targeted (using NPe6) before mitochondria (using BPD) and an additive response was seen when mitochondria were targeted before lysosomes. All these studies have shown that the combination of two photosensitizers is more effective in photokilling of tumor cells than is one photosensitizer.
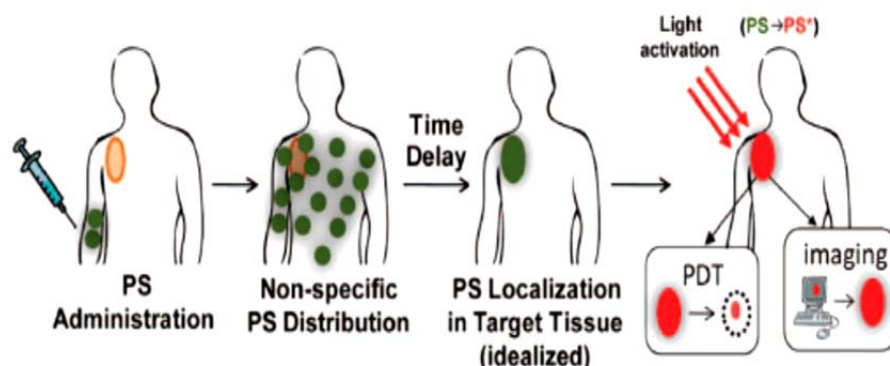
Figure 2.7: Schematic showing sequence of steps for PDT treatment. Photosensitizer is administered systemically and allowed to distribute throughout the body. After an appropriate time interval the photosensitizer preferentially accumulates in the target tissue and is activated by light. Following activation by light at the target location, reactive oxygen species are formed leading to cytotoxic effect (Celli, Spring et al. 2010).

2.2.6 Use of 3D models for PDT

Currently, *in vitro* preclinical models are being developed that can better predict drug responses and success in clinical trials. Some of the first 3D models for modeling of normal breast and breast cancer were developed in the laboratory of Dr. Mina Bissell (Howlett and

Bissell 1993, Bissell, Weaver et al. 1999, Weaver and Bissell 1999, Weigelt, Ghajar et al. 2014). These models utilized reconstituted basement membrane matrix produced from the Engelbreth-Holm-Swarm tumors of mice [commercially available as Matrigel (Corning Life Sciences) or Cultrex (Trevigen)]. These 3D models were found to recapitulate cell-cell and cell-matrix interactions. Non-malignant cells form acini similar as those present in the mammary gland *in vivo* and these acini are functional as they produce milk in the presence of lactogenic hormones (Li, Aggeler et al. 1987, Aggeler, Park et al. 1988, Barcellos-Hoff, Aggeler et al. 1989). The 3D models have also been found to be better predictors of responses to drugs and treatments (Mueller-Klieser 2000, Friedrich, Seidel et al. 2009, Shin, Kwak et al. 2013, Unger, Kramer et al. 2014, Antoni, Burckel et al. 2015).

The majority of pre-clinical PDT studies have been done in cells grown in 2D monolayer cultures with some in animal models. Some of the more recent work on PDT from Dr. Tayabba Hasan's group at Harvard has used 3D models of ovarian and pancreatic cancers (Celli, Rizvi et al. 2010, Celli, Spring et al. 2010, Rizvi, Celli et al. 2010, Celli, Solban et al. 2011, Anbil, Rizvi et al. 2013, Rizvi, Anbil et al. 2013, Celli, Rizvi et al. 2014). Studies from the Hasan lab have also shown that BPD-PDT significantly decreases the size of 3D ovarian cancer nodules and synergistically enhances carboplatin efficacy (Rizvi, Celli et al. 2010). Thus 3D models may play an important role in improving treatment planning for PDT in regard to concentration of photosensitizer and PDT dose.

2.3 Apoptosis

Apoptosis is a highly regulated process that occurs in multicellular organisms and takes place the cell destined to die [reviewed in (Wyllie, Kerr et al. 1980, Strasser, O'Connor et al. 2000, Gallaher, Hille et al. 2001, Renehan, Booth et al. 2001, Kerr 2002, Derradji and Baatout 2003, Chowdhury, Tharakan et al. 2006, Elmore 2007, Taylor, Cullen et al. 2008)]. During this

process of cell death neighboring cells are minimally damaged. Apoptosis, also called programmed cell death, was first used by Kerr, Wyllie and Curie in 1972 to describe a cell death mechanism distinguished by morphological and biochemical characteristics (Kerr, Wyllie et al. 1972, Kerr 2002). Apoptosis normally occurs during important processes such as development, aging, cell cycle regulation, maintenance of homeostasis (King and Cidlowski 1998, Renehan, Bach et al. 2001, Renehan, Booth et al. 2001, Kerr 2002, Opferman and Korsmeyer 2003). Apoptosis is an evolutionary conserved biochemical process that is dependent on ATP as source of energy. Apoptosis can be induced by a variety of physiological and pathophysiological stimuli, such as tumor necrosis factor (TNF alpha) (Ashkenazi 2002), DNA damage (Gentile, Latonen et al. 2003), ultraviolet light (Gentile, Latonen et al. 2003, Zhang, Xing et al. 2009), and cytotoxic drugs (Solary, Droin et al. 2000). Deregulation of the apoptotic pathway results in pathological conditions such as cancer, autoimmune diseases, and neurodegenerative diseases (Thompson 1995, Hanahan and Weinberg 2000).

Apoptosis is known to occur by an extrinsic or an intrinsic pathway [Figure 2.8, reviewed in (Gallaher, Hille et al. 2001, Derradji and Baatout 2003, Chowdhury, Tharakan et al. 2006, Moffitt, Martin et al. 2010, Ola, Nawaz et al. 2011)]. The two pathways have different stimuli but converge to conclude the process. The intrinsic pathway is also known as the mitochondrial pathway or stress pathway and is activated by genomic and metabolic stress, unfolded proteins, mitochondrial membrane permeabilization, and release of pro-apoptotic proteins such as Bid and Bax into the cytoplasm. Disruption of the mitochondrial membrane potential leads to cytochrome c release (Kluck, Bossy-Wetzel et al. 1997, Zhivotovsky, Orrenius et al. 1998). Cytochrome c plays a key role in this pathway leading to formation of an apoptosome by interaction of cytochrome c with the apoptotic protease-activating factor (Apaf1) and deoxyadenosine triphosphate (dATP) (Li, Nijhawan et al. 1997, Riedl and Salvesen 2007, Hu,

Wu et al. 2014, Zamaraev, Kopeina et al. 2015). The apoptosome recruits initiator caspase 9, which gets activated after proteolytic cleavage following dimerization (Salvesen and Dixit 1997, Chowdhury, Tharakan et al. 2008). On the other hand, the extrinsic pathway involves the binding of the extracellular ligands (FAS-L and TNF-alpha L) to trans-membrane death receptors (FAS and TNF-alpha) (Chen and Goeddel 2002, Wajant 2002, Ihnatko and Kubes 2007, Brint, O'Callaghan et al. 2013). After this interaction, the receptor trimerizes and death adaptor molecules are recruited to the cytoplasmic side. Fas recruits Fas-associated death domain protein (FADD) and TNF-alpha receptor recruits TNF-R1-associated death domain protein (TRADD), which in turn recruits FADD (Ashkenazi 2002, Ola, Nawaz et al. 2011). This further leads to formation of a death-inducing signaling complex (DISC) that consists of the receptor, its ligand, the initiator caspase-8 (or caspase-10), and other co-regulators and co-factors [reviewed in (Strasser, O'Connor et al. 2000, Chen and Goeddel 2002, Wajant 2002, Zamaraev, Kopeina et al. 2015)]. Once initiator caspases are activated via either intrinsic or extrinsic pathway, a catalytic cascade begins resulting in activation of the executioner caspases i.e. caspases 3, 6 and 7 (Salvesen and Dixit 1997).

Many substrates for activated executioner caspases are known and the list is growing. The substrates are broadly classified as cytoplasmic proteins (such as actin, β-catenin, keratin 18), nuclear proteins (such as lamins A and B; lamin B receptor, RNA-binding and ribonucleoprotein-associated proteins), DNA metabolism and repair proteins (such as PARP, DNA topoisomerases, RNA-polymerase), protein kinases (such as PKC, MAPK, ERK, Akt), signal transduction pathway proteins (such as cytokines, phospholipases) and cell cycle proteins (such as p21, p27) [(Luthi and Martin 2007), reviewed in (Earnshaw, Martins et al. 1999, Nicholson 1999, Chowdhury, Tharakan et al. 2008)].

The breakdown of cytoplasmic and nuclear proteins by activated executioner caspases results in certain morphologic features that are associated with apoptosis (Kerr, Wyllie et al. 1972, Wyllie, Kerr et al. 1980, Kerr 2002). During early stages of apoptosis cells become smaller in size (cell shrinkage), the cytoplasm becomes dense and chromatin condensation takes place (pyknosis). Pyknosis is followed by karyorrhexis or fragmentation of nuclei. In later stages of apoptosis, plasma membrane blebbing takes place, the cell fragments and separates into apoptotic bodies containing cytoplasm, cellular organelles and fragments of nuclei enclosed in plasma membrane. These apoptotic bodies are either phagocytosed by macrophages or taken up by neighboring cells for recycling of the contents.
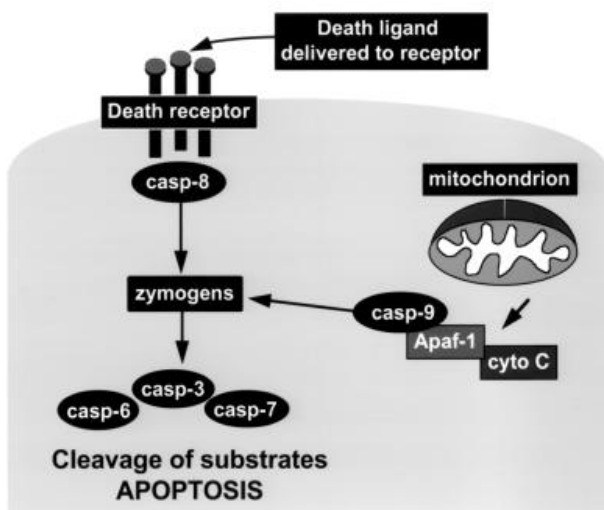
Figure 2.8: Schematic diagram of apoptosis. Cell death via extrinsic pathway takes place by a direct binding of receptors and ligands at the cell surface resulting in activation of initiator caspase-8 (casp-8), which then activates executioner caspases (casp-3, -6 and/or -7). Alternatively for cell death via intrinsic pathway, damage to the genome or radiation causing mitochondrial damage leads to, release of cytochrome c from mitochondria and formation of apoptosome that recruits and activates caspase 9. Activated caspase 9 further results in the activation of executioner caspases (casp-3, -6 and/or -7). (Salvesen and Dixit 1999)

Apoptosis is essential to maintain homeostasis and for the removal of old, damaged or infected cells from the body. Excessive or too little apoptosis is associated with diseases such as atrophy and cancer, respectively. Most drugs currently used in anti-cancer therapy kill target cells by induction of apoptosis, either by the extrinsic or intrinsic pathways.

CHAPTER 3

MATERIALS AND METHODS

3.1 Materials

Dulbecco's Modified Eagles Medium/Ham's F-12, hydrocortisone, insulin from bovine pancreas and dimethyl sulfoxide (DMSO) were obtained from Sigma-Aldrich. Phenol red-free mammary epithelial cell growth medium (MEGM), composed of mammary epithelial basal medium and MEGM SingleQuot kit supplements and growth factors and MycoZap Plus-CL, was procured from Lonza. Fetal bovine serum (FBS) was purchased from Hyclone; epithelial growth factor (EGF) from R&D Systems; and reconstituted basement membrane (rBM, reduced growth factor Cultrex[TM]) from Trevigen. LIVE/DEAD kits, Hoechst 33342, L-Glutamine and trypsin-EDTA were purchased from Life Technologies.

3.2 Tissue Culture

The SUM149 cell line (a kind gift from Dr. Steven Ethier, MUSC) was used as a model of human triple negative inflammatory breast cancer (Table 3.1); cells were maintained in Hams F-12 medium supplemented with 5% FBS, 5µg/ml Insulin, 1µg/ml Hydrocortisone and 1% MycoZap plus-CL. The human invasive TNBC breast cancer cell lines, MDA-MB-231 and Hs578T, were purchased from ATCC. MDA-MB-231 cells were cultured and maintained in medium composed of DMEM supplemented with 10% FBS, 4mM L-glutamine and 1% MycoZap plus-CL (Table 3.1). Hs578T cells were cultured and maintained in DMEM medium supplemented with 10% FBS, 5µg/ml Insulin, 4mM L-glutamine and 1% mycozap plus-CL (Table 3.1). All cell lines were maintained in T-25 flasks in a humidified incubator with 5% CO_2 at 37 °C. MEGM medium was used for 3D cultures.

Table 3.1. Cell lines used for PDT studies

Name	Breast Cancer Subtype	Morphology in 3D Cell Cultures[a]	References
MDA-MB-231	Triple negative	Stellate	(Cailleau, Young et al. 1974, Neve, Chin et al. 2006, Chavez, Garimella et al. 2010)
Hs578T	Triple negative	Stellate	(Hackett, Smith et al. 1977, Neve, Chin et al. 2006, Chavez, Garimella et al. 2010)
SUM149	Triple negative and Inflammatory	Grape-like	(Forozan, Veldman et al. 1999, Neve, Chin et al. 2006, Chavez, Garimella et al. 2010, Barnabas and Cohen 2013)

a: (Kenny, Lee et al. 2007)

3.3 Generation of 3D Mammary Architecture and Microenvironment Engineering (MAME) Models

A reconstituted basement membrane (rBM) overlay model, developed by Bissell and colleagues (Howlett and Bissell 1993, Bissell, Weaver et al. 1999, Weaver and Bissell 1999), has been modified by Brugge and colleagues for analysis of oncogenesis of human MCF-10A (Debnath, Mills et al. 2002, Debnath and Brugge 2005). Dr. Stephanie Mullins trained in the Brugge laboratory and adapted the model to variants of the MCF-10A non-transformed mammary epithelial line (Mullins, Sameni et al. 2012). The model has been used for multiple breast cancer cell lines by our laboratory (Sameni, Dosescu et al. 2008, Victor, Anbalagan et al. 2011, Sameni, Anbalagan et al. 2012) and was used here for all PDT experiments. To generate the MAME model, glass coverslips (12 mm) placed in 35 mm dishes were coated with 50 µl rBM (Cultrex, Trevigen) and the rBM allowed to gel for 15 minutes at 37 °C. 5000 cells were resuspended in 50 µl MEGM medium, seeded on rBM and incubated at 37 °C for an hour to allow cells to adhere. Then overlay medium i.e. MEGM with 2% rBM was added gently. A schematic of the 3D MAME model is shown in Figure 3.1 (Sameni, Anbalagan et al. 2012). 3D structures were then allowed to form over time. MDA-MB-231 and Hs578T cells were grown in

3D MAME cultures for a period of 3 or 6 days allowing us to study effects of treatment on invasive structures of two sizes (Sameni, Dosescu et al. 2008, Sameni, Anbalagan et al. 2012). SUM149 cells were grown in 3D MAME cultures for 7 days.
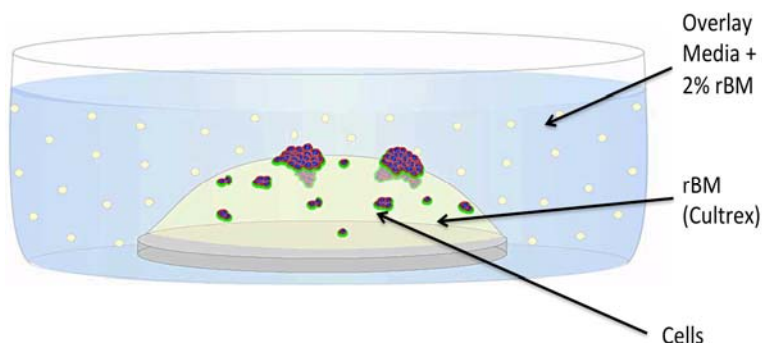
Figure 3.1. Schematic representation of the 3D MAME model. The cartoon illustrates a coverslip placed in a dish and coated with Cultrex. An aliquot of single cells was applied to the coverslip and cells allowed to attach. This was followed by addition of overlay media composed of MEGM medium containing 2% rBM.

3.4. Photodynamic Therapy

A) BPD-PDT

MAME cultures were incubated for 60 minutes at 37 °C with 1.5 μM BPD, washed with PBS and replenished with overlay media. Cells were irradiated using a 700 watt quartz-halogen lamp and an interference filter that confines the irradiation to 690 ± 10 nm, using a power density of 1.5 mW/cm^2. Irradiation was performed for PDT doses ranging from 45 mJ/cm^2 to 540 mJ/cm^2 (corresponding to time period ranging from 30 seconds to 6 minutes). Two additional controls were used: a protocol that results in 100% killing and a dark control (Celli, Rizvi et al. 2014). Following irradiation, samples were placed in an incubator at 37 °C for 18-24 hours before live/dead assays were performed.

B) Combination PDT using BPD and NPe6

SUM149 cells were grown in MAME cultures for 7 days. On day 7, cultures were incubated with 1.5 μM BPD and/or 40 μM NPe6 for 60 minutes. Then cells were irradiated with

light at 690 nm (to initiate photodynamic effects of BPD) and/or at 660 nm (to initiate photodynamic effects of NPe6); see figures for light doses. The sequential treatments are represented as NPe6/BPD when NPe6 was activated before BPD and BPD/NPe6 when BPD was activated before NPe6. Following irradiation, samples were placed in an incubator at 37 °C for approximately 24 hours or 48 hours before live/dead assays were performed.

3.5. Live-dead Assays

The live-dead assay has two components. A dye (calcein AM, CG) that fluoresces green when cleaved by intracellular esterases is used to identify live cells. A second dye, ethidium homodimer-1 (EB), exhibits red fluorescence when incorporated into the DNA of dead cells. Cells were incubated with assay reagents for 30 minutes at 37 °C, washed once with warm PBS, then warm MEGM media was added and cells were imaged live on a Zeiss 510 LSM META NLO confocal microscope using a 20X water-immersion objective. Z-stacks (Figure 3.2) through the entire structures were captured for 16 contiguous fields (Figure 3.3) in at least three separate experiments. The images were reconstructed in 3D using Volocity software and are represented here as either extended depth of focus images (*en face* view) or volume rendered 3D images tilted at a 45° angle (Figure 3.4). Cell viability was calculated by quantifying the green and red fluorescence intensities as described by Celli et al. (Celli, Rizvi et al. 2014) and converted to percentage of dark controls and plotted against the PDT dose.

Cell viability was then calculated using the formula (Celli, Rizvi et al. 2014):

$$Viability = \frac{\overline{CG}}{\overline{CG} + \phi \overline{EB}} \quad \text{where,} \quad \phi = \frac{CG_{NT} - CG_{TK}}{EB_{TK} - EB_{NT}}$$

Here, CG bar and EB bar represent the mean relative intensities of CG (live) and EB (dead) fluorescence signals respectively. The subscripts NT and TK are the mean values for non-treated and total-killing controls. The scaling factor ϕ rescales all values to internal non-treated and

total killing controls and further corrects for inevitable variability in imaging parameters and minor instrumentation drift across evaluation timepoints (Celli, Rizvi et al. 2010, Rizvi, Celli et al. 2010, Celli, Rizvi et al. 2014).
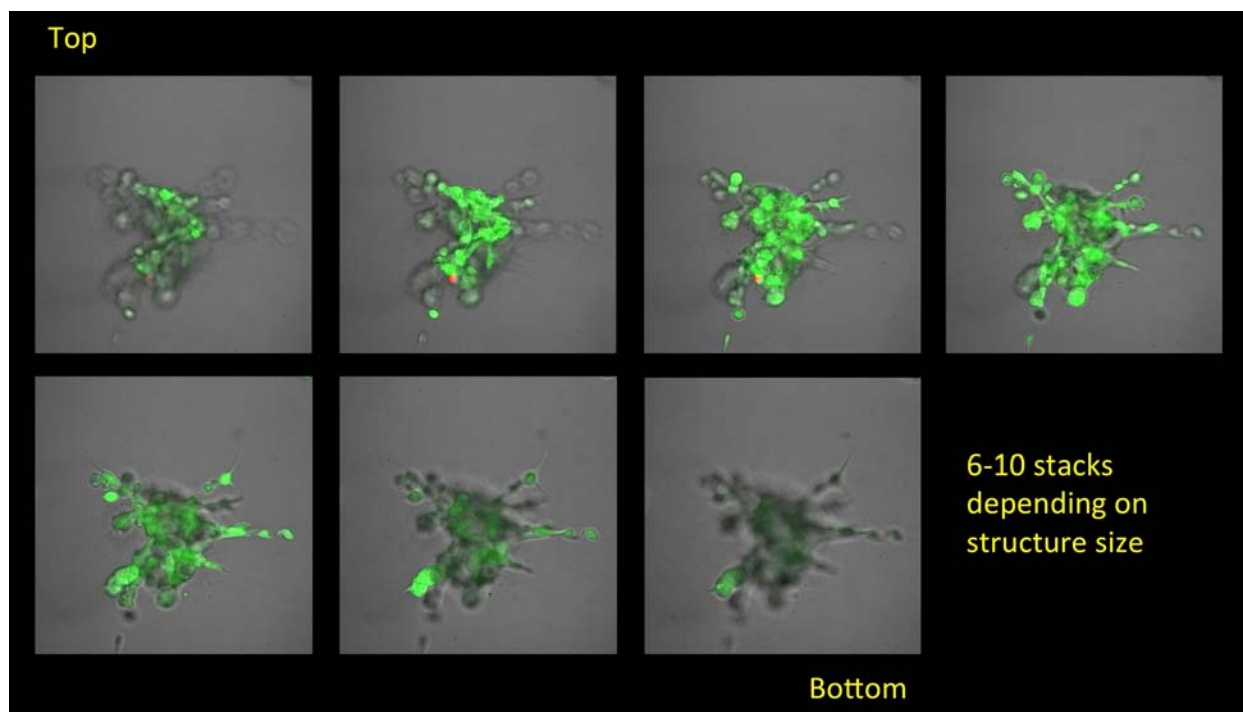
Figure 3.2. An example of a z-stack image of an MDA-MB-231 structure taken through the entire depth of the structure. These images show cells labeled with Calcein (green) overlaid with differential interference contrast (DIC) images.

3.6 Viral Transduction of SUM149 Cells

50,000 cells were seeded in a 6-well dish and allowed to attach. 70% confluent cells were transduced with cignal RFP (Qiagen) viral particles (20 µl) resuspended in 300 µl antibiotic-free media containing 6 µg Sure-Entry reagent (Qiagen) and the dish was placed back in a 37 °C humidified incubator with 5% CO_2. On the next day, the cells were washed with PBS twice and complete media added. Cells were then passaged to a T-25 flask and subsequently to a T-75 flask, and flow-sorted to separate cells that express RFP. The sorted cells were then maintained using the same protocols as for the wild-type SUM149 cell line.

Top
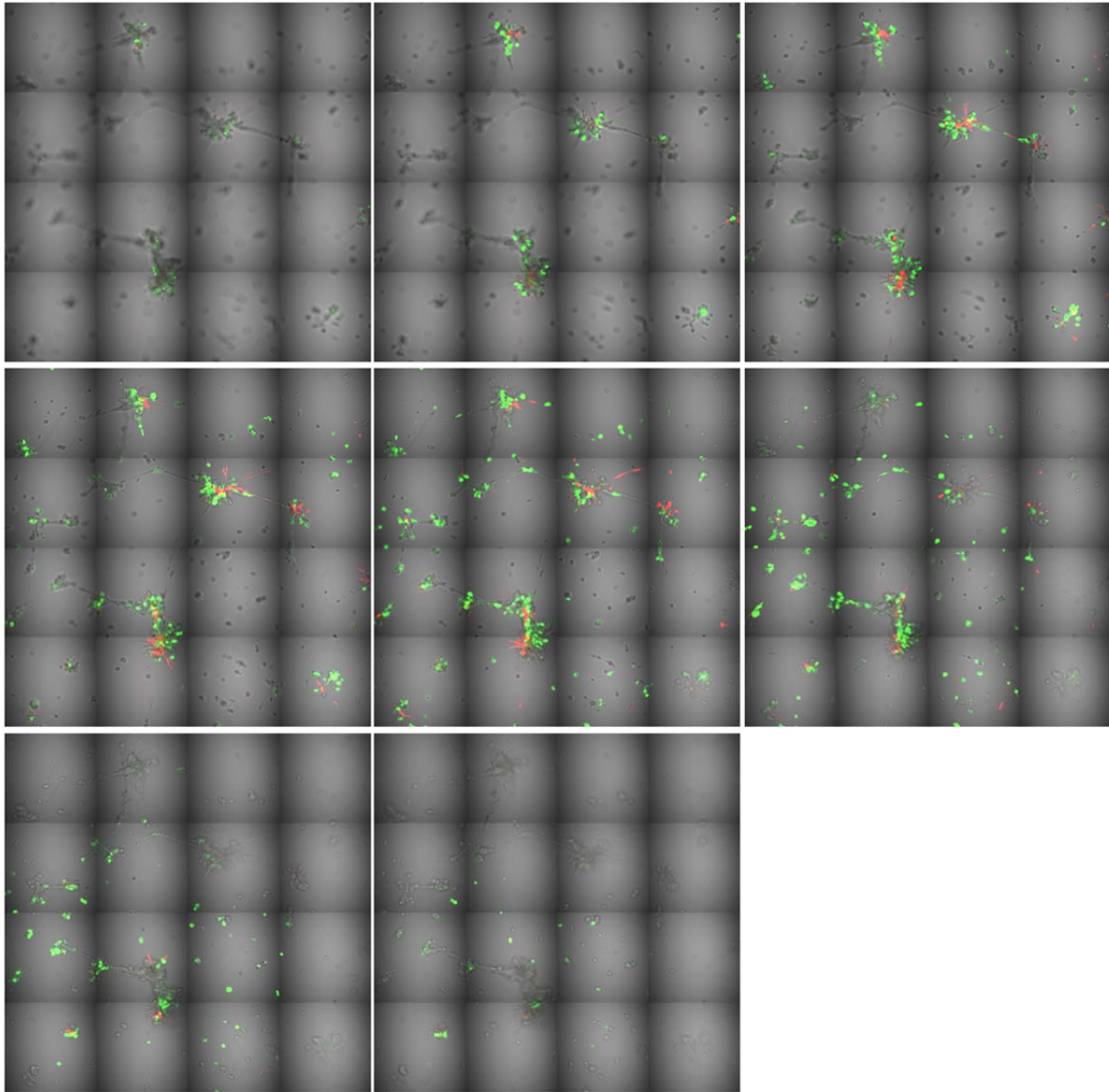
Bottom

Figure 3.3: An example of a z-stack through 3D MAME structures for 16-contiguous fields. These images show optical sections through the depth of MAME structures and are an overlay of differential interference contrast (DIC) images and cells labeled with CG (green) and EB (red).
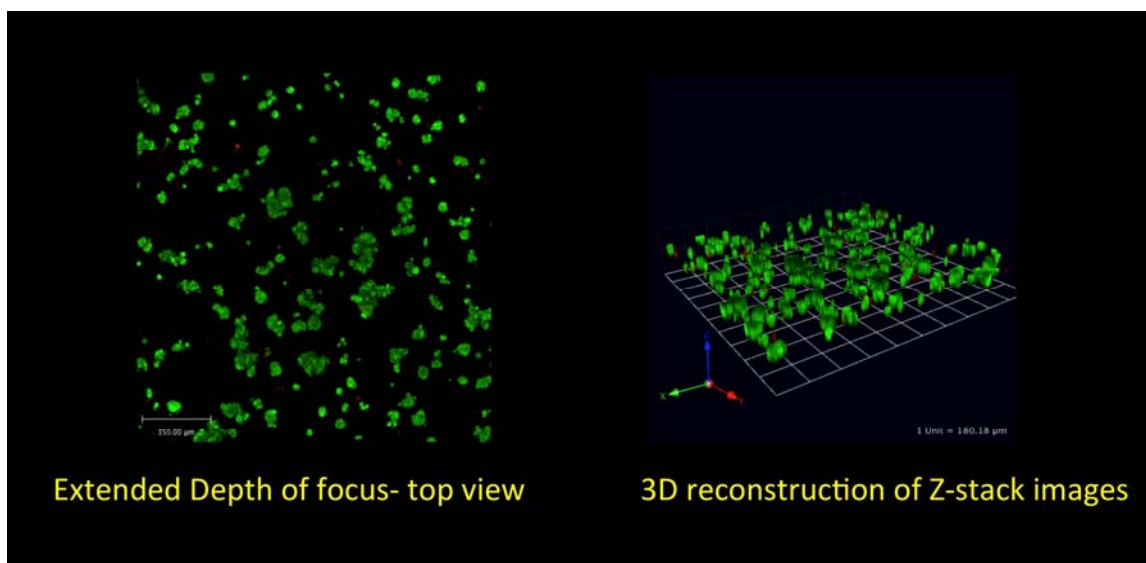
Figure 3.4. Examples of post-processing and representation of 16-contiguous fields and z-stacks images. Panel A shows extended depth of focus (also called an *en face*) view and Panel B shows volume rendered 3D reconstruction of images tilted at an angle of 45 °.

3.7 Methods for Assessing Apoptosis

A) Cleaved caspase-3 immunofluorescence

SUM149 cells were grown in MAME cultures and treated on day 7 using the sequential NPe6/BPD PDT protocol at a dose of 22.5 mJ/cm^2. MAME structures were then fixed at 6, 12 and 24 hours post-PDT using 4% paraformaldehyde for 20 minutes, washed 3 times with PBS and permeabilized using 0.2% Triton X-100 for 5 minutes followed by quenching three times with 0.1 M glycine for 10 minutes. Non-specific binding sites were then blocked with 0.2% BSA for 60 minutes. Samples were incubated overnight at 4 °C with a 1:400 dilution of cleaved caspase-3 antibody (Cell Signaling Technology). The samples were then washed four times with PBS for 10 minutes each. Cells were then treated with a 1:1000 dilution of AlexaFluor 488 (Life Technologies) for an hour at room temperature, washed four times with PBS for 10 minutes each, fresh PBS with Hoechst was added and the samples were imaged on the Zeiss 510 LSM META NLO confocal microscope using a 40X water-immersion objective. The z-stack images were quantified to determine the intensity of cleaved caspase-3 and reconstructed in 3D using

Volocity software.

B) Nuclear-staining with Hoechst

SUM149 cells were grown in MAME cultures for 7 days and treated with the sequential NPe6/BPD-PDT protocol at a dose of 22.5 mJ/cm^2; 24 hours later a 1:1000 dilution of Hoechst dye HO33342 was added for 15 minutes. The medium was replaced and MAME structures were imaged live on a Zeiss 510 LSM META NLO confocal microscope using a 40X water-immersion objective. The images were reconstructed in 3D using Volocity software to show extended depth of focus (*en face* view).

3.8 Live Cell Proteolysis Assay

A detailed protocol for the live cell proteolysis assay has been published (Jedeszko, Sameni et al. 2008). Briefly, glass coverslips in 35-mm dishes were coated with 45 μl of Cultrex containing 25 mg/ml of DQ-collagen IV and placed in a 37 °C incubator for 10 min to allow solidification. 5000 cells were seeded on top of the Cultrex and incubated at 37 °C for 30-60 min until adherent, followed by addition of culture media containing 2% rBM. Media were changed after four days. For inhibitor studies, 10 μM CA074Me, 10 μM E64d, 10 μM PD150606 or DMSO was added to overlay media on day 7 (these inhibitors are in routine use in the Sloane laboratory). Cells were washed thoroughly in phosphate buffered saline (PBS) followed by addition of MEGM media. All experiments were imaged on day 8 with a Zeiss LSM 510 META NLO confocal microscope using a 20X water-dipping objective to capture the 3D structures. Volume of degradation of DQ collagen was assessed using Volocity software.

3.9 Statistical Analysis

Statistical significance was determined using GraphPad Prism 6.0 software. Experiments were analyzed using a two-tailed, unpaired Student's T-test or one-way ANOVA as stated for each experiment.

CHAPTER 4

EFFICACY OF PDT IN PHOTOKILLING IN 3D MAME MODELS OF TNBC AND IBC CELLS

Rationale

There is an unmet need for therapies against TNBCs and IBCs. The dermal metastases of IBC and the chest wall metastases of TNBC are in locations that are accessible to the light needed to activate photosensitizers. Pre-clinical PDT studies have mainly used cell lines cultured in monolayers on plastic (in 2-dimensions). Cells cultured in monolayers do not recapitulate the *in vivo* architecture (e.g. cell-cell and cell-matrix interactions) that is critical for accurately modeling tumor growth and response to therapies. In contrast, cells grown in 3D models do recapitulate cell-cell and cell-matrix interactions (Weigelt and Bissell 2008, Eke and Cordes 2011). Moreover, 3D models have been able to predict resistance to chemo- and radiation therapies, something that is not possible for monolayer cultures (Li, Chow et al. 2010, Storch, Eke et al. 2010, Celli, Solban et al. 2011, Chen, Wang et al. 2014).

PDT that targets mitochondria induces immediate release of cytochrome c thus activating caspase cascade and the apoptotic pathway (Granville, Carthy et al. 1998). PDT that targets lysosomes induces release of lysosomal proteases into the cytoplasm and causes damage to other intracellular organelles (Kessel and Poretz 2000, Reiners, Caruso et al. 2002). Combination PDT using photosensitizers targeting lysosomes and mitochondria sequentially promotes photokilling via apoptosis in 2D murine hepatoma model (Kessel and Reiners 2014). We suggest that combination PDT may have the potential to eradicate chest wall metastases of TNBCs and dermal metastases of IBC, i.e., sites that would be accessible to this therapy. We propose to use 3D models of TNBC and IBC to determine the efficacy of PDT including combination PDT targeting lysosomes and mitochondria. Such a combination therapy protocol has not yet been

tested in 3D cultures yet.

Specific Aim 1: Determine if PDT is more effective in the photokilling of MAME structures of TNBC and IBC when lysosomes and mitochondria are sequentially targeted as compared to targeting only mitochondria.

Hypothesis: Combination PDT will be more efficacious in photokilling as two critical organelles, lysosomes and mitochondria, will be damaged.

Results

4.1 Optimization of BPD Concentration and Incubation Time in 3D MAME Structures

4.1.1 BPD concentration and uptake

BPD was used as the photosensitizer in our experiments; its excitation and emission spectrum is in the UV and far-red region, respectively. We used MDA-MB-231 human breast carcinoma cells grown in MAME models for optimization as they are easy to culture in 3D and are in routine use in the Sloane laboratory. Cultures were incubated for 60 minutes with BPD at concentrations from 0.5 µM to 2.0 µM. Differential interference contrast (DIC) images were taken to illustrate the morphology of the 3D structures at different concentrations of BPD (Figure 4.1 A-E). The fluorescent images represent autofluorescence of BPD at the different concentrations (Figure 4.1 A'-E'). We confirmed that BPD was able to penetrated entire 3D structures and accumulated in the cells in a dose dependent manner as indicated by the increase in red fluorescence. As the intensity of fluorescence was similar at BPD concentrations of 1.5 µM and 2.0 µM, we selected the lower concentration of 1.5 µM for further experiments.
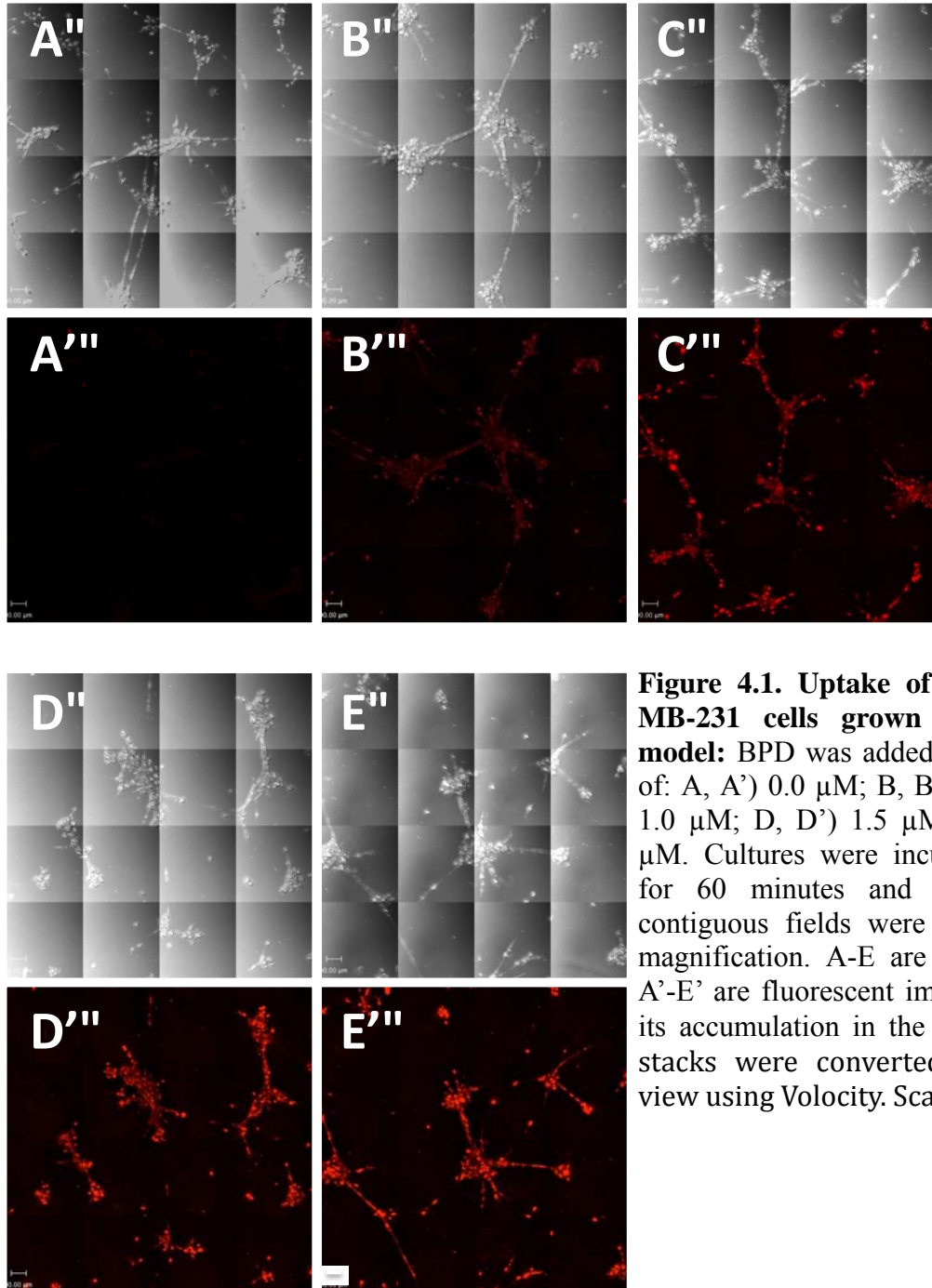
Figure 4.1. Uptake of BPD by MDA-MB-231 cells grown in 3D MAME model: BPD was added at concentrations of: A, A') 0.0 µM; B, B') 0.5 µM; C, C') 1.0 µM; D, D') 1.5 µM; and E, E') 2.0 µM. Cultures were incubated with BPD for 60 minutes and Z-stacks for 16 contiguous fields were captured at 20X magnification. A-E are DIC images and A'-E' are fluorescent images of BPD and its accumulation in the 3D structures. Z-stacks were converted to an *en face* view using Volocity. Scale bar= 80 µm

4.1.2 Incubation time

MDA-MB-231 cells were grown in MAME cultures for 3 days allowing 3D structures to form and then incubated with 1.5 µM BPD for different time periods (Figure 4.2). We found that 1.5 µM BPD penetrates into the structures within the first 15 minutes of incubation as

indicated by the low intensity of red signal (Figure 4.2 A). At longer times of incubation with BPD, accumulation of BPD in the 3D structures is greater as shown by the increases in red fluorescence with time. For all future experiments we used a 60-minute incubation time (Figure 4.2 C). This incubation time is comparable to that used by the Hasan lab at Boston in 3D models of ovarian cancer (Celli, Spring et al. 2010, Anbil, Rizvi et al. 2013).
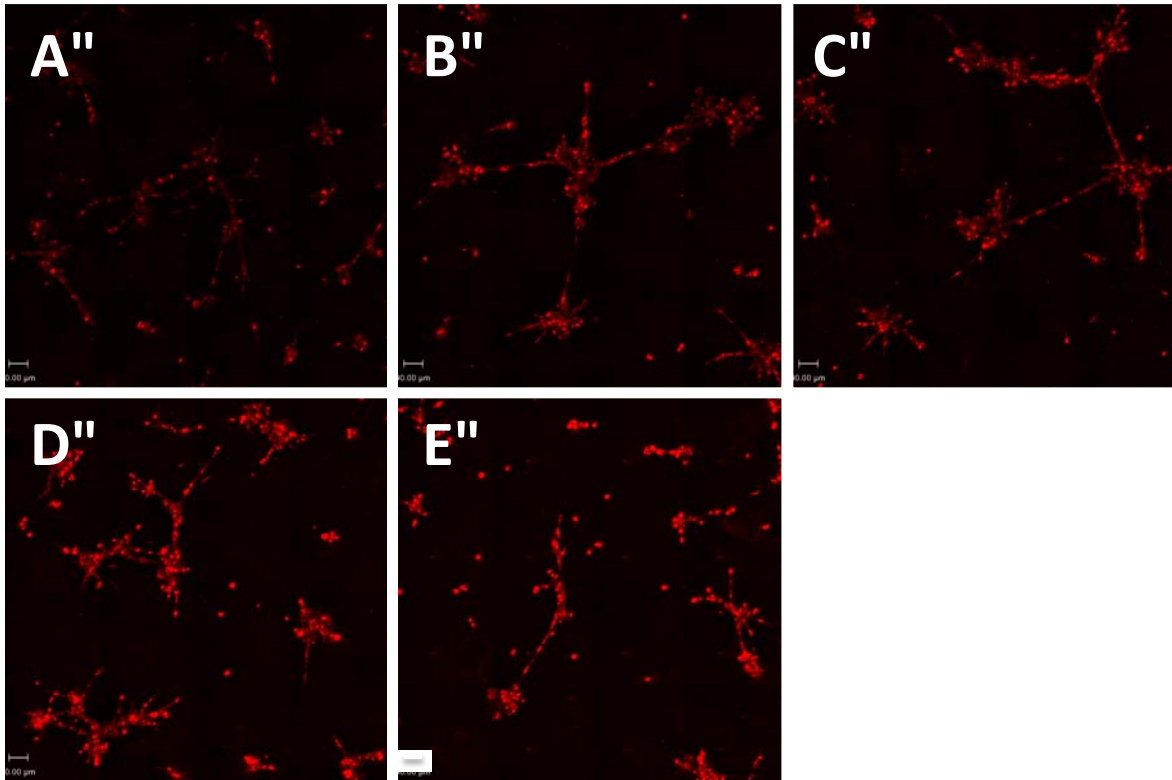
Figure 4.2. Time dependent uptake of BPD by MDA-MB-231 cells grown in MAME model: Cultures were incubated with 1.5 µM BPD for different time periods: A) 15 min; B) 30 min; C) 60 min; D) 120 min; and E) 150 min. Z-stacks were captured at 20X magnification. Images were processed using Volocity software and are presented as extended depth of focus. Red represents fluorescence of BPD and its accumulation in the 3D structures. Scale bar = 80 µm

4.2 Dose Response of MAME Structures of Triple Negative Breast Cancer to Photokilling by BPD-PDT

4.2.1 3 day MDA-MB-231 MAME structures

We utilized a MDA-MB-231 MAME model to assess the dose-response to a PDT

protocol in which mitochondria are targeted using BPD (Figure 4.3, Table 4.1). Approximately 50% of 3D structures were killed at a 45 mJ/cm^2 BPD-PDT dose. When we increased the duration of irradiation, we observed a significant decrease in cell viability resulting in 60% cell death after 90 mJ/cm^2 (one minute), 91% cell death after 180 mJ/cm^2 (two minutes), 98% cell death after 360 mJ/cm^2 (4 minutes) and 99% cell death after 540 mJ/cm^2 (six minutes) of treatment. A decrease in live MAME structures (green) and a corresponding increase in dead MAME structures (red) with increased dose of PDT were observed (Figure 4.3). Thus there was a significant increase in death of TNBC MDA-MB-231 MAME structures in response to escalating the BPD-PDT dose.

To confirm that light alone does not affect MAME structures, we performed PDT at a dose of 540 mJ/cm^2 in the absence of photosensitizer. The representative image shown in Figure 4.4 illustrates that light does not result in photokilling of MAME structures in the absence of a photosensitizer (see green cells).

Table 4.1. Viability (% Control) for 3 day MAME cultures of MDA-MB-231 cells

BPD-Dose (mJ/cm^2)	45	90	180	360	540
Viability(%Control)	49 ± 5	39 ± 8	9 ± 7	2 ± 1	1 ± 2

A
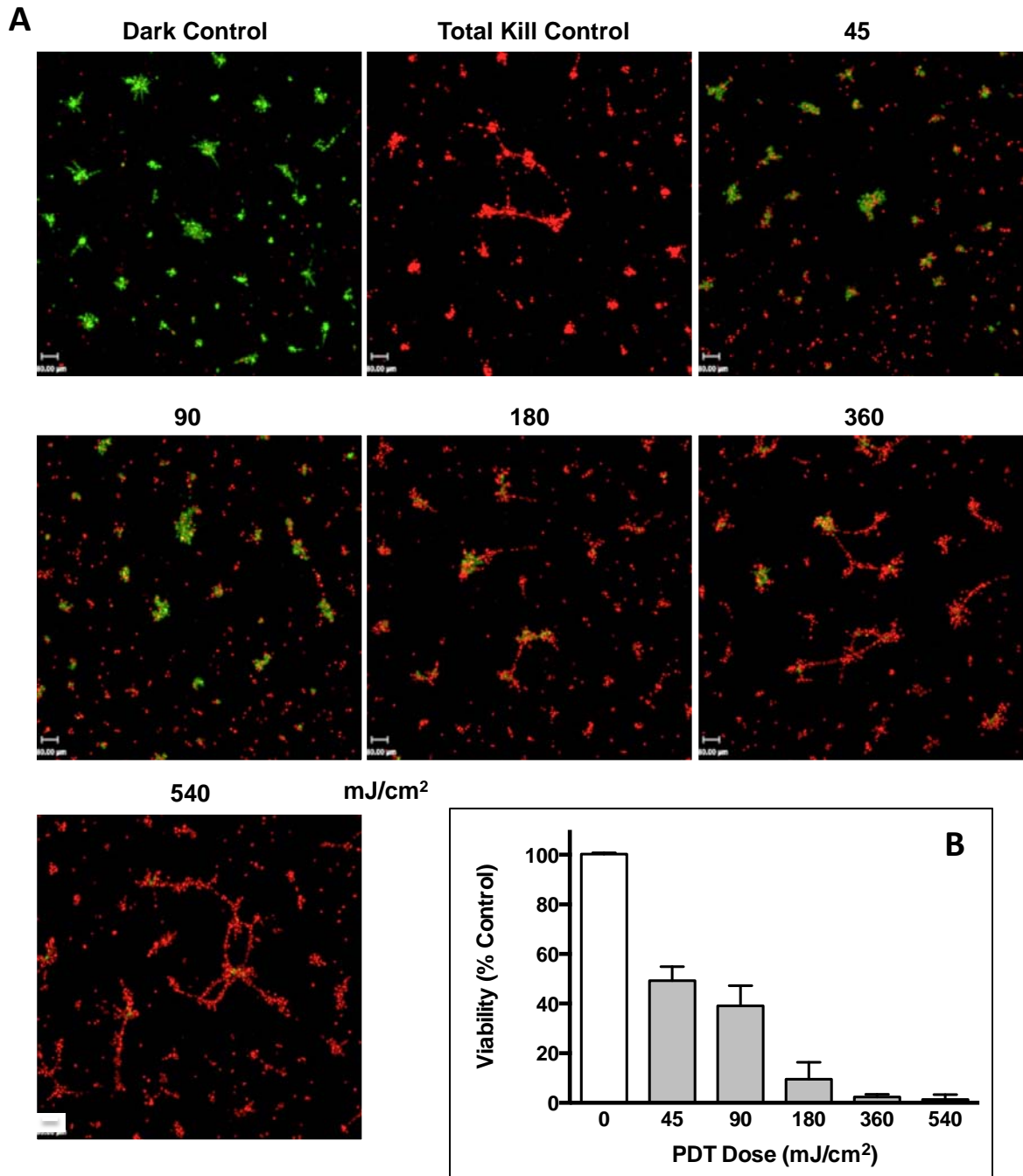
Figure 4.3: MDA-MB-231 cells grown in MAME model for 3 days exhibited a significant dose-response to photokilling by BPD-PDT. Representative live/dead images of optical sections through the 3D structures were captured for 16 contiguous fields and shown in an *en face* view (A). Images were taken 24 hours after PDT with 1.5 µM BPD and show live cells (green, calcein AM) and dead cells (red, ethidium homodimer-1) for non-treated dark control and BPD-PDT treated samples as indicated in the Figure; scale bar = 80 µm. Intensities of red and green fluorescence were used to calculate viability and plotted against PDT dose (B) p-value < 0.0001, one-way ANOVA; n=4, mean ± SD.
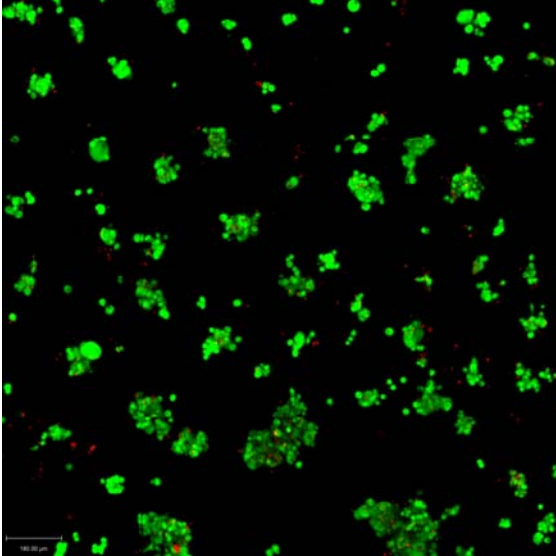
Figure 4.4: Proof of principle confirming that cells grown in MAME model are not photokilled by light in the absence of photosensitizer. Live/dead images of optical sections through the 3D structures were captured for 16 contiguous fields and shown in an *en face* view. Images were taken 24 hours after PDT in the absence of BPD and show live cells (green, calcein AM) and dead cells (red, ethidium homodimer-1).

4.2.2 6 day MDA-MB-231 MAME structures

In the clinics, cancer patients present with tumors of varied sizes. So we next tested if PDT would target larger structures of about 80 microns (formed in 6 day cultures) as compared to structures of less than 50 microns (formed in 3 day cultures). The MDA-MB-231 cells were grown in MAME models for 6 days (Figure 4.5, Table 4.2). Approximately 14% of 6 day 3D structures were killed at a 45 mJ/cm^2 BPD-PDT dose as compared to 50% of 3 day 3D structures. When we increased the duration of irradiation for the 6 day cultures we observed a significant decrease in cell viability resulting in 35% cell death after 90 mJ/cm^2 (one minute), 54% cell death after 180 mJ/cm^2 (two minutes), 74% cell death after 360 mJ/cm^2 (4 minutes) and 86% cell death after 540 mJ/cm^2 (six minutes) of treatment. A decrease in live MAME structures (green) and a corresponding increase in dead MAME structures (red) with increased dose of PDT were observed (Figure 4.5). Thus there was a significant increase in death of 6 day TNBC MDA-MB-231 MAME structures in response to escalating the BPD-PDT dose.
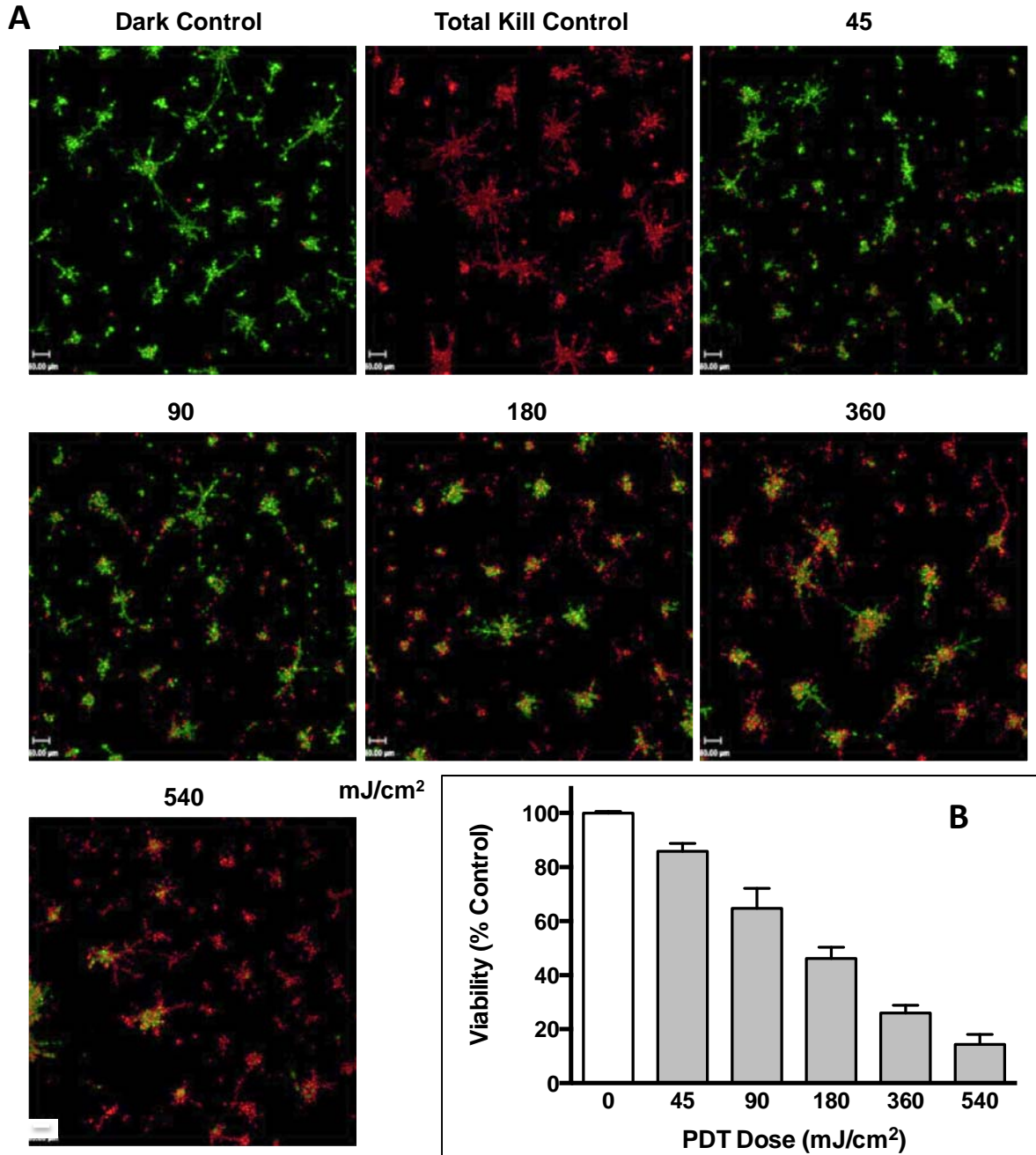
Figure 4.5: Response of 6 day MAME structures of MDA-MB-231 to BPD-PDT: Representative live/dead images of optical sections through 3D structures were captured for 16 contiguous fields and shown in *en face* view (A). Images were taken 24 hours after PDT with 1.5 µM BPD and show live cells (green, calcein AM) and dead cells (red, ethidium homodimer-1) for non-treated dark control and BPD-PDT treated samples; scale bar = 80µm. Intensities of red and green fluorescence were used to calculate viability and plotted against PDT dose (B). p-value < 0.0001, one-way ANOVA; n=6, mean ± SD.

As ~15% of MAME structures of MDA-MB-231 cells were not photokilled by BPD-PDT treatment at a dose of 540 mJ/cm^2, we increased the dose to 620 mJ/cm^2. At the higher dose we observed enhanced photokilling as indicated by an increase in dead structures (red) and a decrease in live structures (green) (Figure 4.6). These data were not quantified as we only tested the effects of the higher dose of 620 mJ/cm^2 once.

Table 4.2. Viability (% Control) for 6 day MAME cultures of MDA-MB-231 cells

BPD-Dose (mJ/cm^2)	45	90	180	360	540
Viability (%Control)	86 ± 3	65 ± 7	46 ± 4	26 ± 3	14 ± 4
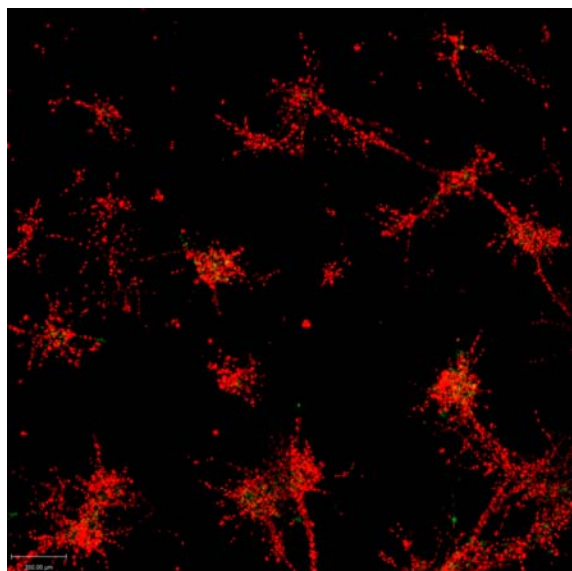
Figure 4.6: Response of MDA-MB-231 6 day MAME structures to BPD-PDT at a dose of 620 mJ/cm^2: Live/dead images of optical sections through the volume of 3D structures were captured for 16 contiguous fields and shown in *en face* view (A). This image taken 24 hours after PDT with 1.5 µM BPD shows primarily dead cells (red, ethidium homodimer-1).

4.2.3 3 day Hs578T MAME structures

To confirm the dose-dependent photokilling effect that was observed using one TNBC cell line i.e. MDA-MB-231, we used another TNBC cell line, Hs578T. The 3D structures formed by Hs578T cells were larger and had more invasive outgrowths (multicellular) than those formed by the MDA-MB-231 cells. Hs578T cells were grown in MAME model for 3 days and then incubated with 1.5 µM BPD for 60 minutes followed by irradiation for 0.5-6 minutes (45-540 mJ/cm^2) (Figure 4.7, Table 4.3). Approximately 50% of 3D structures were killed at a 45

mJ/cm^2 BPD-PDT dose.   When we increased the duration of irradiation, we observed a significant decrease in cell viability resulting in 72% cell death after 90 mJ/cm^2, 20% cell death after 180 mJ/cm^2, 91% cell death after 360 mJ/cm^2 and 93% cell death after 540 mJ/cm^2 of treatment.   A decrease in live MAME structures (green) and a corresponding increase in dead MAME structures (red) with increased dose of PDT were observed (Figure 4.5).   Thus there was a significant increase in death of TNBC Hs578T MAME structures in response to escalating the BPD-PDT dose.

Table 4.3. Viability (% Control) for 3 day MAME cultures of Hs578T cells

BPD-Dose (mJ/cm^2)	45	90	180	360	540
Viability (%Control)	51 ± 1	28 ± 5	20 ± 3	9 ± 6	7 ± 4
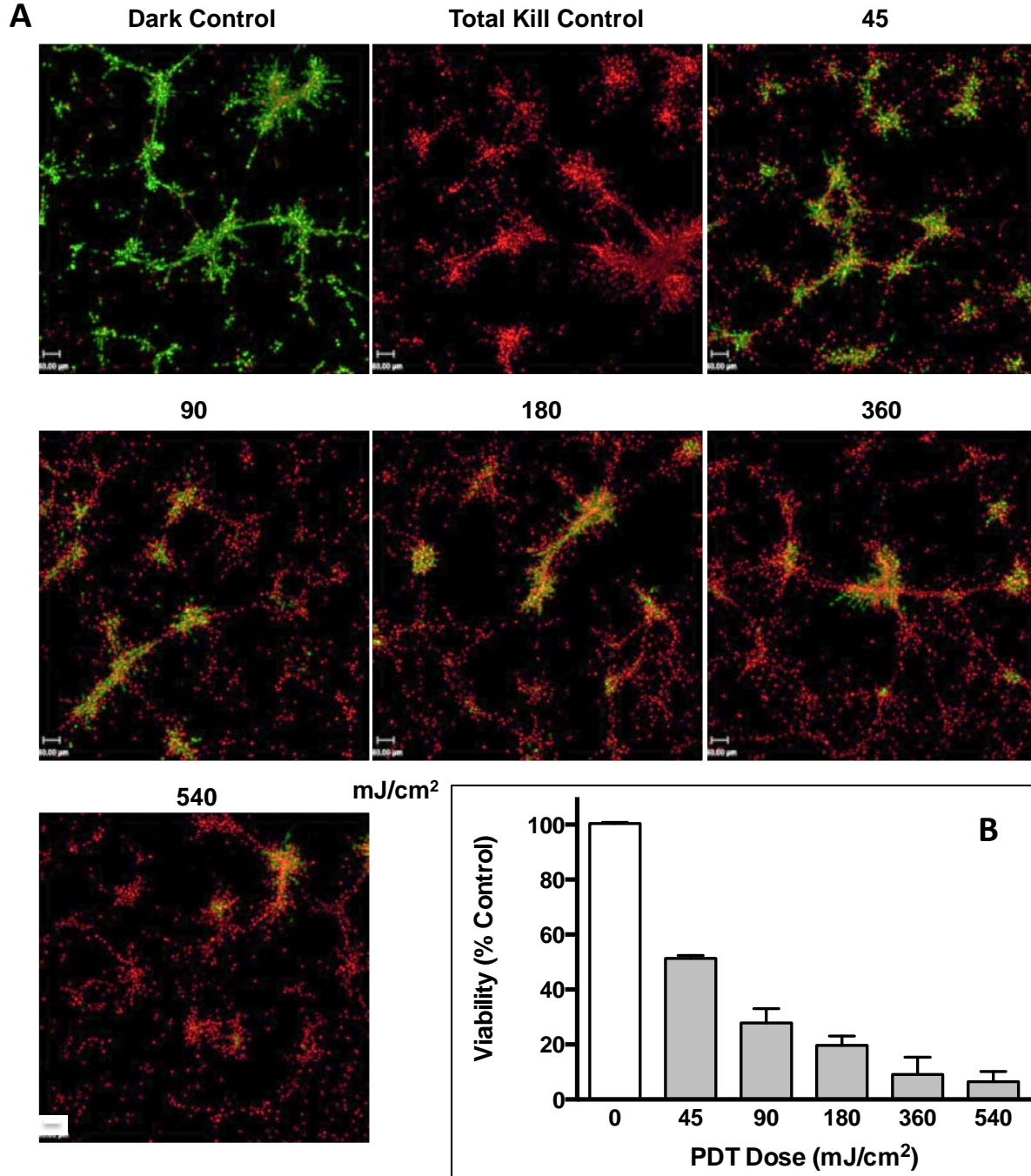
Figure 4.7: Response of Hs578T 3 day MAME structures to BPD-PDT: Representative live/dead images of optical sections through the volume of 3D structures were captured for 16 contiguous fields and shown in *en face* view (A). Images were taken 24 hours after PDT with 1.5 μM BPD and show live cells (green, calcein AM) and dead cells (red, ethidium homodimer-1) for non-treated dark control and BPD-PDT treated samples at multiple doses as indicted in the Figure; scale bar = 80 μm. Intensities of red and green fluorescence were used to calculate viability and plotted against PDT dose (B). p-value < 0.0001, one-way ANOVA; n=4, mean ± SD

4.2.4 6 day Hs578T MAME structures

To confirm the dose-dependent photokilling effect that was observed in the 6 day MAME structures of MDA-MB-231 cells, we grew Hs587T cells for 6 days in MAME cultures. Approximately 20% of 3D structures were killed at a 45 mJ/cm^2 BPD-PDT dose as compared to 50% of 3 day 3D structures (Figure 4.8, Table 4.4). When we increased the duration of irradiation for the 6 day cultures, we observed a significant decrease in cell viability resulting in 34% cell death after 90 mJ/cm^2 (one minute), 53% cell death after 180 mJ/cm^2 (two minutes), 64% cell death after 360 mJ/cm^2 (4 minutes) and 73% cell death after 540 mJ/cm^2 (six minutes) of treatment. A decrease in live MAME structures (green) and a corresponding increase in dead MAME structures (red) with increased dose of PDT were observed (Figure 4.8). Thus there was a significant increase in death of 6 day TNBC Hs578T MAME structures in response to escalating the BPD-PDT dose.

As ~30% of MAME structures of Hs578T cells were not photokilled by BPD-PDT treatment at a dose of 540 mJ/cm^2, we increased the dose to 620 mJ/cm^2. At the higher dose we observed enhanced photokilling as indicated by an increase in dead structures (red) and a decrease in live structures (green) (Figure 4.9). These data were not quantified as we only tested the effects of the higher dose of 620 mJ/cm^2 once.

Table 4.4. Viability (% Control) for 6 day MAME cultures of Hs578T cells

BPD-Dose (mJ/cm^2)	45	90	180	360	540
Viability (%Control)	82 ± 17	66 ± 11	47 ± 11	36 ± 8	27 ± 8
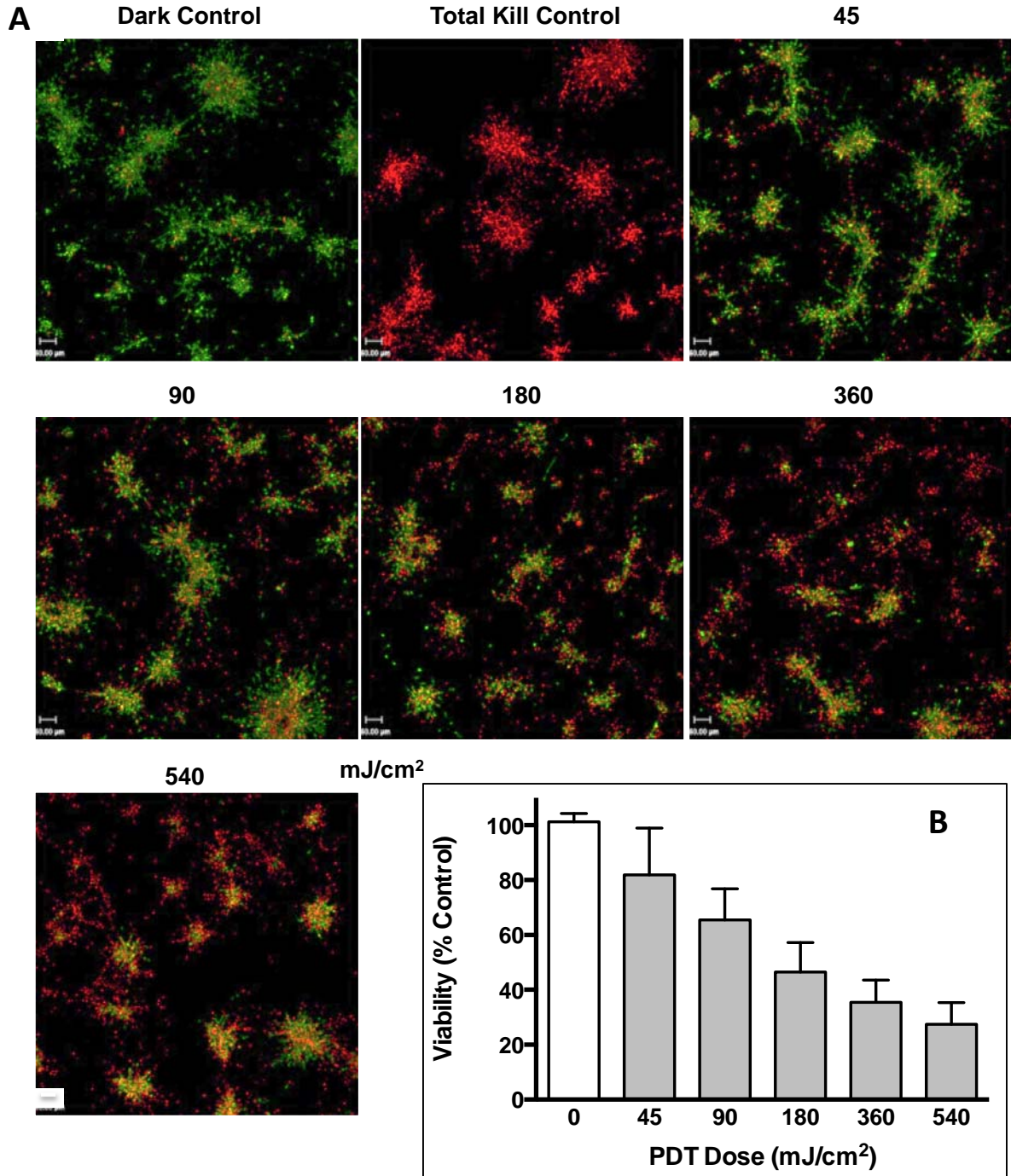
Figure 4.8: Response of Hs578T 6 day MAME structures to BPD-PDT: Representative live/dead images of optical sections through the volume of 3D structures were captured for 16 contiguous fields and shown in *en face* view (A). Images were taken 24 hours after PDT with 1.5 μM BPD and show live cells (green, calcein AM) and dead cells (red, ethidium homodimer-1) for non-treated dark control and BPD-PDT treated samples as indicated in the Figure; scale bar = 80 μm. Intensities of red and green fluorescence were used to calculate viability and plotted against PDT dose (B). p-value < 0.0001, one-way ANOVA; n=6, mean ± SD
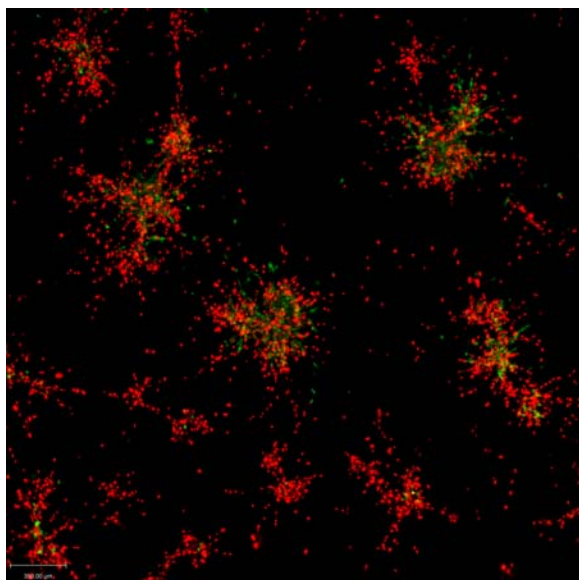
Figure 4.9: Response of Hs578T 6 day MAME structures to BPD-PDT at a dose of 620 mJ/cm^2: Live/dead images of optical sections through the volume of 3D structures were captured for 16 contiguous fields and shown in *en face* view (A). This image taken 24 hours after PDT with 1.5 µM BPD shows primarily dead cells (red, ethidium homodimer-1).

4.3 Dose Response of MAME Structures of Inflammatory Breast Cancer to Photokilling by PDT

4.3.1 BPD-PDT

We utilized MAME model of IBC cells to assess the dose-response to a PDT protocol in which mitochondria are targeted using BPD (Figure 4.10, Table 4.5). Approximately 50% of 3D structures were killed at a 45 mJ/cm^2 BPD-PDT dose. When we increased the duration of irradiation, we observed a significant decrease in cell viability resulting in 60% cell death after 90 mJ/cm^2 (one minute), 79% cell death after 180 mJ/cm^2 (two minutes), 92% cell death after 360 mJ/cm^2 (4 minutes) and 95% cell death after 540 mJ/cm^2 (six minutes) of treatment. A decrease in live MAME structures (green) and a corresponding increase in dead MAME structures (red) with increased dose of PDT were observed (Figure 4.10). Thus there was a significant increase in death of IBC MAME structures in response to escalating the BPD-PDT dose.
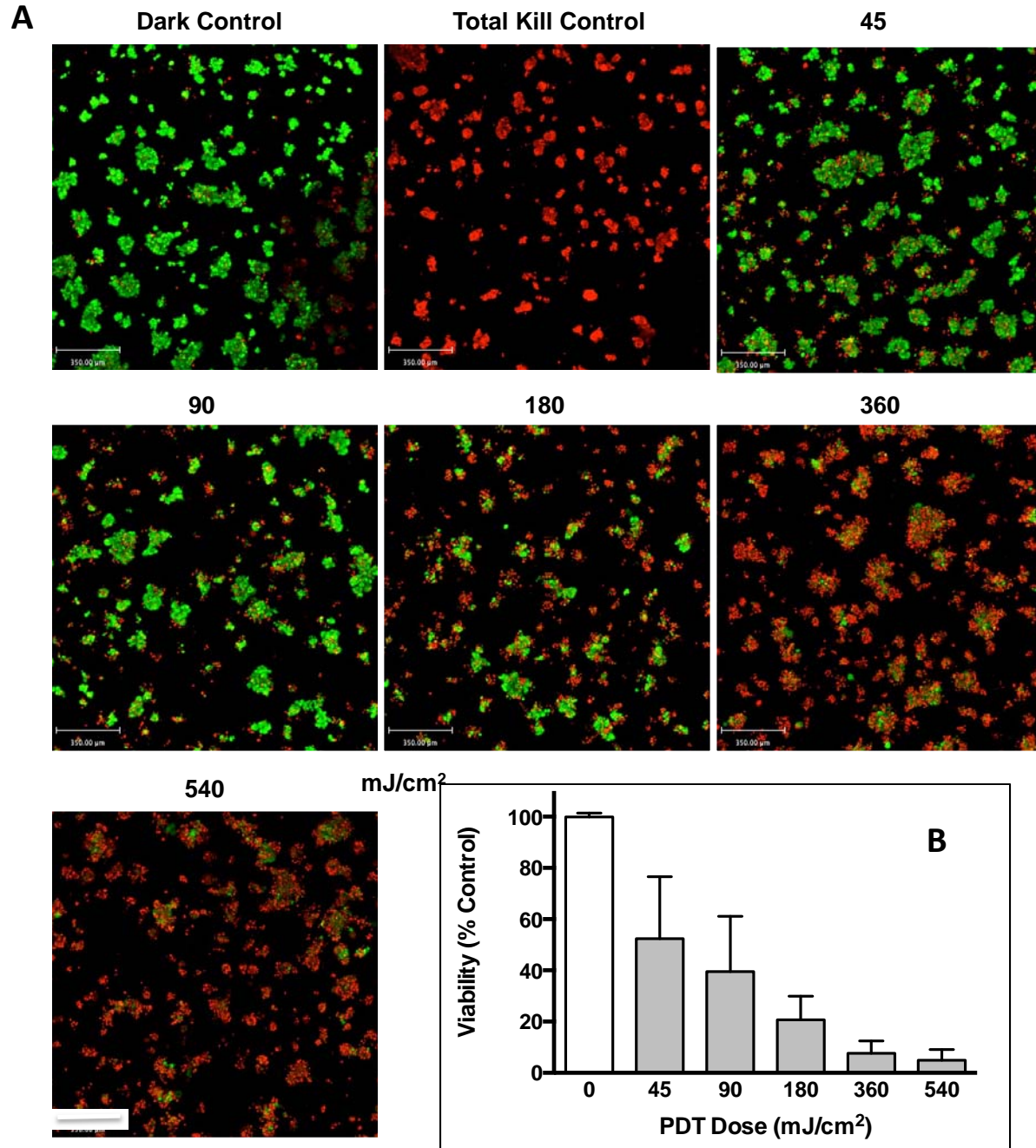
Figure 4.10: BPD-PDT induces dose-dependent photokilling of SUM149 cells in MAME cultures. Tiled 16-panel images and z-stacks through the depth of structures were captured and reconstructed in 3D to show an *en face* view (A). Images show live cells (green, calcein AM) and dead cells (red, ethidium homodimer-1) and were taken 24 hours after PDT with 1.5 µM BPD and for non-treated dark control; scale bar equals 350 µm. Intensities of red (dead) and green (live) fluorescence were used to calculate viability and plotted against PDT dose (B). Significance was calculated by one-way ANOVA, p-value < 0.0001; n=6, mean ± SD.

Table 4.5. Viability (% Control) for BPD-PDT treated IBC cells in MAME model

BPD-Dose (mJ/cm^2)	45	90	180	360	540
Viability (%Control)	52 ± 15	40 ± 14	21 ± 6	8 ± 3	5 ± 3

4.3.2 Combination PDT

Next, we assessed the cytotoxic response of combining two photosensitizers that target two critical organelles within a cell, mitochondria and lysosomes, using BPD and NPe6, respectively. These photosensitizing agents differ in their absorbance spectra and so photodamage with each agent can be separately initiated (Kessel and Reiners 2014). We examined the effects on photokilling of the order of activation of the photosensitizers at three doses of PDT (Figure 4.11, Table 4.6).

At a PDT dose of 22.5 mJ/cm^2, we observed a significant difference in photokilling in response to the order of irradiation of the mitochondrial targeted photosensitizer and the lysosomal targeted photosensitizer (Figure 4.11 I). The response to a combination of BPD and NPe6 was greater than additive compared to either alone. Cell death with BPD was 19% and with NPe6 was 5%. A sequential protocol of irradiation at 690 nm followed by 660 nm, resulted in 35% cell death. In contrast, a sequential protocol of 660 nm irradiation followed by 690 nm irradiation yielded 57% photokilled cells. Thus targeting lysosomes before mitochondria was more efficacious in photokilling of IBC MAME structures.

Additional studies were carried out using a higher PDT dose for NPe6 (45 mJ/cm^2) and keeping the dose for BPD at 22.5 mJ/cm^2 (Figure 4.11 II). We tested a twofold difference in dosage as Kessel and Reiners (Kessel and Reiners 2014) had reported that a twofold difference in dosage of NPe6 followed by BPD resulted in a synergistic response to photokilling in a 2D model of 1c1c7 hepatoma cells. In our IBC MAME model, cell death with BPD alone was 12%

and with NPe6 alone was 27%. A sequential protocol targeting either mitochondria or lysosomes first resulted in ~60% cell death. The two-fold difference in doses when targeting mitochondria followed by lysosomes did however result in an increase in photokilling by 25% compared to that at a dose of 22.5 mJ/cm^2 (see Table 4.6). The order of activation of photosensitizers did not affect photokilling in IBC MAME models.
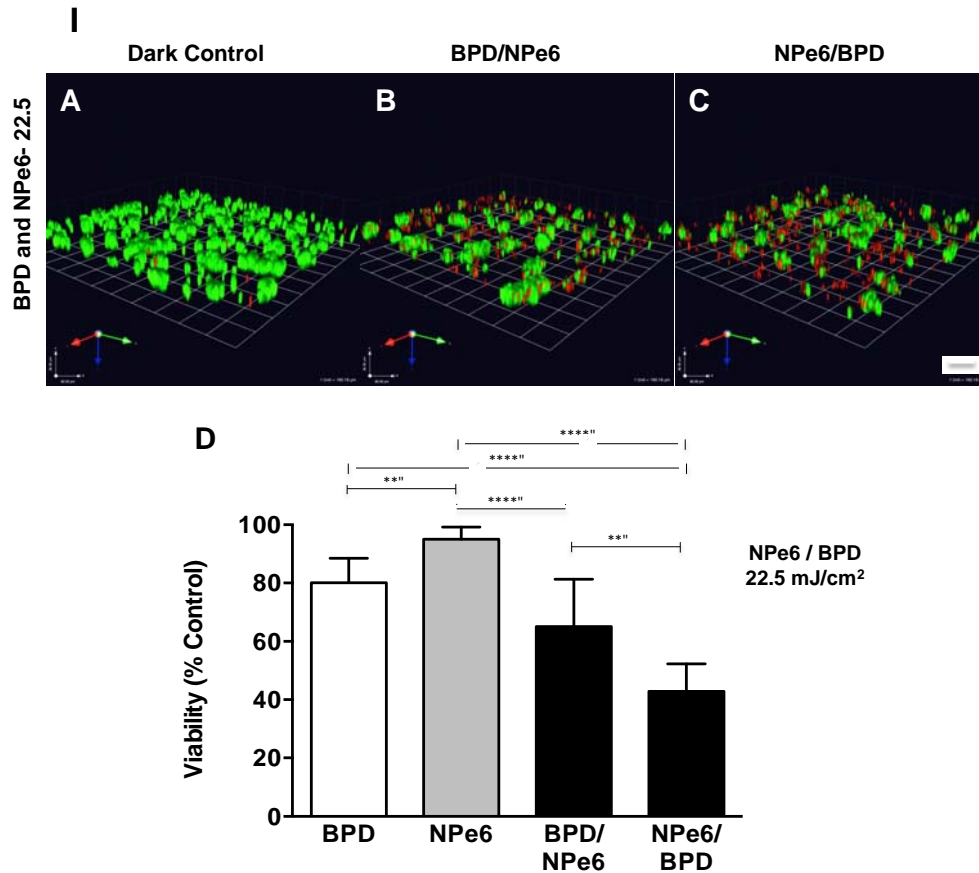
Figure 4.11 I: Combination PDT promotes photokilling of SUM149 cells in MAME cultures. Representative images show live cells (green, calcein AM) and dead cells (red, ethidium homodimer-1) for untreated dark control; light irradiation targeting mitochondria (BPD-690 nm) and lysosomes (NPe6-660 nm) at dose of 22.5mJ/cm^2 each (I). Optical sections through the depth of 3D structures were captured for 16 contiguous fields 24 hours after therapy and reconstructed in 3D; scale bar equals 80 microns. Intensities of red and green fluorescence were used to calculate viability and plotted against treatment. Significance was calculated by one-way ANOVA: *p-value < 0.05, **p-value < 0.01, ***p-value < 0.001, ****p-value < 0.0001; n=6-8, mean ± SD.
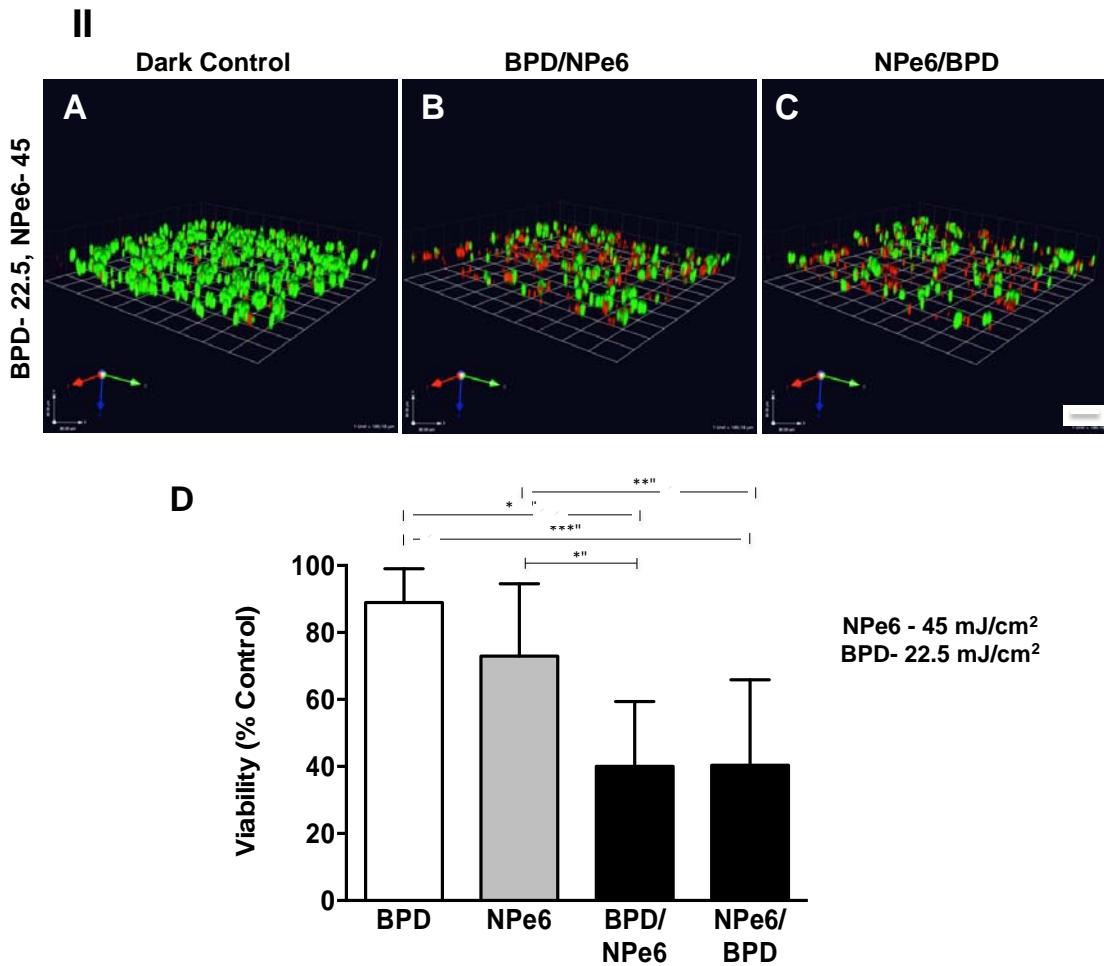
Figure 4.11 II: Combination PDT promotes photokilling of SUM149 cells in MAME cultures. Representative images show live cells (green, calcein AM) and dead cells (red, ethidium homodimer-1) for untreated dark control; PDT targeting mitochondria (BPD) at dose of 22.5 mJ/cm^2 and lysosomes (NPe6) at dose of 45 mJ/cm^2 (II). Optical sections through the depth of 3D structures were captured for 16 contiguous fields 24 hours after therapy and reconstructed in 3D; scale bar equals 80 microns. Intensities of red and green fluorescence were used to calculate viability and plotted against treatment. Significance was calculated by one-way ANOVA: * p-value < 0.05, ** p-value < 0.01, *** p-value < 0.001, **** p-value < 0.0001; n = 6-8, mean ± SD.

At a PDT dose of 45 mJ/cm^2, we observed a substantial degree of photokilling, with the order of activation of the photosensitizers not being significant (Figure 4.11 III). Cell death with either BPD or NPe6 was 36% and 44%, respectively. We observed a significant increase in cell death using sequential protocols targeting mitochondria first or lysosomes first, i.e., cell death of

81% and 94%, respectively. If lysosomes are targeted first, all IBC MAME structures are photokilled at a PDT dose of 45 mJ/cm^2.
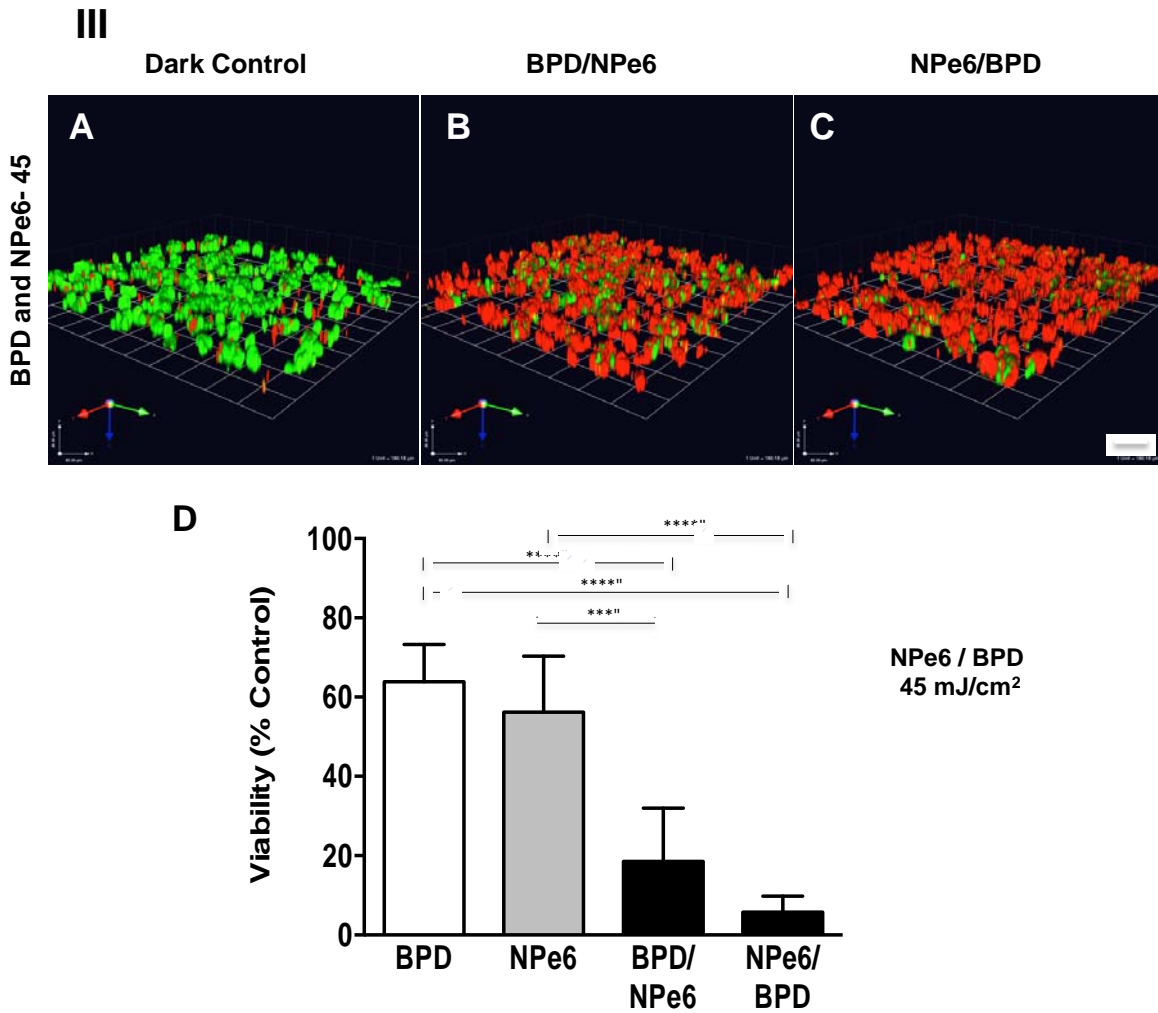
Figure 4.11 III: Combination PDT promotes photokilling of SUM149 cells in MAME cultures. Representative images show live cells (green, calcein AM) and dead cells (red, ethidium homodimer-1) for untreated dark control; PDT targeting mitochondria (BPD) and lysosomes (NPe6) at dose of 45 mJ/cm^2 each (III). Optical sections through the depth of 3D structures were captured for 16 contiguous fields 24 hours after therapy and reconstructed in 3D; scale bar equals 80 microns. Intensities of red and green fluorescence were used to calculate viability and plotted against treatment. Significance was calculated by one-way ANOVA: * p-value < 0.05, **p-value < 0.01, ***p-value < 0.001, ****p-value < 0.0001; n=6-8, mean ± SD.

Table 4.6. Viability (% dark control) for combination PDT of SUM149 3D cultures

Treatment	Irradiation (nm)	690nm-22.5 mJ/cm², 660- 22.5 mJ/cm²	690nm-22.5 mJ/cm², 660- 45 mJ/cm²	690nm-45 mJ/cm², 660- 45 mJ/cm²
BPD	690	80 ± 8	89 ± 10	64 ± 9
NPe6	660	95 ± 4	73 ± 22	56 ± 14
BPD and NPe6	690 »» 660	65 ± 16	40 ± 19	19 ± 13
BPD and NPe6	660 »» 690	43 ± 9	40 ± 25	6 ± 4

4.3.3 Changes in volume of IBC MAME structures indicate response to combination PDT

A decrease in tumor burden is used as a standard measure of response to anti-tumor therapy. In this respect, mathematical algorithms for 3D modeling of patient tumors and prediction of surgical volume better assess breast tumor stage and response to therapies (Guelfi, Masoni et al. 1994, Edgerton, Chuang et al. 2011). Volume of nasopharyngeal carcinoma rather than their size is associated with poorer survival and faster recurrence (Mukherji, Schmalfuss et al. 2004, Lee, Huang et al. 2010, Mozley, Schwartz et al. 2010). Here we measured the volume of MAME structures to determine if this parameter could be used to quantify response to combination PDT (Figure 4.12). We observed an increase in size and volume of MAME structures over a period of 4 days for the dark controls. In contrast, there was significant decrease in the size and volume of MAME structures over the 4 days following NPe6/BPD treatment at a dose of 22.5 mJ/cm². These data suggest that the volumetric measurement of MAME structures can be used as an indirect method to evaluate response to therapy.
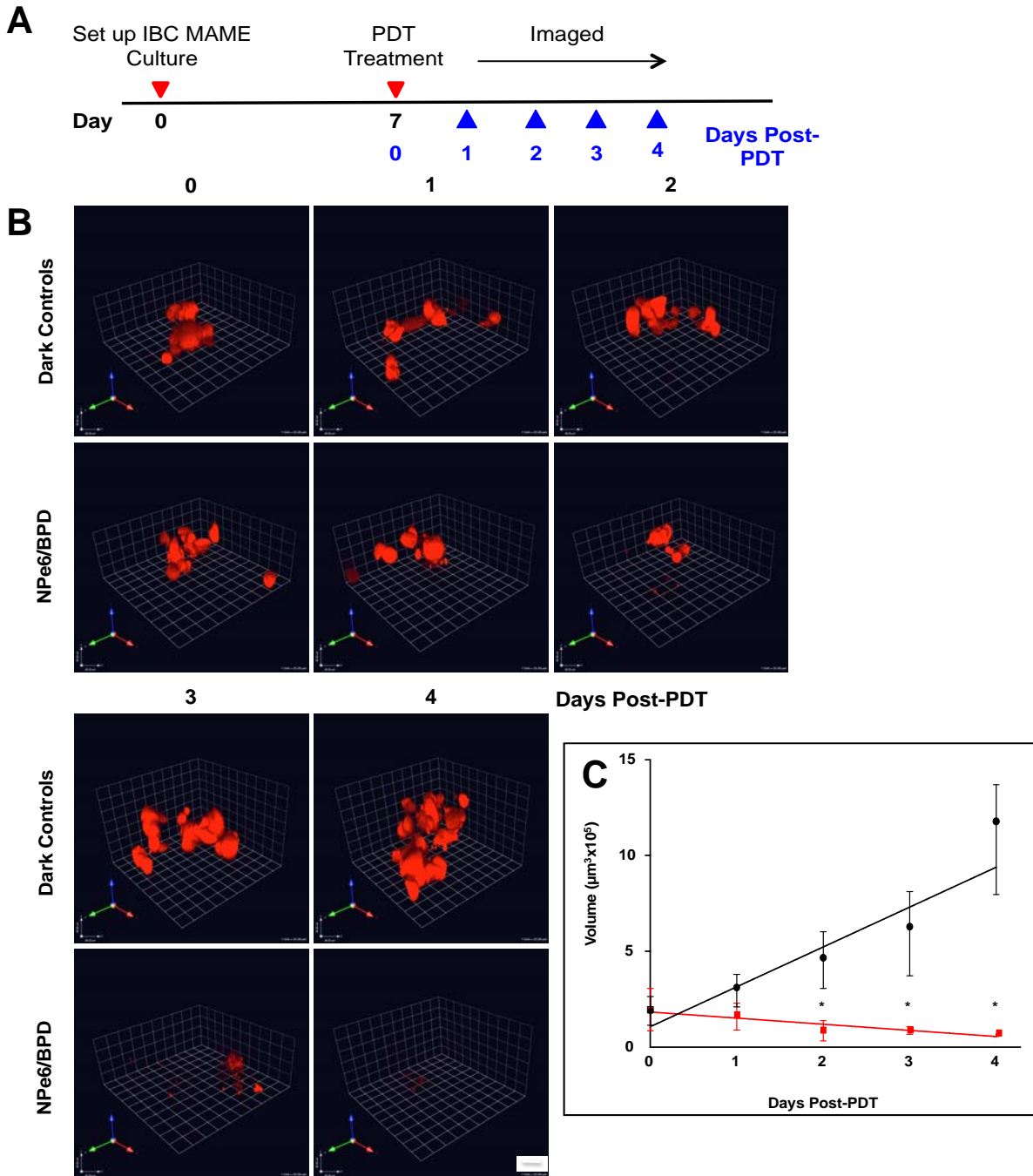
Figure 4.12: SUM149 structure volume assesses phenotypic response to the sequential PDT protocol. Schematic of events during the experiment (A). Representative 3D images of SUM149-RFP cells in MAME cultures (red) treated with sequential PDT (NPe6 followed by BPD at 22.5 mJ/cm^2) (B); scale bars equal 80 microns. Volume of structures was calculated using Volocity and is plotted against days post treatment (C); untreated dark control (black line), NPe6/BPD-PDT (red line). Significance was calculated by two-way ANOVA: * p-value < 0.0001, n = 8, mean ± SD.

CHAPTER 5

MECHANISM OF PHOTOKILLING OF TN-IBC CELLS IN MAME MODELS

Rationale

PDT targeting either mitochondria or lysosomes leads to the initiation of apoptosis, an irreversible route to cell death (Diamond, Granelli et al. 1972, Agarwal, Clay et al. 1991, Dougherty, Gomer et al. 1998, Kessel and Luo 1998, Dolmans, Fukumura et al. 2003, Kessel and Reiners 2007, Kessel and Oleinick 2010, Agostinis, Berg et al. 2011, Andrzejak, Price et al. 2011). PDT that targets mitochondria induces immediate release of cytochrome c thus activating the caspase cascade and apoptotic pathway (Granville, Carthy et al. 1998). PDT that targets lysosomes induces release of lysosomal proteases into the cytoplasm and causes damage to other intracellular organelles resulting in activation of the caspase cascade and death via apoptosis (Kessel, Luo et al. 2000, Reiners, Caruso et al. 2002). Combining the targeting of lysosomes by PDT with targeting of mitochondria by PDT has been shown to promote cell death. Indeed, targeting lysosomes and mitochondria sequentially significantly increases photokilling by PDT of 1c1c7 murine hepatoma cells in monolayer cultures (Kessel and Reiners 2014). The mechanism of photokilling by sequential targeting of lysosomes and mitochondria is under study.

Specific Aim 2: Identify mechanism(s) involved in photokilling by sequential targeting of lysosomes and mitochondria.

Hypothesis: Sequential targeting of lysosomes and mitochondria causes cell death via apoptosis.

Results

5.1 Cysteine Cathepsins and Calpains are not Involved in Cell Death by Combination PDT

The additive effect that was observed upon photodamage to lysosomes prior to mitochondria might be due to the release of lysosomal proteases (Figure 5.1). Yousefi et al.

(Yousefi, Perozzo et al. 2006) have reported that calpains cleave ATG5, an autophagy-related protein. Truncated ATG5 amplifies the pro-apoptotic signal. For PDT, we hypothesized that lysosomal proteases or calpains may alter ATG5 cleavage. We tested Ca074Me, a selective inhibitor of lysosomal cysteine cathepsins B and L (Montaser, Lalmanach et al. 2002); E64d, an inhibitor of cysteine proteases including lysosomal cysteine cathepsins and calpains (Tamai, Matsumoto et al. 1986, McGowan, Becker et al. 1989); and PD150606, an inhibitor of calpains (Wang, Posner et al. 1996). We did not observe any changes in viability. This indicates that cysteine proteases including lysosomal cathepsins B and L and calpains do not contribute to cell death in our models.
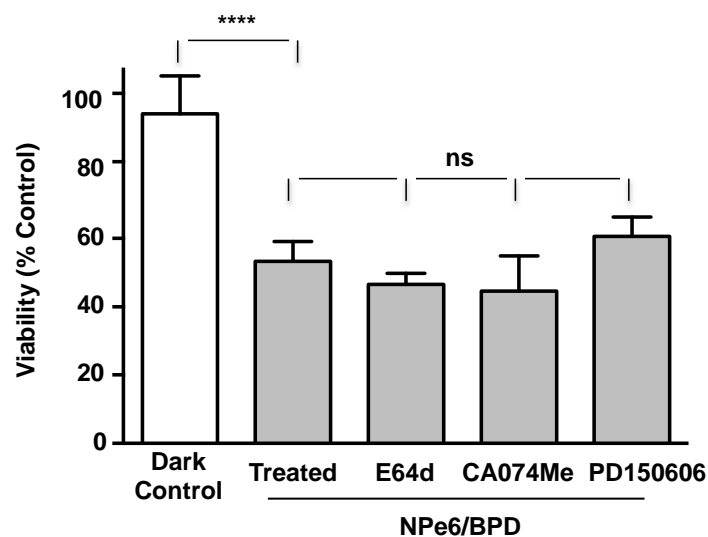
Figure 5.1: Inhibitors of cysteine cathepsins and calpains do not alter response to combination PDT. SUM149 cells were grown in MAME cultures for 8 days followed by combination PDT (NPe6 followed by BPD at 22.5 mJ/cm^2) in the presence of cell permeable inhibitors: E64d (cysteine proteases), CA074Me (CTSB and L) and PD150606 (calpains). Significance was calculated by multiple comparison t-test: **** p-value < 0.0001; bars represent mean ± SD from at least four 16-field images.

Our laboratory has previously shown that E64d, CA074Me, and PD150606 inhibitors do inhibit protease activities in breast cancer cell types (Victor, Anbalagan et al. 2011, Moin, Sameni et al. 2012, Mullins, Sameni et al. 2012). However to demonstrate that these inhibitors are cell permeable and function to decrease protease activities in IBC MAME model, we performed a live-cell proteolysis assay. We observed a significant reduction in the proteolytic activity as shown by the decrease in degradation of DQ collagen IV (Figure 5.2).

Figure 5.2 Evidence that inhibitors are functionally active. 3D cultures were grown in presence of DQ Collagen IV for 8 days with treatment with inhibitors as indicated for 24 hours. Images through the depth of structures were captured for 16 contiguous fields and fluorescence intensity from images was measured using Volocity and plotted against treatment. Significance was calculated by an unpaired Student's t-test, p-value < 0.0001, n=4-8, mean ± SD.
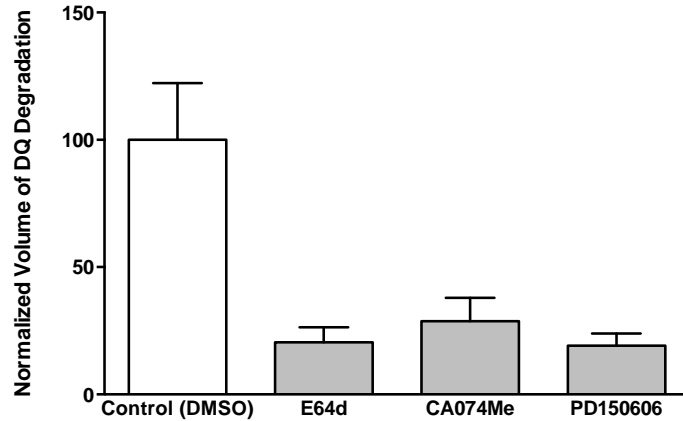
5.2 Mechanism of Cell Death Following Combination PDT is Apoptosis

PDT targeting either mitochondria or lysosomes results in initiation of apoptosis (Diamond, Granelli et al. 1972, Agarwal, Clay et al. 1991, Dougherty, Gomer et al. 1998, Kessel and Luo 1998, Dolmans, Fukumura et al. 2003, Kessel and Reiners 2007, Kessel and Oleinick 2010, Agostinis, Berg et al. 2011, Andrzejak, Price et al. 2011). Morphologic features associated with apoptosis include cell shrinkage, dense cytoplasm, chromatin condensation (pyknosis) and nuclear fragmentation (karyorrhexis) (Kerr, Wyllie et al. 1972, Wyllie, Kerr et al. 1980, Kerr 2002). The apoptotic process is very tightly regulated; however, once executioner caspases (i.e. caspases-3, 6 or 7) are activated, a cell is destined to undergo programmed cell death (Wyllie, Kerr et al. 1980, Granville, Carthy et al. 1998, Janicke, Sprengart et al. 1998, Porter and Janicke 1999, Renehan, Booth et al. 2001). We observed a time-dependent increase in activated caspase-3 as a result of NPe6/BPD treatment at a dose of 22.5 mJ/cm^2 (Figure 5.3 A, B). By 24 hours post-PDT, nuclear fragmentation and chromatin condensation were present (Figure 5.3 C). The activated caspase-3 and changes in nuclear morphology observed here in response to sequential PDT protocol are consistent with cell death occurring by apoptosis.
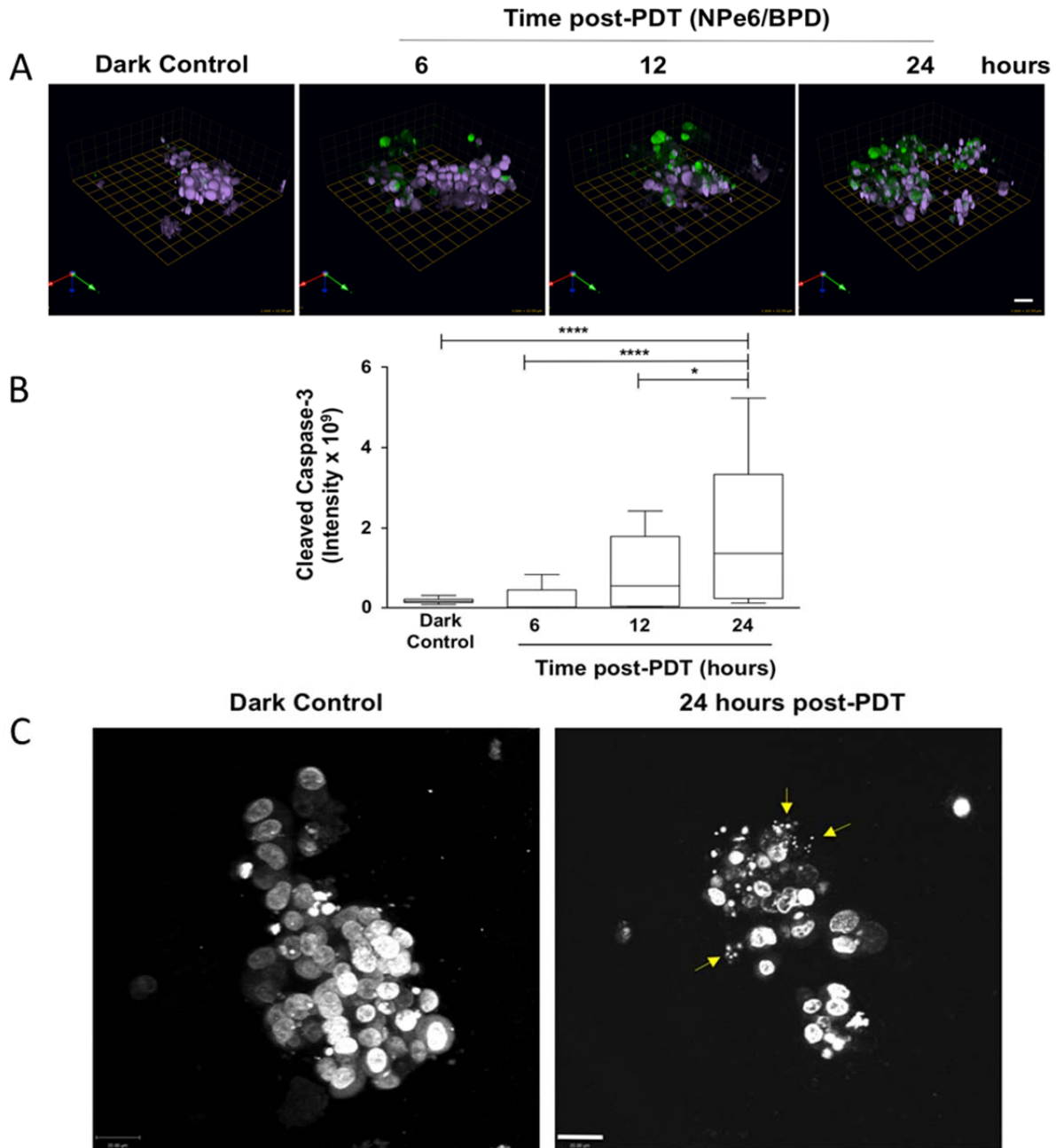
Figure 5.3 Mechanism of cell death following sequential PDT protocol is apoptosis. Panel A shows representative images of expression of cleaved caspase-3 in response to the sequential PDT protocol PDT or a dark control. Images through the depth of structures were captured at 6 hours, 12 hours and 24 hours after treatment and images were reconstructed in 3D using Volocity; each square unit equals 22.59 microns. Green florescence represents cleaved caspase-3 and purple represents nuclei (pseudocolored, Hoechst). Fluorescent intensity was quantified using Volocity and plotted against treatment (B); significance was calculated by one-way ANOVA: **** p-value < 0.0001, n=20, mean ± SD. Representative images showing fragmented nuclei (yellow arrows) stained with Hoechst (gray scale) 24 hours after sequential PDT protocol compared to intact nuclei for dark control (C); images show an *en face* view of single 3D structure and scale bars equal 22 microns.

5.3 MAME Structures of IBC Cells do not Show a Bystander Effect to Combination PDT

In a recent study in which much higher PDT doses were used for combination PDT in 2D, the tumor cells (HeLa, HaCaT and MCF-7 cell lines) were found to be photokilled by necrosis (Acedo, Stockert et al. 2014). Calcium and metabolic byproducts such as cytokines that are released by necrotic cells can damage neighboring cells due to a bystander effect (Henderson and Donovan 1989, Dahle, Kaalhus et al. 1997, Dahle, Bagdonas et al. 2000, Ding, Xu et al. 2004). In contrast, apoptosis initiated by low dose PDT does not induce a bystander effect or immune response because toxic metabolites are not leaked from apoptotic cells (Dahle, Kaalhus et al. 1997, Dahle, Bagdonas et al. 2000). Here we evaluated whether there was a bystander response to low dose PDT in the IBC MAME models. A PDT dose of 45 mJ/cm^2 photokilled all 3D MAME structures within 24 hours following treatment (Figure 5.4). To test for a bystander effect we used a lower PDT dose, i.e., 22.5 mJ/cm^2. We observed that photokilling was comparable on days 1 and 2 post combination PDT, which is consistent with the absence of a bystander effect.
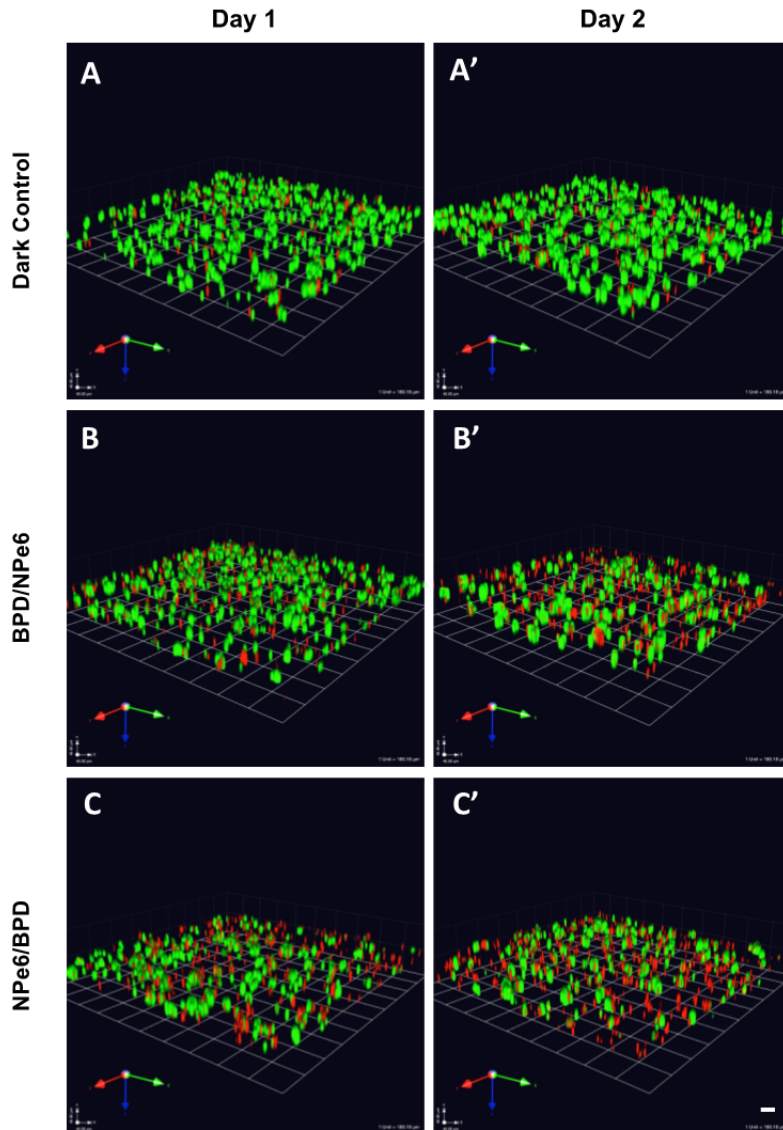
Figure 5.4: A bystander effect is not induced by sequential PDT protocol. Optical sections through the depth of 3D structures were captured for 16 contiguous fields and reconstructed in 3D. Images were taken on day 1 (A-C) and day 2 (A'-C') after combination PDT for 22.5 mJ/cm^2 each with 1.5 μM BPD and 40μM NPe6 and show live cells (green, calcein AM) and dead cells (red, ethidium homodimer-1) for untreated dark control (A, A'); sequential light irradiation targeting mitochondria then lysosomes (B, B'); and sequential light irradiation targeting lysosomes then mitochondria (C, C'); scale bars equal 40 microns. Intensities of red and green fluorescence were used to calculate viability and plotted against days post-PDT (D); Significance was calculated by ANOVA: **** p-value < 0.0001, n=8-10, mean ± SD.
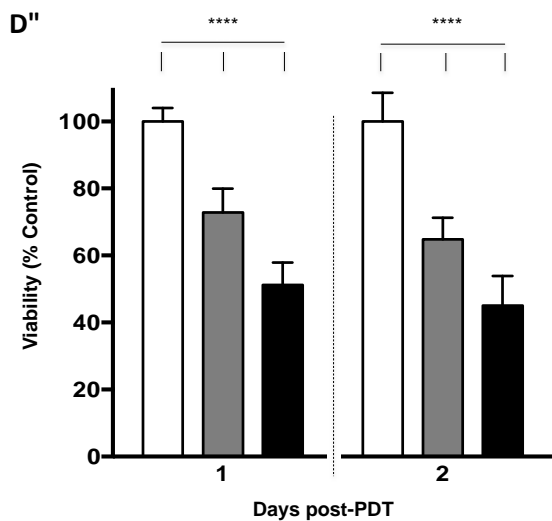
CHAPTER 6

DISCUSSION

Initial site for metastasis of breast cancer is lymphatics. TNBC often recurs with chest wall metastases. IBC is a subtype of breast cancer that spreads rapidly. By the time a correct diagnosis is made, the prognosis is poor because the cancer has already metastasized to dermal lymphatics. PDT, a FDA approved therapy for some cancers, can shut down lymphatic vasculature (Henderson and Dougherty 1992, Dougherty, Gomer et al. 1998, Dolmans, Fukumura et al. 2003, Tammela, Saaristo et al. 2011). Thus, we hypothesize that PDT could be a valid modality for treating breast cancer metastases. Indeed, PDT has offered excellent clinical response in treating chest wall metastases of breast cancer (Allison, Mang et al. 2001, Allison, Sibata et al. 2004, Rogers 2012).

TNBCs and IBCs are the most lethal subtypes of breast cancers. TNBC accounts for about 20-40% of IBC cases and 15-20% of non-IBC breast cancers (Lehmann, Bauer et al. 2011, Dawood, Ueno et al. 2012). Experiments in this study have been done using two highly invasive TNBC cell lines (MDA-MB-231 and Hs578T) and one IBC cell line that is also triple negative (SUM149) (Lehmann, Bauer et al. 2011, Victor, Anbalagan et al. 2011, Barnabas and Cohen 2013). Recently, TNBCs were subtyped into 6 categories based on cluster analysis following gene expression profiling of 587 TNBC cases (Lehmann, Bauer et al. 2011). Based on this classification, MDA-MB-231 and Hs578T lines belong to the mesenchymal-stem like (MSL) subtype, a subtype that has a higher expression of genes involved in the epithelial-mesenchymal transition and responds to mTOR and src inhibitors. SUM149 belongs to the basal like 2 (BL2) subtype, a subtype that has a higher expression of cell cycle and DNA damage response genes and responds to cisplatin treatment. There are not presently targeted therapies for use in clinics for either IBC or TNBC. Our data demonstrate that PDT is an effective modality for

photokilling of 3D MAME structures of TNBC and IBC providing support for use in clinics.

PDT that targets mitochondria can induce release of cytochrome c, a known trigger for apoptosis (Granville, Carthy et al. 1998). Lysosomal photodamage results in release of lysosomal proteases into the cytoplasm leading to cleavage (activation) of the pro-apoptotic protein Bid, cytochrome c release and apoptosis (Kessel and Poretz 2000, Reiners, Caruso et al. 2002). Targeting lysosomes before mitochondria promotes cell death by PDT in 2D models (Kessel and Reiners 2014). In our study, such a sequential PDT protocol eradicated IBC structures. To our knowledge this is the first study to show using an IBC MAME model that combinatorial targeting of lysosomes and mitochondria with PDT is significantly more efficacious than targeting mitochondria alone. Our studies do, however, suggest that before a sequential protocol is taken to the clinic one should also consider the potential effects of varying the PDT dose. A serious side effect of PDT at higher doses is skin ulceration and necrosis (Oleinick and Evans 1998, Allison and Moghissi 2013). We surmise that these side effects could be reduced or eliminated by using combination PDT.

Mechanistically, PDT photokills cells via apoptosis, necrosis or autophagy. To our knowledge our studies are the first to show that sequential targeting of lysosomes before mitochondria leads to cell death by apoptosis. This was shown by the presence of cleaved caspase-3 and the condensation and fragmentation of nuclei. Inhibiting cysteine proteases (both lysosomal and cytosolic) did not alter cell death in our 3D MAME models suggesting that cysteine proteases do not play a role in photokilling of the IBC structures. We did not observe a bystander effect as has also been shown for apoptotic cell death induced by PDT and treatments other than PDT (Dahle, Kaalhus et al. 1997, Dahle, Bagdonas et al. 2000, Staudacher, Blyth et al. 2010, Blyth and Sykes 2011). Our study suggests that use of PDT and in particular the lower doses possible with combination PDT should be explored for the treatment of IBC and TNBC.

PDT has not been evaluated for treatment of IBC dermal metastases. Nonetheless, the success of PDT against chest wall recurrences of breast cancer (Allison, Mang et al. 2001, Allison, Sibata et al. 2004) suggests that PDT may be an efficacious therapeutic approach for IBC and TNBC.

CHAPTER 7

ADDITIONAL STUDIES

Effects of cellular components of tumor microenvironment on photokilling by PDT

I. Develop and optimize coculture model of SUM149 cells and carcinoma associated fibroblasts (CAFs). Use different PDT doses and sequential PDT to treat cells in the coculture and quantify dose response of respective cell types to photokilling.

To study the effects of cellular components, we performed some preliminary studies; the results of those are shown and discussed below:

Carcinoma Associated Fibroblasts (CAFs) are a predominant cell type in the tumor microenvironment that can promote malignant progression (Campbell, Polyak et al. 2009, Madar, Goldstein et al. 2013, Augsten 2014). Our lab has previously designed and optimized MAME culture models to mimic breast tumors in context of their cellular and (Jedeszko, Victor et al. 2009, Sameni, Anbalagan et al. 2012). Previous studies from the Sloane laboratory have shown that when TNBC cells are cultured with CAFs, the tumor cells become more invasive, exhibit increased degradation of extracellular matrix proteins and form larger stellate structures with multicellular outgrowths (Jedeszko, Victor et al. 2009, Sameni, Anbalagan et al. 2012). Similar coculture experiments would allow us to determine whether interactions between IBC cells and CAFs affect malignant phenotype.

An association of IBC tumors with CAFs clinically is yet to be established. Therefore, we performed immunohistochemistry (IHC) on IBC patient samples obtained from Dr. Mona Mohamed (Cairo University, Egypt). The samples were stained using an antibody to vimentin that will label all fibroblasts and an antibody to fibroblast activation protein (FAP) to selectively label active (carcinoma associated) fibroblasts. Here, we show that there are CAFs in human IBC tissue samples (Figure 7.1). These preliminary studies need to be confirmed with tissue

microarrays containing normal, non-IBC and IBC tissue samples, preferentially microarrays annotated for breast cancer subtypes.
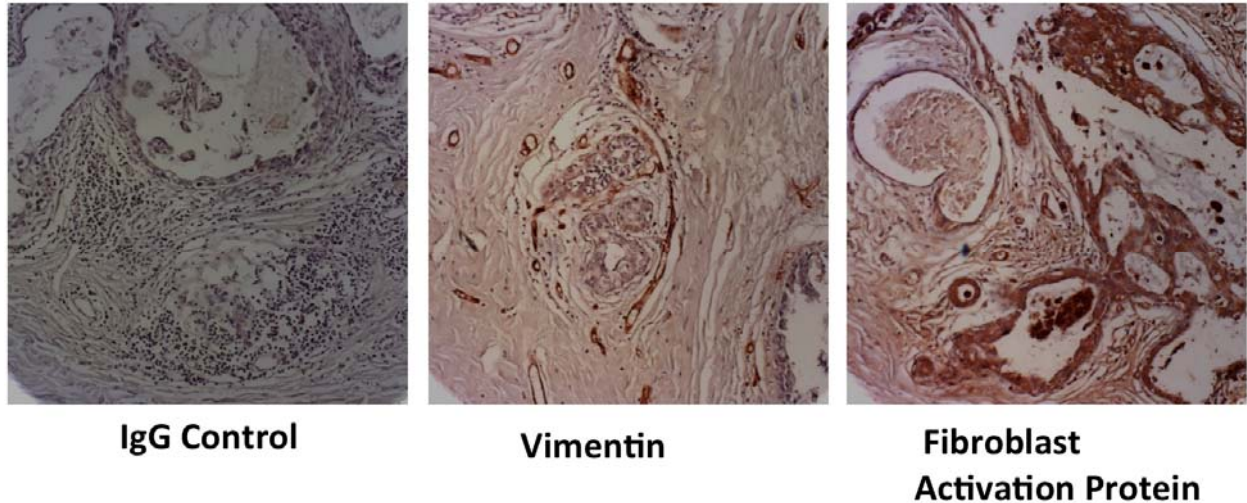
Figure 7.1 Fibroblasts are associated with IBC tumors. Representative images of IBC patient tissue samples stained with IgG (control antibody), Vimentin and Fibroblast Activation Protein (FAP). Magnification: 20X

We adapted the MAME coculture model (Sameni, Cavallo-Medved et al. 2009, Sameni, Anbalagan et al. 2012, Osuala, Sameni et al. in press). We seeded 5000 SUM149-RFP cells and 1600 CAF40TKi cells (a human breast fibroblast line that has been immortalized by Dr. Kingsley Osuala (Osuala, Sameni et al. in press) that were stained with CFSE (green). Images were captured on days 2 and 6 through the entire depth of 3D structures for 16 contiguous fields using LSM 510 confocal microscope. Interactions among the two cell types were observed: CAFs (green) infiltrated into SUM149 structures (red) (Figure 7.2).
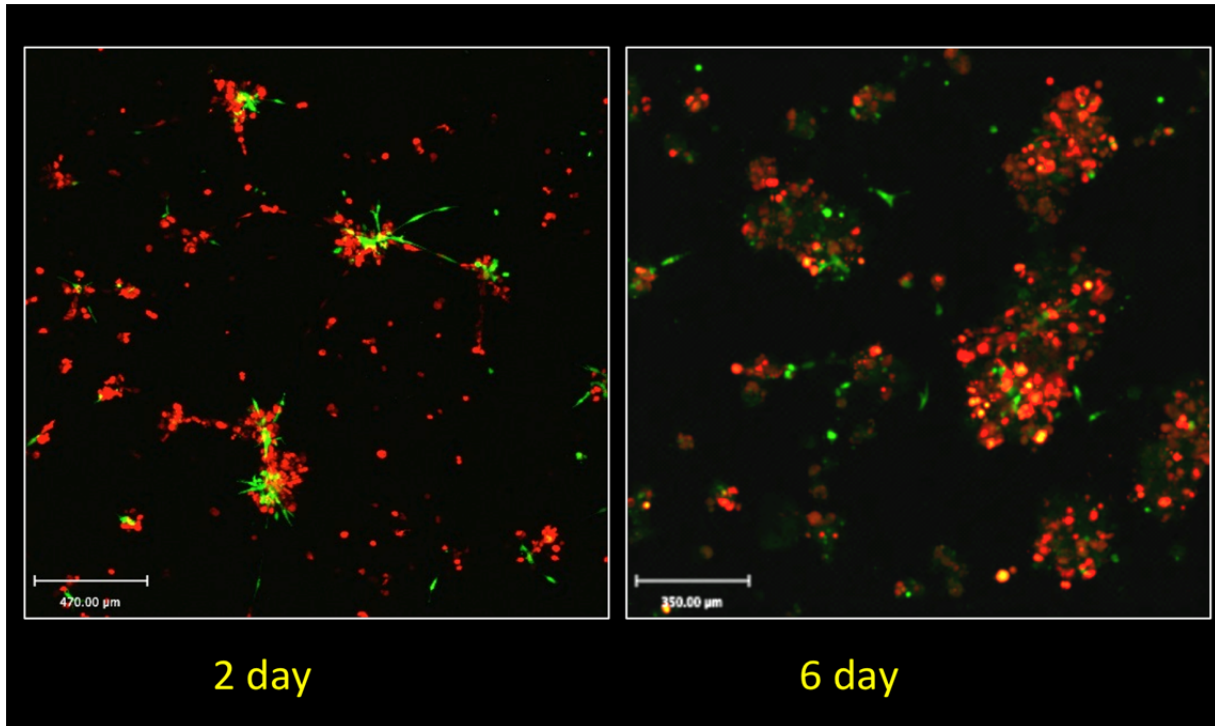
Figure 7.2: MAME coculture model of SUM149-RFP cells (red) and CAFs (green). Tiled 16-panel images and z-stacks through the depth of structures were captured and reconstructed in 3D to show an *en face* view and show cells in coculture growing over time (2 day culture compared to 6 day culture); scale bar= 350 microns.

We determined whether PDT could photokill tumor cells and CAFs in these coculture models. Limitations for these experiments were availability of dyes to maintain staining of cells over time needed for long-term cultures and the need to perform live-dead assays that require fluorophores that emit in red and green regions. ToPro-3 is a nuclear dye that labels dead cells and fluoresces in the far-red region so we used ToPro-3 along with the RFP (red)- labeled SUM149 cells and CFSE (green)- labeled CAF40TKi cells. In Figure 7.3 we show that a majority of cells were photokilled after treatment with NPe6/BPD-PDT (45 mJ/cm^2) as indicated by the magenta staining (TopPro3). These experiments were done to optimize conditions and as proof of principle that PDT could be effectively used in coculture models. We have yet to prove whether both cell types are photokilled by PDT and what dose of PDT would be more

efficacious. In addition, we cannot quantify viability due to lack of a live cell marker that fluoresces in range other than red, green and far red.
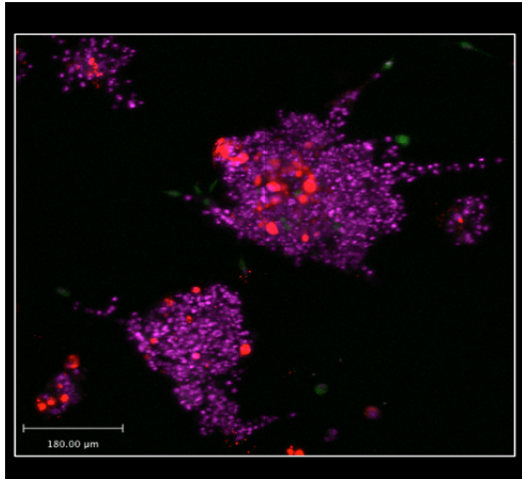
Figure 7.3: PDT is effective in killing cocultures of SUM149-RFP cells (red) and CAFs (stained with CFSE; green). The image was captured for 4 contiguous fields, through the depth of structures and shows effect of combination PDT (sequential NPe6/BPD-PDT at dose of 45 mJ/cm^2) on the coculture where magenta (pseudocolored ToPro3) represents dead cells; scale bar = 180 microns.

II. Develop and optimize coculture model of SUM149 cells and lymphatic endothelial cells. Use different PDT doses and sequential PDT to treat cells in the coculture and quantify the dose response of respective cell types to photokilling.

Preliminary studies are shown below:

IBC spreads via the dermal lymphatic vasculature. Hence a coculture of the two types would provide a better insight of cell-cell interactions and how these interactions might affect PDT. We adapted the MAME coculture model (Sameni, Cavallo-Medved et al. 2009, Sameni, Anbalagan et al. 2012, Osuala, Sameni et al. in press). We seeded 5000 SUM149 cells and 20,000 human dermal lymphatic endothelial cells (HDLEC). The 3D MAME structures were allowed to form for 4 days. PDT was then performed and a live/dead assay was done for analysis of photokilling (Figure 7.4). We observed that PDT could photokill tumor cells and HDLECs in these coculture models. A limitation for these experiments was ability the to maintain HDLEC cells in culture for long-term cultures. The other limitation was availability of dyes to maintain staining of live cells over long periods of time and the need to perform live-

dead assays that requires fluorophores that emit in red and green region.
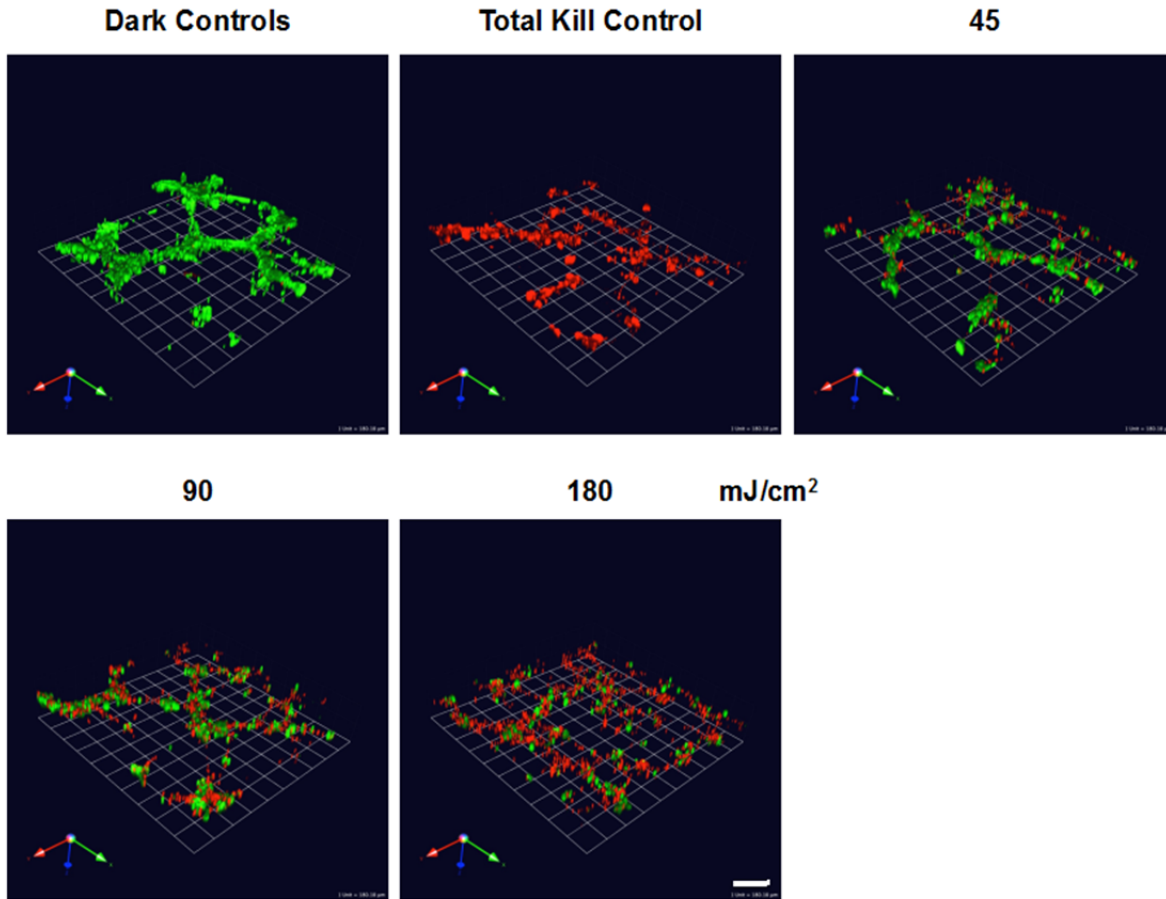
Figure 7.4: PDT is effective in killing cocultures of SUM149 cells and HDLECs. Optical sections. through the depth of structures were captured for 16 contiguous fields. Images show effect of BPD-PDT on the coculture where red (Ethidium Homodimer 1) represents dead cells and green (Calcein AM) represents live cells; scale bar = 180 microns.

Effects of non-cellular components of tumor microenvironment on photokilling by PDT

I. Optimize the MAME model of SUM149 cells to study the effects of pH on photokilling by PDT.

Previous studies from the Sloane laboratory have shown that the acidic pH found in the breast tumor microenvironment enhances the activity of secreted cysteine cathepsins (e.g. cathepsin B) thus contributing to increased malignancy of breast tumors (Rothberg, Bailey et al. 2013). We would like to study if PDT would is affected by an acidic tumor microenvironment.

II. Optimize the MAME model of SUM149 cells to study the effects of hypoxia on photokilling by PDT.

One of the important components for an effective PDT is availability of oxygen. Solid tumors such as those of the breast often have hypoxic cores, which might decrease the efficacy of therapy. We would like to study in future the effect of PDT on MAME structures when availability of oxygen is limited.

REFERENCES

1. Acedo, P., J. C. Stockert, M. Canete and A. Villanueva (2014). "Two combined photosensitizers: a goal for more effective photodynamic therapy of cancer." Cell Death Dis 5: e1122.

2. Adriance, M. C., J. L. Inman, O. W. Petersen and M. J. Bissell (2005). "Myoepithelial cells: good fences make good neighbors." Breast Cancer Res 7(5): 190-197.

3. Agarwal, M. L., M. E. Clay, E. J. Harvey, H. H. Evans, A. R. Antunez and N. L. Oleinick (1991). "Photodynamic therapy induces rapid cell death by apoptosis in L5178Y mouse lymphoma cells." Cancer Res 51(21): 5993-5996.

4. Aggeler, J., C. S. Park and M. J. Bissell (1988). "Regulation of milk protein and basement membrane gene expression: the influence of the extracellular matrix." J Dairy Sci 71(10): 2830-2842.

5. Agostinis, P., K. Berg, K. A. Cengel, T. H. Foster, A. W. Girotti, S. O. Gollnick, S. M. Hahn, M. R. Hamblin, A. Juzeniene, D. Kessel, M. Korbelik, J. Moan, P. Mroz, D. Nowis, J. Piette, B. C. Wilson and J. Golab (2011). "Photodynamic therapy of cancer: an update." CA Cancer J Clin 61(4): 250-281.

6. Akens, M. K., M. R. Hardisty, B. C. Wilson, J. Schwock, C. M. Whyne, S. Burch and A. J. Yee (2010). "Defining the therapeutic window of vertebral photodynamic therapy in a murine pre-clinical model of breast cancer metastasis using the photosensitizer BPD-MA (Verteporfin)." Breast Cancer Res Treat 119(2): 325-333.

7. Akens, M. K., A. J. Yee, B. C. Wilson, S. Burch, C. L. Johnson, L. Lilge and S. K. Bisland (2007). "Photodynamic therapy of vertebral metastases: evaluating tumor-to-neural tissue uptake of BPD-MA and ALA-PpIX in a murine model of metastatic human breast carcinoma." Photochem Photobiol 83(5): 1034-1039.

8. Allison, B. A., P. H. Pritchard, A. M. Richter and J. G. Levy (1990). "The plasma distribution of benzoporphyrin derivative and the effects of plasma lipoproteins on its biodistribution." Photochem Photobiol 52(3): 501-507.

9. Allison, R., T. Mang, G. Hewson, W. Snider and D. Dougherty (2001). "Photodynamic therapy for chest wall progression from breast carcinoma is an underutilized treatment modality." Cancer 91(1): 1-8.

10. Allison, R. R. and K. Moghissi (2013). "Photodynamic Therapy (PDT): PDT Mechanisms." Clin Endosc 46(1): 24-29.

11. Allison, R. R., C. Sibata, T. S. Mang, V. S. Bagnato, G. H. Downie, X. H. Hu and R. Cuenca (2004). "Photodynamic therapy for chest wall recurrence from breast cancer." Photodiagnosis Photodyn Ther 1(2): 157-171.

12. Anbil, S., I. Rizvi, J. P. Celli, N. Alagic, B. W. Pogue and T. Hasan (2013). "Impact of treatment response metrics on photodynamic therapy planning and outcomes in a three-dimensional model of ovarian cancer." J Biomed Opt 18(9): 098004.

13. Andrzejak, M., M. Price and D. H. Kessel (2011). "Apoptotic and autophagic responses to photodynamic therapy in 1c1c7 murine hepatoma cells." Autophagy 7(9): 979-984.

14. Antoni, D., H. Burckel, E. Josset and G. Noel (2015). "Three-dimensional cell culture: a breakthrough *in vivo*." Int J Mol Sci 16(3): 5517-5527.

15. Ashkenazi, A. (2002). "Targeting death and decoy receptors of the tumour-necrosis factor superfamily." Nat Rev Cancer 2(6): 420-430.

16. Augsten, M. (2014). "Cancer-associated fibroblasts as another polarized cell type of the tumor microenvironment." Front Oncol 4: 62.

17. Aveline, B., T. Hasan and R. W. Redmond (1994). "Photophysical and photosensitizing properties of benzoporphyrin derivative monoacid ring A (BPD-MA)." Photochem

Photobiol 59(3): 328-335.

18. Badylak, S. F. (2005). "Regenerative medicine and developmental biology: the role of the extracellular matrix." Anat Rec B New Anat 287(1): 36-41.

19. Barcellos-Hoff, M. H., J. Aggeler, T. G. Ram and M. J. Bissell (1989). "Functional differentiation and alveolar morphogenesis of primary mammary cultures on reconstituted basement membrane." Development 105(2): 223-235.

20. Barnabas, N. and D. Cohen (2013). "Phenotypic and Molecular Characterization of MCF10DCIS and SUM Breast Cancer Cell Lines." Int J Breast Cancer 2013: 872743.

21. Biel, M. A. (2007). "Photodynamic therapy treatment of early oral and laryngeal cancers." Photochem Photobiol 83(5): 1063-1068.

22. Bissell, M. J., V. M. Weaver, S. A. Lelievre, F. Wang, O. W. Petersen and K. L. Schmeichel (1999). "Tissue structure, nuclear organization, and gene expression in normal and malignant breast." Cancer Res 59(7 Suppl): 1757-1763s; discussion 1763s-1764s.

23. Blyth, B. J. and P. J. Sykes (2011). "Radiation-induced bystander effects: what are they, and how relevant are they to human radiation exposures?" Radiat Res 176(2): 139-157.

24. Bosch, A., P. Eroles, R. Zaragoza, J. R. Vina and A. Lluch (2010). "Triple-negative breast cancer: molecular features, pathogenesis, treatment and current lines of research." Cancer Treat Rev 36(3): 206-215.

25. Bowen, R. L., S. W. Duffy, D. A. Ryan, I. R. Hart and J. L. Jones (2008). "Early onset of breast cancer in a group of British black women." Br J Cancer 98(2): 277-281.

26. Brint, E., G. O'Callaghan and A. Houston (2013). "Life in the Fas lane: differential outcomes of Fas signaling." Cell Mol Life Sci 70(21): 4085-4099.

27. Brown, S. B. and K. J. Mellish (2001). "Verteporfin: a milestone in opthalmology and photodynamic therapy." Expert Opin Pharmacother 2(2): 351-361.

28. Burch, S., S. K. Bisland, A. Bogaards, A. J. Yee, C. M. Whyne, J. A. Finkelstein and B. C. Wilson (2005). "Photodynamic therapy for the treatment of vertebral metastases in a rat model of human breast carcinoma." J Orthop Res 23(5): 995-1003.

29. Cailleau, R., R. Young, M. Olive and W. J. Reeves, Jr. (1974). "Breast tumor cell lines from pleural effusions." J Natl Cancer Inst 53(3): 661-674.

30. Campbell, I., K. Polyak and I. Haviv (2009). "Clonal mutations in the cancer-associated fibroblasts: the case against genetic coevolution." Cancer Res 69(17): 6765-6768; discussion 6769.

31. Caruso, J. A., P. A. Mathieu, A. Joiakim, B. Leeson, D. Kessel, B. F. Sloane and J. J. Reiners, Jr. (2004). "Differential susceptibilities of murine hepatoma 1c1c7 and Tao cells to the lysosomal photosensitizer NPe6: influence of aryl hydrocarbon receptor on lysosomal fragility and protease contents." Mol Pharmacol 65(4): 1016-1028.

32. Celli, J. P., I. Rizvi, A. R. Blanden, I. Massodi, M. D. Glidden, B. W. Pogue and T. Hasan (2014). "An imaging-based platform for high-content, quantitative evaluation of therapeutic response in 3D tumour models." Sci Rep 4: 3751.

33. Celli, J. P., I. Rizvi, C. L. Evans, A. O. Abu-Yousif and T. Hasan (2010). "Quantitative imaging reveals heterogeneous growth dynamics and treatment-dependent residual tumor distributions in a three-dimensional ovarian cancer model." J Biomed Opt 15(5): 051603.

34. Celli, J. P., N. Solban, A. Liang, S. P. Pereira and T. Hasan (2011). "Verteporfin-based photodynamic therapy overcomes gemcitabine insensitivity in a panel of pancreatic cancer cell lines." Lasers Surg Med 43(7): 565-574.

35. Celli, J. P., B. Q. Spring, I. Rizvi, C. L. Evans, K. S. Samkoe, S. Verma, B. W. Pogue and T. Hasan (2010). "Imaging and photodynamic therapy: mechanisms, monitoring, and optimization." Chem Rev 110(5): 2795-2838.

36. Chang, S., S. L. Parker, T. Pham, A. U. Buzdar and S. D. Hursting (1998). "Inflammatory breast carcinoma incidence and survival: the surveillance, epidemiology, and end results program of the National Cancer Institute, 1975-1992." Cancer 82(12): 2366-2372.

37. Chavez, K. J., S. V. Garimella and S. Lipkowitz (2010). "Triple negative breast cancer cell lines: one tool in the search for better treatment of triple negative breast cancer." Breast Dis 32(1-2): 35-48.

38. Chen, G. and D. V. Goeddel (2002). "TNF-R1 signaling: a beautiful pathway." Science 296(5573): 1634-1635.

39. Chen, J., J. Wang, Y. Zhang, D. Chen, C. Yang, C. Kai, X. Wang, F. Shi and J. Dou (2014). "Observation of ovarian cancer stem cell behavior and investigation of potential mechanisms of drug resistance in three-dimensional cell culture." J Biosci Bioeng 118(2): 214-222.

40. Cheresh, D. A. and D. G. Stupack (2008). "Regulation of angiogenesis: apoptotic cues from the ECM." Oncogene 27(48): 6285-6298.

41. Chiorean, R., C. Braicu and I. Berindan-Neagoe (2013). "Another review on triple negative breast cancer. Are we on the right way towards the exit from the labyrinth?" Breast 22(6): 1026-1033.

42. Chowdhury, I., B. Tharakan and G. K. Bhat (2006). "Current concepts in apoptosis: the physiological suicide program revisited." Cell Mol Biol Lett 11(4): 506-525.

43. Chowdhury, I., B. Tharakan and G. K. Bhat (2008). "Caspases - an update." Comp Biochem Physiol B Biochem Mol Biol 151(1): 10-27.

44. Cincotta, L., D. Szeto, E. Lampros, T. Hasan and A. H. Cincotta (1996). "Benzophenothiazine and benzoporphyrin derivative combination phototherapy effectively eradicates large murine sarcomas." Photochem Photobiol 63(2): 229-237.

45. Cirman, T., K. Oresic, G. D. Mazovec, V. Turk, J. C. Reed, R. M. Myers, G. S. Salvesen and B. Turk (2004). "Selective disruption of lysosomes in HeLa cells triggers apoptosis mediated by cleavage of Bid by multiple papain-like lysosomal cathepsins." J Biol Chem 279(5): 3578-3587.

46. Corkery, B., J. Crown, M. Clynes and N. O'Donovan (2009). "Epidermal growth factor receptor as a potential therapeutic target in triple-negative breast cancer." Ann Oncol 20(5): 862-867.

47. Cuenca, R. E., R. R. Allison, C. Sibata and G. H. Downie (2004). "Breast cancer with chest wall progression: treatment with photodynamic therapy." Ann Surg Oncol 11(3): 322-327.

48. Dahle, J., S. Bagdonas, O. Kaalhus, G. Olsen, H. B. Steen and J. Moan (2000). "The bystander effect in photodynamic inactivation of cells." Biochim Biophys Acta 1475(3): 273-280.

49. Dahle J., O. Kaalhus J. Moan and HB. Steen (1997). "Cooperative effects of photodynamic treatment of cells in microcolonies." Proc Natl Acad Sci USA 94(5):1773-78.

50. Dawood, S., N. T. Ueno, V. Valero, W. A. Woodward, T. A. Buchholz, G. N. Hortobagyi, A. M. Gonzalez-Angulo and M. Cristofanilli (2011). "Differences in survival among women with stage III inflammatory and noninflammatory locally advanced breast cancer appear early: a large population-based study." Cancer 117(9): 1819-1826.

51. Dawood, S., N. T. Ueno, V. Valero, W. A. Woodward, T. A. Buchholz, G. N. Hortobagyi, A. M. Gonzalez-Angulo and M. Cristofanilli (2012). "Identifying factors that impact survival among women with inflammatory breast cancer." Ann Oncol 23(4): 870-875.

52. de Ruijter, T. C., J. Veeck, J. P. de Hoon, M. van Engeland and V. C. Tjan-Heijnen (2011). "Characteristics of triple-negative breast cancer." J Cancer Res Clin Oncol 137(2):183-192.

53. Debnath, J. and J. S. Brugge (2005). "Modelling glandular epithelial cancers in three-

dimensional cultures." Nat Rev Cancer 5(9): 675-688.

54. Debnath, J., K. R. Mills, N. L. Collins, M. J. Reginato, S. K. Muthuswamy and J. S. Brugge (2002). "The role of apoptosis in creating and maintaining luminal space within normal and oncogene-expressing mammary acini." Cell 111(1): 29-40.

55. Dent, R., M. Trudeau, K. I. Pritchard, W. M. Hanna, H. K. Kahn, C. A. Sawka, L. A. Lickley, E. Rawlinson, P. Sun and S. A. Narod (2007). "Triple-negative breast cancer: clinical features and patterns of recurrence." Clin Cancer Res 13(15 Pt 1): 4429-4434.

56. Derradji, H. and S. Baatout (2003). "Apoptosis: a mechanism of cell suicide." *In vivo* 17(2): 185-192.

57. Diamond, I., S. G. Granelli, A. F. McDonagh, S. Nielsen, C. B. Wilson and R. Jaenicke (1972). "Photodynamic therapy of malignant tumours." Lancet 2(7788): 1175-1177.

58. Dimofte A, TC. Zhu, SM. Hahn, R A. Lustig (2002). "*In vivo* light dosimetry for motexafin lutetium-mediated PDT of recurrent breast cancer." Lasers Surg Med 31(5):305-12.

59. Ding, X., Q. Xu, F. Liu, P. Zhou, Y. Gu, J. Zeng, J. An, W. Dai and X. Li (2004). "Hematoporphyrin monomethyl ether photodynamic damage on HeLa cells by means of reactive oxygen species production and cytosolic free calcium concentration elevation." Cancer Lett 216(1): 43-54.

60. Dolmans, D. E., D. Fukumura and R. K. Jain (2003). "Photodynamic therapy for cancer." Nat Rev Cancer 3(5): 380-387.

61. Dougherty, T. J., C. J. Gomer, B. W. Henderson, G. Jori, D. Kessel, M. Korbelik, J. Moan and Q. Peng (1998). "Photodynamic therapy." J Natl Cancer Inst 90(12): 889-905.

62. Dougherty, T. J., J. E. Kaufman, A. Goldfarb, K. R. Weishaupt, D. Boyle and A. Mittleman (1978). "Photoradiation therapy for the treatment of malignant tumors." Cancer Res 38(8): 2628-2635.

63. Dougherty, T. J., G. Lawrence, J. H. Kaufman, D. Boyle, K. R. Weishaupt and A. Goldfarb (1979). "Photoradiation in the treatment of recurrent breast carcinoma." J Natl Cancer Inst 62(2): 231-237.

64. Dreyer, G., T. Vandorpe, A. Smeets, K. Forceville, B. Brouwers, P. Neven, H. Janssens, K. Deraedt, P. Moerman, B. Van Calster, M. R. Christiaens, R. Paridaens and H. Wildiers (2013). "Triple negative breast cancer: clinical characteristics in the different histological subtypes." Breast 22(5): 761-766.

65. Drife, J. O. (1986). "Breast development in puberty." Ann N Y Acad Sci 464: 58-65.

66. Duanmu, J., J. Cheng, J. Xu, C. J. Booth and Z. Hu (2011). "Effective treatment of chemoresistant breast cancer *in vitro* and *in vivo* by a factor VII-targeted photodynamic therapy." Br J Cancer 104(9): 1401-1409.

67. Earnshaw, W. C., L. M. Martins and S. H. Kaufmann (1999). "Mammalian caspases: structure, activation, substrates, and functions during apoptosis." Annu Rev Biochem 68: 383-424.

68. Edgerton, M. E., Y. L. Chuang, P. Macklin, W. Yang, E. L. Bearer and V. Cristini (2011). "A novel, patient-specific mathematical pathology approach for assessment of surgical volume: application to ductal carcinoma in situ of the breast." Anal Cell Pathol (Amst) 34(5): 247-263.

69. Eke, I. and N. Cordes (2011). "Radiobiology goes 3D: how ECM and cell morphology impact on cell survival after irradiation." Radiother Oncol 99(3): 271-278.

70. Elmore, S. (2007). "Apoptosis: a review of programmed cell death." Toxicol Pathol 35(4): 495-516.

71. Epstein, J. H. (1990). "Induction of melanomas in experimental animals." Photodermatol Photoimmunol Photomed 7(3): 95-97.

72. Epstein, J. H. (1990). "Phototherapy and photochemotherapy." N Engl J Med 322(16): 1149-1151.

73. Fingar, V. H., W. R. Potter and B. W. Henderson (1987). "Drug and light dose dependence of photodynamic therapy: a study of tumor cell clonogenicity and histologic changes." Photochem Photobiol 45(5): 643-650.

74. Forozan, F., R. Veldman, C. A. Ammerman, N. Z. Parsa, A. Kallioniemi, O. P. Kallioniemi and S. P. Ethier (1999). "Molecular cytogenetic analysis of 11 new breast cancer cell lines." Br J Cancer 81(8): 1328-1334.

75. Friedrich, J., C. Seidel, R. Ebner and L. A. Kunz-Schughart (2009). "Spheroid-based drug screen: considerations and practical approach." Nat Protoc 4(3): 309-324.

76. Gallaher, B. W., R. Hille, K. Raile and W. Kiess (2001). "Apoptosis: live or die--hard work either way!" Horm Metab Res 33(9): 511-519.

77. Gentile, M., L. Latonen and M. Laiho (2003). "Cell cycle arrest and apoptosis provoked by UV radiation-induced DNA damage are transcriptionally highly divergent responses." Nucleic Acids Res 31(16): 4779-4790.

78. Ghajar, C. M. and M. J. Bissell (2008). "Extracellular matrix control of mammary gland morphogenesis and tumorigenesis: insights from imaging." Histochem Cell Biol 130(6): 1105-1118.

79. Gonzalez-Angulo, A. M., N. Sneige, A. U. Buzdar, V. Valero, S. W. Kau, K. Broglio, Y. Yamamura, G. N. Hortobagyi and M. Cristofanilli (2004). "p53 expression as a prognostic marker in inflammatory breast cancer." Clin Cancer Res 10(18 Pt 1): 6215-6221.

80. Granville, D.J., C.M. Carthy, H. Jiang, G.C. Shore, B.M. McManus and D.W. Hunt (1998). "Rapid cytochrome c release, activation of caspases 3, 6, 7 and 8 followed by Bap31 cleavage in HeLa cells treated with photodynamic therapy." FEBS Lett 437(1-2):5-10.

81. Gudjonsson, T., L. Ronnov-Jessen, R. Villadsen, F. Rank, M. J. Bissell and O. W. Petersen (2002). "Normal and tumor-derived myoepithelial cells differ in their ability to interact with luminal breast epithelial cells for polarity and basement membrane deposition." J Cell Sci 115(Pt 1): 39-50.

82. Guelfi, M. R., M. Masoni, G. Torelli, S. Fonda and D. Caramella (1994). "[A proposal for the use of tridimensional reconstruction in oncology to better assess tumor stage and response to therapy]." Radiol Med 87(5): 669-676.

83. Hackett, A. J., H. S. Smith, E. L. Springer, R. B. Owens, W. A. Nelson-Rees, J. L. Riggs and M. B. Gardner (1977). "Two syngeneic cell lines from human breast tissue: the aneuploid mammary epithelial (Hs578T) and the diploid myoepithelial (Hs578Bst) cell lines." J Natl Cancer Inst 58(6): 1795-1806.

84. Hanahan, D. and R. A. Weinberg (2000). "The hallmarks of cancer." Cell 100(1): 57-70.

85. Hance, K. W., W. F. Anderson, S. S. Devesa, H. A. Young and P. H. Levine (2005). "Trends in inflammatory breast carcinoma incidence and survival: the surveillance, epidemiology, and end results program at the National Cancer Institute." J Natl Cancer Inst 97(13): 966-975.

86. Henderson, B. W. and J. M. Donovan (1989). "Release of prostaglandin E2 from cells by photodynamic treatment *in vitro*." Cancer Res 49(24 Pt 1): 6896-6900.

87. Henderson, B. W. and T. J. Dougherty (1992). "How does photodynamic therapy work?" Photochem Photobiol 55(1): 145-157.

88. Howlett, A. R. and M. J. Bissell (1993). "The influence of tissue microenvironment (stroma and extracellular matrix) on the development and function of mammary epithelium." Epithelial Cell Biol 2(2): 79-89.

89. Hu, Q., D. Wu, W. Chen, Z. Yan, C. Yan, T. He, Q. Liang and Y. Shi (2014). "Molecular

determinants of caspase-9 activation by the Apaf-1 apoptosome." Proc Natl Acad Sci U S A 111(46): 16254-16261.

90. Hu, Z., B. Rao, S. Chen and J. Duanmu (2010). "Targeting tissue factor on tumour cells and angiogenic vascular endothelial cells by factor VII-targeted verteporfin photodynamic therapy for breast cancer *in vitro* and *in vivo* in mice." BMC Cancer 10: 235.

91. Hu, Z., B. Rao, S. Chen and J. Duanmu (2011). "Selective and effective killing of angiogenic vascular endothelial cells and cancer cells by targeting tissue factor using a factor VII-targeted photodynamic therapy for breast cancer." Breast Cancer Res Treat 126(3): 589-600.

92. Hynes, R. O. (1992). "Integrins: versatility, modulation, and signaling in cell adhesion." Cell 69(1): 11-25.

93. Ihnatko, R. and M. Kubes (2007). "TNF signaling: early events and phosphorylation." Gen Physiol Biophys 26(3): 159-167.

94. Janicke, R. U., M. L. Sprengart, M. R. Wati and A. G. Porter (1998). "Caspase-3 is required for DNA fragmentation and morphological changes associated with apoptosis." J Biol Chem 273(16): 9357-9360.

95. Jedeszko, C., M. Sameni, M. B. Olive, K. Moin and B. F. Sloane (2008). "Visualizing protease activity in living cells: from two dimensions to four dimensions." Curr Protoc Cell Biol Chapter 4: Unit 4 20.

96. Jedeszko, C., B. C. Victor, I. Podgorski and B. F. Sloane (2009). "Fibroblast hepatocyte growth factor promotes invasion of human mammary ductal carcinoma in situ." Cancer Res 69(23): 9148-9155.

97. Kalluri, R. (2003). "Basement membranes: structure, assembly and role in tumour angiogenesis." Nat Rev Cancer 3(6): 422-433.

98. Keam, S. J., L. J. Scott and M. P. Curran (2003). "Verteporfin : a review of its use in the management of subfoveal choroidal neovascularisation." Drugs 63(22): 2521-2554.

99. Kenny, P. A., G. Y. Lee, C. A. Myers, R. M. Neve, J. R. Semeiks, P. T. Spellman, K. Lorenz, E. H. Lee, M. H. Barcellos-Hoff, O. W. Petersen, J. W. Gray and M. J. Bissell (2007). "The morphologies of breast cancer cell lines in three-dimensional assays correlate with their profiles of gene expression." Mol Oncol 1(1): 84-96.

100. Kerr, J. F. (2002). "History of the events leading to the formulation of the apoptosis concept." Toxicology 181-182: 471-474.

101. Kerr, J. F., A. H. Wyllie and A. R. Currie (1972). "Apoptosis: a basic biological phenomenon with wide-ranging implications in tissue kinetics." Br J Cancer 26(4): 239-57.

102. Kessel, D. (1992). "The role of low-density lipoprotein in the biodistribution of photosensitizing agents." J Photochem Photobiol B 14(3): 261-262.

103. Kessel, D. (2006). "Death pathways associated with photodynamic therapy." Med Laser Appl 21(4): 219-224.

104. Kessel, D. (2015). "Apoptosis and associated phenomena as a determinants of the efficacy of photodynamic therapy." Photochem Photobiol Sci.

105. Kessel, D. and A. S. Arroyo (2007). "Apoptotic and autophagic responses to Bcl-2 inhibition and photodamage." Photochem Photobiol Sci 6(12): 1290-1295.

106. Kessel, D. and Y. Luo (1998). "Mitochondrial photodamage and PDT-induced apoptosis." J Photochem Photobiol B 42(2): 89-95.

107. Kessel, D. and Y. Luo (1999). "Photodynamic therapy: a mitochondrial inducer of apoptosis." Cell Death Differ 6(1): 28-35.

108. Kessel, D., Y. Luo, P. Mathieu and J. J. Reiners, Jr. (2000). "Determinants of the apoptotic response to lysosomal photodamage." Photochem Photobiol 71(2): 196-200.

109. Kessel, D. and N. L. Oleinick (2010). "Photodynamic therapy and cell death pathways." Methods Mol Biol 635: 35-46.

110. Kessel, D., RD. Poretz (2000). "Sites of photodamage induced by photodynamic therapy with a chlorin e6 triacetoxymethyl ester (CAME)." Photochem Photobiol 71(1): 94-96.

111. Kessel, D. and J. J. Reiners, Jr. (2007). "Apoptosis and autophagy after mitochondrial or endoplasmic reticulum photodamage." Photochem Photobiol 83(5): 1024-1028.

112. Kessel, D. and J. J. Reiners, Jr. (2014). "Enhanced efficacy of photodynamic therapy via a sequential targeting protocol." Photochem Photobiol 90(4): 889-895.

113. King, K. L. and J. A. Cidlowski (1998). "Cell cycle regulation and apoptosis." Annu Rev Physiol 60: 601-617.

114. Kluck, R. M., E. Bossy-Wetzel, D. R. Green and D. D. Newmeyer (1997). "The release of cytochrome c from mitochondria: a primary site for Bcl-2 regulation of apoptosis." Science 275(5303): 1132-1136.

115. Lakhani, S. R. and M. J. O'Hare (2001). "The mammary myoepithelial cell--Cinderella or ugly sister?" Breast Cancer Res 3(1): 1-4.

116. Lara-Medina, F., V. Perez-Sanchez, D. Saavedra-Perez, M. Blake-Cerda, C. Arce, D. Motola-Kuba, C. Villarreal-Garza, A. M. Gonzalez-Angulo, E. Bargallo, J. L. Aguilar, A. Mohar and O. Arrieta (2011). "Triple-negative breast cancer in Hispanic patients: high prevalence, poor prognosis, and association with menopausal status, body mass index, and parity." Cancer 117(16): 3658-3669.

117. Lee, C. C., T. T. Huang, M. S. Lee, S. H. Hsiao, H. Y. Lin, Y. C. Su, F. C. Hsu and S. K. Hung (2010). "Clinical application of tumor volume in advanced nasopharyngeal carcinoma to predict outcome." Radiat Oncol 5: 20.

118. Lehmann, B. D., J. A. Bauer, X. Chen, M. E. Sanders, A. B. Chakravarthy, Y. Shyr and J.

A. Pietenpol (2011). "Identification of human triple-negative breast cancer subtypes and preclinical models for selection of targeted therapies." J Clin Invest 121(7): 2750-2767.

119. Li, J., A. M. Gonzalez-Angulo, P. K. Allen, T. K. Yu, W. A. Woodward, N. T. Ueno, A. Lucci, S. Krishnamurthy, Y. Gong, M. L. Bondy, W. Yang, J. S. Willey, M. Cristofanilli, V. Valero and T. A. Buchholz (2011). "Triple-negative subtype predicts poor overall survival and high locoregional relapse in inflammatory breast cancer." Oncologist 16(12): 1675-1683.

120. Li, M. L., J. Aggeler, D. A. Farson, C. Hatier, J. Hassell and M. J. Bissell (1987). "Influence of a reconstituted basement membrane and its components on casein gene expression and secretion in mouse mammary epithelial cells." Proc Natl Acad Sci U S A 84(1): 136-140.

121. Li, P., D. Nijhawan, I. Budihardjo, S. M. Srinivasula, M. Ahmad, E. S. Alnemri and X. Wang (1997). "Cytochrome c and dATP-dependent formation of Apaf-1/caspase-9 complex initiates an apoptotic protease cascade." Cell 91(4): 479-489.

122. Li, Q., A. B. Chow and R. R. Mattingly (2010). "Three-dimensional overlay culture models of human breast cancer reveal a critical sensitivity to mitogen-activated protein kinase kinase inhibitors." J Pharmacol Exp Ther 332(3): 821-828.

123. Linderholm, B. K., H. Hellborg, U. Johansson, G. Elmberger, L. Skoog, J. Lehtio and R. Lewensohn (2009). "Significantly higher levels of vascular endothelial growth factor (VEGF) and shorter survival times for patients with primary operable triple-negative breast cancer." Ann Oncol 20(10): 1639-1646.

124. Lo, A. C., C. G. Kleer, M. Banerjee, S. Omar, H. Khaled, S. Eissa, A. Hablas, J. A. Douglas, S. H. Alford, S. D. Merajver and A. S. Soliman (2008). "Molecular epidemiologic features of inflammatory breast cancer: a comparison between Egyptian and US patients."

Breast Cancer Res Treat 112(1): 141-147.

125. Lochter, A. and M. J. Bissell (1995). "Involvement of extracellular matrix constituents in breast cancer." Semin Cancer Biol 6(3): 165-173.

126. Lund, M. J., K. F. Trivers, P. L. Porter, R. J. Coates, B. Leyland-Jones, O. W. Brawley, E. W. Flagg, R. M. O'Regan, S. G. Gabram and J. W. Eley (2009). "Race and triple negative threats to breast cancer survival: a population-based study in Atlanta, GA." Breast Cancer Res Treat 113(2): 357-370.

127. Luthi, A. U. and S. J. Martin (2007). "The CASBAH: a searchable database of caspase substrates." Cell Death Differ 14(4): 641-650.

128. Madar, S., I. Goldstein and V. Rotter (2013). "'Cancer associated fibroblasts'--more than meets the eye." Trends Mol Med 19(8): 447-453.

129. Mang, T. S., R. Allison, G. Hewson, W. Snider and R. Moskowitz (1998). "A phase II/III clinical study of tin ethyl etiopurpurin (Purlytin)-induced photodynamic therapy for the treatment of recurrent cutaneous metastatic breast cancer." Cancer J Sci Am 4(6): 378-384.

130. Masuda, H., K. A. Baggerly, Y. Wang, T. Iwamoto, T. Brewer, L. Pusztai, K. Kai, T. Kogawa, P. Finetti, D. Birnbaum, L. Dirix, W. A. Woodward, J. M. Reuben, S. Krishnamurthy, W. Symmans, S. J. Van Laere, F. Bertucci, G. N. Hortobagyi and N. T. Ueno (2013). "Comparison of molecular subtype distribution in triple-negative inflammatory and non-inflammatory breast cancers." Breast Cancer Res 15(6): R112.

131. Maziere, J. C., R. Santus, P. Morliere, J. P. Reyftmann, C. Candide, L. Mora, S. Salmon, C. Maziere, S. Gatt and L. Dubertret (1990). "Cellular uptake and photosensitizing properties of anticancer porphyrins in cell membranes and low and high density lipoproteins." J Photochem Photobiol B 6(1-2): 61-68.

132. McGowan, E. B., E. Becker and T. C. Detwiler (1989). "Inhibition of calpain in intact

platelets by the thiol protease inhibitor E-64d." Biochem Biophys Res Commun 158(2): 432-435.

133. Mitra, S. and T. H. Foster (2008). "*In vivo* confocal fluorescence imaging of the intratumor distribution of the photosensitizer mono-L-aspartylchlorin-e6." Neoplasia 10(5): 429-438.

134. Moan, J. and K. Berg (1991). "The photodegradation of porphyrins in cells can be used to estimate the lifetime of singlet oxygen." Photochem Photobiol 53(4): 549-553.

135. Moan, J., E. O. Pettersen and T. Christensen (1979). "The mechanism of photodynamic inactivation of human cells *in vitro* in the presence of haematoporphyrin." Br J Cancer 39(4): 398-407.

136. Moffitt, K. L., S. L. Martin and B. Walker (2010). "From sentencing to execution--the processes of apoptosis." J Pharm Pharmacol 62(5): 547-562.

137. Moin, K., M. Sameni, B. C. Victor, J. M. Rothberg, R. R. Mattingly and B. F. Sloane (2012). "3D/4D functional imaging of tumor-associated proteolysis: impact of microenvironment." Methods Enzymol 506: 175-194.

138. Montaser, M., G. Lalmanach and L. Mach (2002). "CA-074, but not its methyl ester CA-074Me, is a selective inhibitor of cathepsin B within living cells." Biol Chem 383(7-8): 1305-1308.

139. Morris, G. J., S. Naidu, A. K. Topham, F. Guiles, Y. Xu, P. McCue, G. F. Schwartz, P. K. Park, A. L. Rosenberg, K. Brill and E. P. Mitchell (2007). "Differences in breast carcinoma characteristics in newly diagnosed African-American and Caucasian patients: a single-institution compilation compared with the National Cancer Institute's Surveillance, Epidemiology, and End Results database." Cancer 110(4): 876-884.

140. Morrison, S. A., S. L. Hill, G. S. Rogers and R. A. Graham (2014). "Efficacy and safety of continuous low-irradiance photodynamic therapy in the treatment of chest wall progression

of breast cancer." J Surg Res 192(2): 235-241.

141. Mozley, P. D., L. H. Schwartz, C. Bendtsen, B. Zhao, N. Petrick and A. J. Buckler (2010). "Change in lung tumor volume as a biomarker of treatment response: a critical review of the evidence." Ann Oncol 21(9): 1751-1755.

142. Mueller-Klieser, W. (2000). "Tumor biology and experimental therapeutics." Crit Rev Oncol Hematol 36(2-3): 123-139.

143. Mukherji, S. K., I. M. Schmalfuss, J. Castelijns and A. A. Mancuso (2004). "Clinical applications of tumor volume measurements for predicting outcome in patients with squamous cell carcinoma of the upper aerodigestive tract." AJNR Am J Neuroradiol 25(8): 1425-1432.

144. Mullins, S. R., M. Sameni, G. Blum, M. Bogyo, B. F. Sloane and K. Moin (2012). "Three-dimensional cultures modeling premalignant progression of human breast epithelial cells: role of cysteine cathepsins." Biol Chem 393(12): 1405-1416.

145. Neve, R. M., K. Chin, J. Fridlyand, J. Yeh, F. L. Baehner, T. Fevr, L. Clark, N. Bayani, J. P. Coppe, F. Tong, T. Speed, P. T. Spellman, S. DeVries, A. Lapuk, N. J. Wang, W. L. Kuo, J. L. Stilwell, D. Pinkel, D. G. Albertson, F. M. Waldman, F. McCormick, R. B. Dickson, M. D. Johnson, M. Lippman, S. Ethier, A. Gazdar and J. W. Gray (2006). "A collection of breast cancer cell lines for the study of functionally distinct cancer subtypes." Cancer Cell 10(6): 515-527.

146. Nicholson, D. W. (1999). "Caspase structure, proteolytic substrates, and function during apoptotic cell death." Cell Death Differ 6(11): 1028-1042.

147. Nogi, H., T. Kobayashi, M. Suzuki, I. Tabei, K. Kawase, Y. Toriumi, H. Fukushima and K. Uchida (2009). "EGFR as paradoxical predictor of chemosensitivity and outcome among triple-negative breast cancer." Oncol Rep 21(2): 413-417.

83

148. Nouh, M. A., M. M. Mohamed, M. El-Shinawi, M. A. Shaalan, D. Cavallo-Medved, H. M. Khaled and B. F. Sloane (2011). "Cathepsin B: a potential prognostic marker for inflammatory breast cancer." J Transl Med 9: 1.

149. Ola, M. S., M. Nawaz and H. Ahsan (2011). "Role of Bcl-2 family proteins and caspases in the regulation of apoptosis." Mol Cell Biochem 351(1-2): 41-58.

150. Oleinick, N. L. and H. H. Evans (1998). "The photobiology of photodynamic therapy: cellular targets and mechanisms." Radiat Res 150(5 Suppl): S146-156.

151. Opferman, J. T. and S. J. Korsmeyer (2003). "Apoptosis in the development and maintenance of the immune system." Nat Immunol 4(5): 410-415.

152. Osaki, T, S. Takagi, Y Hoshin,o M Okumura T. Fujinaga (2006). "Intracellular localization and concentration as well as photodynamic effects of benzoporphyrin derivative monoacid ring A in four types of rodent tumor cells." Cancer Lett 243(2):281-92.

153. Osuala, K. O., M. Sameni, S. Shah, N. Aggarwal, M. L. Simonait, O. E. Franco, Y. Hong, S. W. Hayward, F. Behbod, R. R. Mattingly and B. F. Sloane (in press). "Il-6 signaling between ductal carcinoma in situ cells and carcinoma-associated fibroblasts mediates tumor cell growth and migration."

154. Porter, A. G. and R. U. Janicke (1999). "Emerging roles of caspase-3 in apoptosis." Cell Death Differ 6(2): 99-104.

155. Raab, O. (1904). "Ueber die Wirkung Fluorescierenden Stoffe auf Infusorien." Z. Biol. 39: 524-546.

156. Reiners, J. J., Jr., J. A. Caruso, P. Mathieu, B. Chelladurai, X. M. Yin and D. Kessel (2002). "Release of cytochrome c and activation of pro-caspase-9 following lysosomal photodamage involves Bid cleavage." Cell Death Differ 9(9): 934-944.

157. Renehan, A. G., S. P. Bach and C. S. Potten (2001). "The relevance of apoptosis for

cellular homeostasis and tumorigenesis in the intestine." Can J Gastroenterol 15(3):166-76.

158. Renehan, A. G., C. Booth and C. S. Potten (2001). "What is apoptosis, and why is it important?" BMJ 322(7301): 1536-1538.

159. Richter, A. M., E. Waterfield, A. K. Jain, B. Allison, E. D. Sternberg, D. Dolphin and J. G. Levy (1991). "Photosensitising potency of structural analogues of benzoporphyrin derivative (BPD) in a mouse tumour model." Br J Cancer 63(1): 87-93.

160. Richter, A. M., E. Waterfield, A. K. Jain, E. D. Sternberg, D. Dolphin and J. G. Levy (1990). "*In vitro* evaluation of phototoxic properties of four structurally related benzoporphyrin derivatives." Photochem Photobiol 52(3): 495-500.

161. Riedl, S. J. and G. S. Salvesen (2007). "The apoptosome: signalling platform of cell death." Nat Rev Mol Cell Biol 8(5): 405-413.

162. Riou, G., M. G. Le, J. P. Travagli, A. J. Levine and U. M. Moll (1993). "Poor prognosis of p53 gene mutation and nuclear overexpression of p53 protein in inflammatory breast carcinoma." J Natl Cancer Inst 85(21): 1765-1767.

163. Rizvi, I., S. Anbil, N. Alagic, J. Celli, L. Z. Zheng, A. Palanisami, M. D. Glidden, B. W. Pogue and T. Hasan (2013). "PDT dose parameters impact tumoricidal durability and cell death pathways in a 3D ovarian cancer model." Photochem Photobiol 89(4): 942-952.

164. Rizvi, I., J. P. Celli, C. L. Evans, A. O. Abu-Yousif, A. Muzikansky, B. W. Pogue, D. Finkelstein and T. Hasan (2010). "Synergistic enhancement of carboplatin efficacy with photodynamic therapy in a three-dimensional model for micrometastatic ovarian cancer." Cancer Res 70(22): 9319-9328.

165. Robertson, F. M., M. Bondy, W. Yang, H. Yamauchi, S. Wiggins, S. Kamrudin, S. Krishnamurthy, H. Le-Petross, L. Bidaut, A. N. Player, S. H. Barsky, W. A. Woodward, T. Buchholz, A. Lucci, N. T. Ueno and M. Cristofanilli (2010). "Inflammatory breast cancer:

the disease, the biology, the treatment." CA Cancer J Clin 60(6): 351-375.

166. Rogers, G. S. (2012). "Continuous low-irradiance photodynamic therapy: a new therapeutic paradigm." J Natl Compr Canc Netw 10 Suppl 2: S14-17.

167. Ronnov-Jessen, L., O. W. Petersen and M. J. Bissell (1996). "Cellular changes involved in conversion of normal to malignant breast: importance of the stromal reaction." Physiol Rev 76(1): 69-125.

168. Rothberg, J. M., K. M. Bailey, J. W. Wojtkowiak, Y. Ben-Nun, M. Bogyo, E. Weber, K. Moin, G. Blum, R. R. Mattingly, R. J. Gillies and B. F. Sloane (2013). "Acid-mediated tumor proteolysis: contribution of cysteine cathepsins." Neoplasia 15(10): 1125-1137.

169. Salvesen, G. S. and V. M. Dixit (1997). "Caspases: intracellular signaling by proteolysis." Cell 91(4): 443-446.

170. Salvesen, G. S. and V. M. Dixit (1999). "Caspase activation: the induced-proximity model." Proc Natl Acad Sci U S A 96(20): 10964-10967.

171. Sameni, M., A. Anbalagan, M. B. Olive, K. Moin, R. R. Mattingly and B. F. Sloane (2012). "MAME models for 4D live-cell imaging of tumor: microenvironment interactions that impact malignant progression." J Vis Exp(60).

172. Sameni, M., D. Cavallo-Medved, J. Dosescu, C. Jedeszko, K. Moin, S. R. Mullins, M. B. Olive, D. Rudy and B. F. Sloane (2009). "Imaging and quantifying the dynamics of tumor-associated proteolysis." Clin Exp Metastasis 26(4): 299-309.

173. Sameni, M., J. Dosescu, K. M. Yamada, B. F. Sloane and D. Cavallo-Medved (2008). "Functional live-cell imaging demonstrates that beta1-integrin promotes type IV collagen degradation by breast and prostate cancer cells." Mol Imaging 7(5): 199-213.

174. Schroder, T., I. W. Chen, M. Sperling, R. H. Bell, Jr., K. Brackett and S. N. Joffe (1988). "Hematoporphyrin derivative uptake and photodynamic therapy in pancreatic carcinoma." J

Surg Oncol 38(1): 4-9.

175. Schultz, G. S. and A. Wysocki (2009). "Interactions between extracellular matrix and growth factors in wound healing." Wound Repair Regen 17(2): 153-162.

176. Shin, C. S., B. Kwak, B. Han and K. Park (2013). "Development of an *in vitro* 3D tumor model to study therapeutic efficiency of an anticancer drug." Mol Pharm 10(6): 2167-2175.

177. Solary, E., N. Droin, A. Bettaieb, L. Corcos, M. T. Dimanche-Boitrel and C. Garrido (2000). "Positive and negative regulation of apoptotic pathways by cytotoxic agents in hematological malignancies." Leukemia 14(10): 1833-1849.

178. Soliman, A. S., C. G. Kleer, K. Mrad, M. Karkouri, S. Omar, H. M. Khaled, A. L. Benider, F. B. Ayed, S. S. Eissa, M. S. Eissa, E. J. McSpadden, A. C. Lo, K. Toy, E. D. Kantor, Q. Xiao, C. Hampton and S. D. Merajver (2011). "Inflammatory breast cancer in north Africa: comparison of clinical and molecular epidemiologic characteristics of patients from Egypt, Tunisia, and Morocco." Breast Dis 33(4): 159-169.

179. Spikes, J. D. and J. C. Bommer (1993). "Photosensitizing properties of mono-L-aspartyl chlorin e6 (NPe6): a candidate sensitizer for the photodynamic therapy of tumors." J Photochem Photobiol B 17(2): 135-143.

180. Staudacher, A. H., B. J. Blyth, M. D. Lawrence, R. J. Ormsby, E. Bezak and P. J. Sykes (2010). "If bystander effects for apoptosis occur in spleen after low-dose irradiation *in vivo* then the magnitude of the effect falls within the range of normal homeostatic apoptosis." Radiat Res 174(6): 727-731.

181. Stead, L. A., T. L. Lash, J. E. Sobieraj, D. D. Chi, J. L. Westrup, M. Charlot, R. A. Blanchard, J. C. Lee, T. C. King and C. L. Rosenberg (2009). "Triple-negative breast cancers are increased in black women regardless of age or body mass index." Breast Cancer Res 11(2): R18.

182. Sternlicht, M. D., P. Kedeshian, Z. M. Shao, S. Safarians and S. H. Barsky (1997). "The human myoepithelial cell is a natural tumor suppressor." Clin Cancer Res 3(11):1949-1958.

183. Steward, L., L. Conant, F. Gao and J. A. Margenthaler (2014). "Predictive factors and patterns of recurrence in patients with triple negative breast cancer." Ann Surg Oncol 21(7): 2165-2171.

184. Storch, K., I. Eke, K. Borgmann, M. Krause, C. Richter, K. Becker, E. Schrock and N. Cordes (2010). "Three-dimensional cell growth confers radioresistance by chromatin density modification." Cancer Res 70(10): 3925-3934.

185. Strasser, A., L. O'Connor and V. M. Dixit (2000). "Apoptosis signaling." Annu Rev Biochem 69: 217-245.

186. Tamai, M., K. Matsumoto, S. Omura, I. Koyama, Y. Ozawa and K. Hanada (1986). "*In vitro* and *in vivo* inhibition of cysteine proteinases by EST, a new analog of E-64." J Pharmacobiodyn 9(8): 672-677.

187. Tammela, T., A. Saaristo, T. Holopainen, S. Yla-Herttuala, L. C. Andersson, S. Virolainen, I. Immonen and K. Alitalo (2011). "Photodynamic ablation of lymphatic vessels and intralymphatic cancer cells prevents metastasis." Sci Transl Med 3(69): 69ra11.

188. Taylor, R. C., S. P. Cullen and S. J. Martin (2008). "Apoptosis: controlled demolition at the cellular level." Nat Rev Mol Cell Biol 9(3): 231-241.

189. Thompson, C. B. (1995). "Apoptosis in the pathogenesis and treatment of disease." Science 267(5203): 1456-1462.

190. Trauner, K. B., R. Gandour-Edwards, M. Bamberg, S. Shortkroff, C. Sledge and T. Hasan (1998). "Photodynamic synovectomy using benzoporphyrin derivative in an antigen-induced arthritis model for rheumatoid arthritis." Photochem Photobiol 67(1): 133-139.

191. Tutt, A., M. Robson, J. E. Garber, S. M. Domchek, M. W. Audeh, J. N. Weitzel, M.

Friedlander, B. Arun, N. Loman, R. K. Schmutzler, A. Wardley, G. Mitchell, H. Earl, M. Wickens and J. Carmichael (2010). "Oral poly(ADP-ribose) polymerase inhibitor olaparib in patients with BRCA1 or BRCA2 mutations and advanced breast cancer: a proof-of-concept trial." Lancet 376(9737): 235-244.

192. Unger, C., N. Kramer, A. Walzl, M. Scherzer, M. Hengstschlager and H. Dolznig (2014). "Modeling human carcinomas: physiologically relevant 3D models to improve anti-cancer drug development." Adv Drug Deliv Rev 79-80: 50-67.

193. Usuda, J., H. Kato, T. Okunaka, K. Furukawa, H. Tsutsui, K. Yamada, Y. Suga, H. Honda, Y. Nagatsuka, T. Ohira, M. Tsuboi and T. Hirano (2006). "Photodynamic therapy (PDT) for lung cancers." J Thorac Oncol 1(5): 489-493.

194. Van der Auwera, I., S. J. Van Laere, G. G. Van den Eynden, I. Benoy, P. van Dam, C. G. Colpaert, S. B. Fox, H. Turley, A. L. Harris, E. A. Van Marck, P. B. Vermeulen and L. Y. Dirix (2004). "Increased angiogenesis and lymphangiogenesis in inflammatory versus noninflammatory breast cancer by real-time reverse transcriptase-PCR gene expression quantification." Clin Cancer Res 10(23): 7965-7971.

195. Victor, B. C., A. Anbalagan, M. M. Mohamed, B. F. Sloane and D. Cavallo-Medved (2011). "Inhibition of cathepsin B activity attenuates extracellular matrix degradation and inflammatory breast cancer invasion." Breast Cancer Res 13(6): R115.

196. Victor, B. C. and B. F. Sloane (2007). "Cysteine cathepsin non-inhibitory binding partners: modulating intracellular trafficking and function." Biol Chem 388(11): 1131-1140.

197. Villanueva, A., J. C. Stockert, M. Canete and P. Acedo (2010). "A new protocol in photodynamic therapy: enhanced tumour cell death by combining two different photosensitizers." Photochem Photobiol Sci 9(3): 295-297.

198. von Tappeiner, H. and A. Jodlbauer (1904). "Uber die Wirkung der photodynamischen

(fluorescierenden) Stoffe auf Protozoen und Enzyme." Dtsch. Arch. Klin. Med. 80:427–87.

199. von Tappeiner, H. and A. Jodlbauer (1907). "Die Sensibilisierende Wirkung Fluorescierender Substanzen: Gesammelte Untersuchungen Über die Photodynamische Erscheinung. ." Leipzig, Germany: F.C.W. Vogel 1: 210.

200. Wajant, H. (2002). "The Fas signaling pathway: more than a paradigm." Science 296(5573): 1635-1636.

201. Wan, Q., L. Liu, D. Xing and Q. Chen (2008). "Bid is required in NPe6-PDT-induced apoptosis." Photochem Photobiol 84(1): 250-257.

202. Wang, K. K., A. Posner, K. J. Raser, M. Buroker-Kilgore, R. Nath, I. Hajimohammadreza, A. W. Probert, F. W. Marcoux, E. A. Lunney, S. J. Hays and P. W. Yuen (1996). "Alpha-mercaptoacrylic acid derivatives as novel selective calpain inhibitors." Adv Exp Med Biol 389: 95-101.

203. Weaver, V. M. and M. J. Bissell (1999). "Functional culture models to study mechanisms governing apoptosis in normal and malignant mammary epithelial cells." J Mammary Gland Biol Neoplasia 4(2): 193-201.

204. Webber, J., Y. Luo, R. Crilly, D. Fromm and D. Kessel (1996). "An apoptotic response to photodynamic therapy with endogenous protoporphyrin *in vivo*." J Photochem Photobiol B 35(3): 209-211.

205. Weigelt, B. and M. J. Bissell (2008). "Unraveling the microenvironmental influences on the normal mammary gland and breast cancer." Semin Cancer Biol 18(5): 311-321.

206. Weigelt, B., C. M. Ghajar and M. J. Bissell (2014). "The need for complex 3D culture models to unravel novel pathways and identify accurate biomarkers in breast cancer." Adv Drug Deliv Rev 69-70: 42-51.

207. Wingo, P. A., P. M. Jamison, J. L. Young and P. Gargiullo (2004). "Population-based

statistics for women diagnosed with inflammatory breast cancer (United States)." Cancer Causes Control 15(3): 321-328.

208. Wyld, L., M. W. Reed and N. J. Brown (2001). "Differential cell death response to photodynamic therapy is dependent on dose and cell type." Br J Cancer 84(10): 1384-1386.

209. Wyllie, A. H., J. F. Kerr and A. R. Currie (1980). "Cell death: the significance of apoptosis." Int Rev Cytol 68: 251-306.

210. Yang, Y. C. (2004). "Preserving vision with verteporfin photodynamic therapy." Hosp Med 65(1): 39-43.

211. Yousefi, S., R. Perozzo, I. Schmid, A. Ziemiecki, T. Schaffner, L. Scapozza, T. Brunner and H. U. Simon (2006). "Calpain-mediated cleavage of Atg5 switches autophagy to apoptosis." Nat Cell Biol 8(10): 1124-1132.

212. Zamaraev, A. V., G. S. Kopeina, B. Zhivotovsky and I. N. Lavrik (2015). "Cell death controlling complexes and their potential therapeutic role." Cell Mol Life Sci 72(3):505-17.

213. Zell, J. A., W. Y. Tsang, T. H. Taylor, R. S. Mehta and H. Anton-Culver (2009). "Prognostic impact of human epidermal growth factor-like receptor 2 and hormone receptor status in inflammatory breast cancer (IBC): analysis of 2,014 IBC patient cases from the California Cancer Registry." Breast Cancer Res 11(1): R9.

214. Zhang, L., C. Fang, X. Xu, A. Li, Q. Cai and X. Long (2015). "Androgen receptor, EGFR, and BRCA1 as biomarkers in triple-negative breast cancer: a meta-analysis." Biomed Res Int 2015: 357485.

215. Zhang, Y., D. Xing and L. Liu (2009). "PUMA promotes Bax translocation by both directly interacting with Bax and by competitive binding to Bcl-X L during UV-induced apoptosis." Mol Biol Cell 20(13): 3077-3087.

216. Zhivotovsky, B., S. Orrenius, O. T. Brustugun and S. O. Doskeland (1998). "Injected

cytochrome c induces apoptosis." Nature 391(6666): 449-450.

ABSTRACT

PHOTODYNAMIC THERAPY AS AN EFFECTIVE THERAPEUTIC APPROACH IN MAME MODELS OF TRIPLE NEGATIVE AND INFLAMMATORY BREAST CANCERS

by

NEHA AGGARWAL

August 2015

Advisor: Bonnie Sloane, Ph.D., and Douglas R. Yingst, Ph.D.

Major: Physiology

Degree: Doctor of Philosophy

Introduction: Photodynamic therapy (PDT) is a minimally invasive, FDA approved therapy for treatment of several indications including endobronchial and esophageal cancers that are accessible to light. Triple negative breast cancer (TNBC) and inflammatory breast cancer (IBC) are aggressive and lethal subtypes of breast cancer that spread to chest wall and dermal lymphatics, respectively, sites that would be accessible to light. Both TNBC and IBC patients have a relatively poor survival rate due to lack of targeted therapies. Use of PDT is underexplored for breast cancers but has been proposed for treatment of subtypes for which a targeted therapy is unavailable.

Methods: We optimized and used a mammary architecture and microenvironment engineering (MAME) model of IBC to examine the effects of PDT using two treatment protocols. The first protocol used the benzoporphyrin derivative monoacid A (BPD) activated at doses ranging from 45 mJ/cm^2 to 540 mJ/cm^2. The second PDT protocol used two photosensitizers: BPD and mono-L-aspartyl chlorin e6 (NPe6), which were sequentially activated. Effects of PDT were assessed by live-dead assays.

Results: Using a MAME model of TNBC and IBC, we demonstrate a significant dose-response

in photokilling by BPD-PDT. We found that sequential activation of NPe6 followed by BPD is more effective in photokilling of tumor cells than is BPD alone. Sequential activation at a dose of 45 mJ/cm^2 each resulted in >90% cell death, a response only achieved by BPD-PDT at a dose of 360 mJ/cm^2. Furthermore, our data show that volumetric measurement of 3D MAME structures reflect efficacy of PDT treatment. We also show that the mechanism of cell death after sequential activation of NPe6 followed by BPD is apoptosis.

Conclusion: Our study is the first to demonstrate the potential of PDT in treating MAME structures of TNBC and IBC.

AUTOBIOGRAPHICAL STATEMENT

Neha Aggarwal

Education

Ph.D. (Physiology), 2010- 2015
Wayne State University School of Medicine (WSU SOM), Detroit, MI, USA
    Mentors: Dr. Bonnie F. Sloane and Dr. Douglas Yingst
    Dissertation topic: Effects of photodynamic therapy on 3D models of triple negative and inflammatory breast cancers

MS (Thesis option- Biology), 2007- 2010
Cleveland State University (CSU), Cleveland, Ohio, USA.
    Mentor: Dr. Girish Shukla
    Thesis title: Characterization of a microRNA harboring intron for pre-mRNA splicing and microRNA processing

Master of Science (Honors- Thesis option), Biochemistry, 2005-2007
Panjab University, Chandigarh – INDIA. GPA: 3.8 distinction
    Mentor: Dr. Sanjeev Puri
    Thesis title: Molecular studies on stem cell differentiation: Paradigm for adipogenesis & nephrogenesis

Bachelor of Science (Honors), Biochemistry, 2002-2005
Panjab University, Chandigarh – INDIA. GPA: 3.8

Peer Reviewed Publications

1. **Aggarwal, N.**, Kessel, D., and Sloane, B.F.: Photodynamic therapy as a therapeutic approach for inflammatory breast cancer cells grown in 3D models, 2015, (*Submitted)*

2. Osuala, K.O., Sameni, M., Shah, S., **Aggarwal, N.,** *et.al.*: Il-6 signaling between ductal carcinoma in situ cells and carcinoma-associated fibroblasts mediates tumor cell migration, 2015, (*In Press*)

3. Ramalho, S., Sharma, R., **Aggarwal, N.**, *et.al.*: Visualizing inhibition of proteolysis by a light-activated ruthenium compound in live breast cancer cells, 2015, (*Submitted*)

4. **Aggarwal, N.** and Sloane, B.F.: Cathepsin B: multiple roles in cancer, Proteomics Clin. Appl., 2014, PMID: 24677670

5. Kessel, D., **Aggarwal, N.** and Sloane, B.F.: Increased efficacy of photodynamic therapy via sequential targeting. SPIE (the international society for optics and photonics), 2014, doi: 10.1117/12.2042421

Awards and Honors

- Marion I. Barnhart Graduate Student Award, Department of Physiology- 2014
- American Society for Photobiology's Frederick Urbach Memorial Student Award- 2014
- Third position award for poster presentation at Graduate Research Exhibition- 2014
- Graduate School Travel Award- 2014, 2012
- Department of Physiology Travel Award- 2014, 2012
- Department of Pharmacology Travel Award- 2014, 2012
- Thomas C. Rumble Fellowship, WSU SOM- 2013-2014
- GRA Fellowship from Graduate school, WSU SOM- 2012-2013
- IBS fellowship from Graduate school, WSU SOM- 2010-2012